FACULDADE DE ENGENHARIA DA UNIVERSIDADE DO PORTO

Fracture behavior of refractory silica bricks

João Paulo Couto Cardoso

Mestrado em Engenharia Mecânica

Advisor FEUP: Jorge Lino

Co-advisor FEUP: Marco Parente

Supervisor Tata Steel: Bruno Luchini ; Sido Sinnema

October 20, 2022

Fracture behavior of refractory silica bricks

João Paulo Couto Cardoso

Mestrado em Engenharia Mecânica

October 20, 2022

Abstract

The present dissertation main focus is to study the development of damage and cracks in silica refractories subjected to thermo-mechanical loading. This type of loading is the principal source of damage of these materials and, in order to study them, three prime methodologies of test were carried out: finite element modeling simulations, mechanical testing (three-point bending) and thermal-shock cyclic testing (X-ray diffraction and Impulse excitation technique).

The two materials tested were crystalline silica and fused silica, both sourced from bricks of the same material used in coke ovens present in the factory. The samples were tested until 1400ºC on all tests.

Modeling of a 2D three-point bending test of a silica brick was done using *Abaqus*. The simulations were performed for varying mechanical properties, and using different crack methods and crack lengths. The force-displacement curves were extracted and studied alongside the stress intensity factor and J-integral at failure. Three-point bending tests were performed both at room temperature and high temperature, for either virgin samples and thermally treated ones. Impulse excitation technique was used as a means to study the variation of Young's modulus (E) across varying temperature under different thermal cycles. X-Ray diffraction (XRD) was used to evaluate the phase proportion changes across a thermal cycle.

It was found that for finite element modeling in *Abaqus*, Extended finite element method (XFEM) cracks did not allow to retrieve stress intensity factor and J-integral values with crack growth, making it not suitable as a tool to analyse this parameter. Contour integral crack is a simpler method for this case since it is able to analyse a stationary crack and, at the same time, the stress intensity factor and J-integral values could be retrieved.

Impulse Excitation Technique (IET) tests showed various changes to sample's E, with a crystalline silica sample that increased its Young's modulus at room temperature after being submited to thermal cycle, and fused silica sample showed a great amount of damage when cooled down from high temperature.

Three-point bending (3PB) results did not always come with agreement with impulse excitation technique results. In 3PB tests, longer dwell times and a cyclic testing approach was found to yield very different results from the other tests, meaning more testing needs to be performed with those parameters.

XRD helped to explain some of the behaviour of the samples, which was ruled by phase transformations, clearing out the point of phase transformation of cristobalite and the different polymorphs of tridymite. It backed up some of the findings of impulse excitation technique and helped explain the variations seen in the Young's modulus across the varying temperature of the thermal cycle.

Resumo

A presente dissertação tem como foco principal o estudo dos mecanismos e parâmetros que levam à falha de tijolos refratários de sílica submetidos a cargas termomecânicas. As fendas são a principal causa da falha deste material em serviço e para as estudar, foram usadas três metodologias: simulação pelo método dos elementos finitos, ensaio de flexão em 3 pontos, cristalografia de Raio-X (XRD) e técnica de excitação por impulso (IET).

Os dois materiais testados foram a sílica cristalina e a sílica amorfa, amostras estas retiradas do mesmo material usado nos fornos de carvão presentes na fábrica. As amostras foram testadas até 1400ºC em todos os testes.

O software *Abaqus* foi usado para modelação 2D de um teste de flexão em três pontos de um tijolo refratário de silica. Nas simulações, foram realizados vários testes variando-se as propriedades mecânicas do modelo, o tipo de fenda e o comprimento da mesma. Estudou-se os gráficos de força-deslocamento, assim como o fator de concentração de tensão e Integral J no ponto de rutura. Os ensaios em três pontos foram realizados tanto à temperatura ambiente como a temperaturas elevadas, testando tanto amostras virgens como outras já submetidas previamente a um ciclo térmico. De maneira a estudar a variação do módulo de young com a variação da temperatura para diferentes ciclos térmicos, fez-se recurso á ténica de excitação por impulso. A XRD é responsável por fornecer as mudanças nas proporções de cada fase da sílica quando submetida a um ciclo térmico.

Foi possível observar que para as simulações com elementos finitos que, para fendas com recurso ao "Extended Finite Element Method" (XFEM), não foi possível simular a propagação de fenda e simultaneamente obter os valores para as propriedades desejadas na rutura. Este método foi então abandonado e fendas do tipo "contour integral" foram adotadas devido a serem um método mais simples e que neste caso são capazes de obter os mesmo resultados que XFEM com uma malha mais organizado, permitindo analisar um fenda estacionária usando as propriedades desejadas (fator de concentração de tensão e Integral J).

Nos testes de IET, foram observadas várias mudanças no módulo de Young em ambas as amostras ao longo do ciclo térmico. Para a amostra de sílica cristalina o módulo de Young à temperatura ambiente antes do ciclo é inferior do após à finalização do mesmo, enquanto que a amostra de silica amorfa estava extremamente danificada após ser arrefecida de altas temperaturas, apresentando um módulo de Young muito inferior ao medido no início do teste.

Para os teste de ensaio em três pontos, os resultados nem sempre estiveram de acordo com os observação dos testes de IET. Para além de que se verificou quando as amostras eram mantidas à temperatura de teste por uma duração prolongada antes da realização do ensaio, os resultados eram completamente diferentes. Também quando analisando os ciclos de carga e descarga no inicio dos testes,foram obtidos resultados diferentes. É necessário a realização de mais testes tendo em atenção estes dois parâmetros.

A XRD foi útil para explicar e confirmar certos comportamentos observados nestes materiais que são dominados pelas transformações entre fases. Permitiu também confirmar os pontos de

transformação de cristobalite e tridimite, assim como reforçar algumas das conclusões dos testes de IET.

Acknowledgements

Firstly, I would like to thank Bruno Luchini for guiding me throughout all this project and always being available to answer my questions and clarify my doubts.

I would also like to thank Sido Sinnema for the possibility to participate in this internship and other fun events.

Additionally, I would like to thank Japp Koster for always making the effort to help me and teach me using 3PB machine, Stefan Melzer for the help in XRD experiments, Donald Mittertreiner, Frank Van der Does and Mustafa Keskin for the support related to 3PB experiments, and Pieter Put for making IET experiments possible.

Moreover, I would like to thank all my internship colleagues for making work a funner environment and always willing to help me out. Also to thank every employee at the Ceramic Research Centre for all the welcoming and nice work environment.

I would also like to thank the University of Porto and specially my supervisor and co supervisor at FEUP, Jorge Lino, and Marco Parente, respectively, which were always available for my questions and doubts throughout the project.

I would like to thank my family and friends for all the support they gave me along this project.

Lastly, I thank both Tata Steel IJmuiden and the Erasmus+ programme for the financial support.

João Cardoso

"Perfection is the enemy,
of good enough."

Bad Obsession Motorsport

Contents

List of Figures

List of Tables

Symbols and Acronyms

3PB	Three-point bending
a	Crack length
b	Width
CRC	Ceramics Research Center
CPS4	Four node, bilinear, plane stress/plane strain quadrilateral
E	Young's modulus
f_r	Resonant frequencies
G	Strain energy release rate
G_C	Fracture energy
IET	Impulse excitation technique
K^1	Linear thermal expansion coefficient
K_I	Stress intensity factor in mode I
K_C	Fracture toughness
K_{IC}	Fracture toughness in mode I
KOK	Crystalline silica material code name
l	Displacement
m	Mass
P	Load
t	Thickness
T_1	Correction factor
T_i	Traction forces in a differential element
u_i	Displacement in each element
W	Deformation energy density
XRD	X-ray diffraction
ZEB	Fused silica material code name
σ	Stress
σ_{ij}	Stress tensor
ε_{ij}	Strain tensor
γ_S	Bond energy

Chapter 1

Introduction

1.1 Project Framing

The development of this work was done at the Ceramics Research Center, part of Tata Steel IJmuiden (located in the Netherlands), in a cooperation with the Mechanical Engineering Department of the Faculty of Engineering of the University of Porto, Portugal, as a Master Thesis Dissertation within the Production, Conception and Manufacturing option of the Master in Mechanical Engineering.

1.2 Motivation

The most widely used materials for high temperature linings are ceramic refractory materials, because of their refractoriness, corrosion and erosion resistance, dimensional stability, availability and cost/effectiveness. From coke ovens to high temperature furnaces, refractory bricks are widely used at Tata Steel. They are suitable materials but have limitations and problems which if not taken into account, can cost the company millions. This is where the Ceramics Research Center at Tata Steel IJmuidem comes in. They have the job of providing the company with the best and most cost effective refractories for the in-company applications. To do this, they constantly track the market in search of the best options. Aside from that, the Center has other major task. They are responsible for testing refractories, modeling linings, keeping track of the linings in work, predict the work-life of refractories and constantly improve on the methods applied to achieve their end goals.

Three-point bending and thermal fatigue testing of a specimen are both two methods used to predict the life time of refractory and measure its properties. Both are very important tests, yet it takes time and resources to perform them. Multiple tests have to be made, samples need to be provided and money spent on the equipment and staff necessary to perform these tests. When looking at finite element simulation, although it can be more expensive to use because of the price

of the software and the increased wage of capable staff, it brings advantages over the traditional methods. It is possible to obtain final results in a shorter time span, to evaluate the effect of changing a few parameters and test specimens in complex situations that would be hard to replicate in real operating conditions. However, the results obtained from finite element modeling (FEM) simulation could prove to be unreliable and deviate from the experimental ones. So, it is a must to first assess the reliability of FEM simulation in each situation.

1.3 Project Goals

The aim of this project is to contribute to the development of advanced techniques to assess and predict silica bricks failure in service and the behaviour of this material when subjected to certain thermal cycles. Successful 3D modeling of a three-point bending test of a silica brick using finite element testing is to be achieved. The damage development in silica bricks when in service will be studied using various methods (Impulse excitation technique, X-Ray Diffraction, and three-point bending tests). These tests aim to evaluate the damaged developed by different thermal cycles, as well as the effect of silica's phase transformations in the brick's integrity.

1.4 Project Methodology

The project was mainly divided into 5 main activities: literature survey, finite element modeling, conduction of experiments and post processing of the results, analysis of the experimental results, and finally writing of the final report. The layout and time plan of this activities thought out the internship is presented in Table 1.1. Weekly meetings with the supervisor were carried out to update on the progress made, the results found and help in guiding the project and decision making. The development of the finite element model was done in an iterative and stepped way. First, more simple exercises of modeling were performed to quickly validate the reliability of the process. Depending on the outcome, a new approach would be taken, evolving the method each time. The experimental work was defined in the beginning, but was also adapted according to the results gathered. This dissertation was developed continuously throughout the internship, having the major work of writing and brainstorming performed in final weeks.

Project plan:

- Activity 1: Literature Survey
- Activity 2: Finite Element Modeling
- Activity 3: Conduction of the experiments and post processing of the results
- Activity 4: Analysis of the experimental results
- Activity 5: Writing of the final report

- Xx* - mid-term presentation

Table 1.1: Weakly project planing

	Weeks 01-03-2022 - 12-08-2022												
	1-2	3-4	5-6	7-8	9-10	11-12	13-14	15-16	17-18	19-20	21-22	23-24	25-26
Activity 1	xx	xx	xx	xx	xx	xx	xx	xx					
Activity 2			xx	xx	xx	xx	xx	xx	xx	xx	xx	xx	
Activity 3				xx	xx	xx	xx	xx	xx	xx	xx		
Activity 4				xx	xx			xx	xx		xx		
Activity 5						Xx*				xx	xx	xx	xx

1.5 Structure

The structure of this dissertation was done in a manner that would allow a simple understanding of all the subjects and problems engaged. Firstly, a bibliographic review is presented. This chapter starts with an introduction to silica and silica refractories, their behaviour, characteristics and properties. Following, fracture mechanics concepts are introduced, as its concepts for failure of materials and the crack formation will be explored. The last section in the bibliographic review is dedicated to the techniques used during the project. Some background information was required to fully understand them, therefore, a brief presentation of them was made.

The materials and methods are presented in the chapter that succeeds it. In this chapter, the methods are divided in two paths: the experimental and the finite element modelling (FEM) simulation. Both are used to study the same material but look to answer different questions, both related to the study of damage development and crack propagation.

The chapter that follows is "Results and discussion". The results and discussion were presented simultaneously since it enables a better understanding of the results and the conclusions taken from every experiment. First the results and discussion for the FEM simulations are presented. Following that, the experimental results are introduced and discussed, starting on impulse excitation technique (IET), then three-point bending and lastly X-Ray diffraction (XRD).

Finally, the conclusions drawn from this work are exposed, followed by considerations for future work.

In order to avoid a clustered dissertation, some results and details were placed in the Appendix chapter.

Chapter 2

Literature Review

2.1 Silica

From the latim, silex or silicis, meaning “hard rock”, silicon is a hard solid of dark grey colour that presents itself with a certain metallic shin and it is only available in a combined state. The most abundant chemical compound in our planet’s crust is the combination of silicon and oxygen, forming the compound known as silicon dioxide (SiO_2) (Figure 2.1) [1].

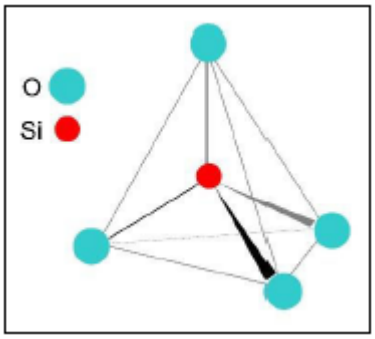

Figure 2.1: Chemical structure of SiO_2

The designation silica is commonly used as an abbreviation for silicon dioxide, either for its crystalline or amorphous state. Silica is found as various units of tetrahedral molecules of SiO_4, constituted of 1 atom of silicon surrounded by 4 atoms of oxygen, for a total charge of -4. But because this structure permits the formation of a three-dimensional crystalline network of molecules, when together, they have a medium stoichiometric formula of SiO_2. The reason behind the ability that the tetrahedral $(SiO_4)^{-4}$ has of connecting to other tetrahedral in various ways, comes down to the fact that the electrostatic

valence between $(SiO_4)^{-4}$ and oxygen is equal to 18. This value is exactly half of the connection strength of the oxygen ion. Because of it, $(SiO_4)^{-4}$ can connect trough an oxygen atom, making a bridge between both tetrahedral molecules and originating bigger structures [1].

The high thermal resistance and refractory property that silica is known for, could mostly be attributed to the interaction between the two unpaired electrons p in the 2py and 2pz orbitals of oxygen and the void in the orbital d of silicon. These interactions result in 2 different type of connections, that when together, elevate the energy of Si-O bonds [1].

2.1.1 Crystalline Silica

The most common types of crystalline silica are quartz, cristobalite and tridymite. Each one of them have a low temperature variant (denominated by α), and a high temperature one (denominated by γ and β). Besides these, another 2 types of crystalline silica could be formed synthetically, stishovite, and coesite (higher pressure) [1]. The p-T (pressure-temperature) diagram of silica in Figure 2.2 represents the conditions (regarding pressure and temperature) at which the phases of silica polymorphs remain stable and their transformations conditions [2].

Si-O-Si connection angles are not rigid, but have a considerable flexibility which permits the occurrence of thermal transformations and form different orientations of the 3D orbitals of silicon. This results in connections of type π for whatever the spatial location of the oxygen atoms. This is believed to be part of the reason why silica has so many types of tetrahedrals of SiO_4 [1].

Two types of transformations between phases can be distinguished: reconstructive transformations and displacive transformations. The phase transformations between the stable phases are reconstructive, requiring breaking and formation of new Si-O bonds [2]. Reconstructive transformations are sluggish and, if they occur at all, require the addition of materials which act as a solvent in order to occur in a reasonable time. Many times, crystalline phases are present outside of their balanced phase, remaining in this metastable state because they need a greater amount of energy to fully convert to a stable phase. This is rather common with tridymite and cristobalite [4].

On the other hand, the displacive transformations between the high and low-temperature forms of each basic structure occur rapidly, without structure reconstruction and cannot be restrained from taking place. Only due to mutual turn and rotation of the tetrahedral does the transformation occur [5]. As a consequence, very little amount of energy is required for it to occur, being also easily reversible.[1] This can also justify the very similar crystalline structure of this quartz polymorphs, as well as the high symmetry of the structure

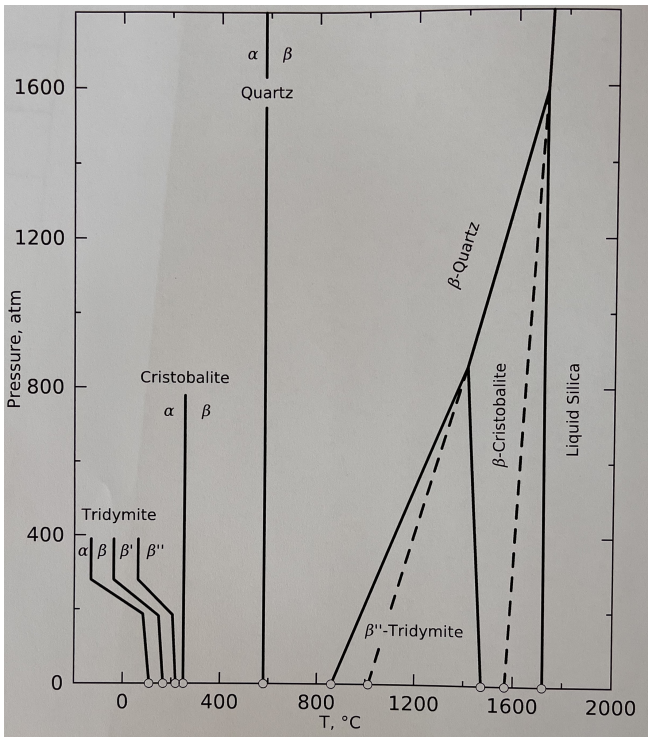

Figure 2.2: System SiO_2 (p-T diag.). Solid lines represent transitions of phases stable in the respective adjoining regions. Broken lines represent transitions of metastable phases. Tridymite and cristobalite in the regions of their alpha-beta transitions are each metastable with respect to alpha quartz, which is here the stable phase [3]

of the high-temperature forms of the polymorphs [5]. The high to low quartz transformation are known for very fast and substantial volume change. This can lead to the fracture and micro fractures of silica bricks and a consequent reduction in the strength. Table 2.1 summarises the transformations of silica polymorphs.

The stable form of quartz at room temperature is low quartz, which transforms into high quartz with a displacive transformation at 573°C. The same type of transformation occurs from quartz to tridymite at 870°C. This phase can only occur when certain impurities are present to act as mineralizers. Tridymite remains stable until 1470°C, when it transforms into cristobalite, another reconstructive transformation. Displacive transformations of cristobalite and tridymite happen on cooling from high temperatures. High cristobalite transforms by distorting its structure into low cristobalite at the temperature range of 200 to 270°C. High tridymite transforms into middle tridymite at 160°C. Finally, it transforms into low tridymite when it reaches 105°C [4].

Table 2.1: Modifications, volume and rate of changes in SiO_2 [6, 7]

Modifications changes $\leftrightarrow$ reversible $\rightarrow$ irreversible	Transformation temperature ºC	Volume change %	Type of transformation
$\alpha \leftrightarrow \gamma$-tridymite	105-163	0.5	Displacive
$\alpha \leftrightarrow \beta$-cristobalite	$\sim$260	2.0-2.8	Displacive
$\alpha \leftrightarrow \beta$-quartz	573	0.8-1.3	Displacive
α-quartz $\rightarrow$ α-tridymite	$\sim$870	14.4	Reconstructive
α-quartz $\rightarrow$ α-cristobalite	1250	17.4	Reconstructive
α-tridymite $\rightarrow$ α-cristobalite	1470	-	Reconstructive

2.1.2 Amorphous Silica

Amorphous silica is the result of the action of either natural or artificial conditions on silicon dioxide, forming generic solids without spatially organized long-range atoms . Also, not all types of amorphous silica show the same X ray diffraction, unlike crystalline silica. Diatomaceous earth and biogenic silicas are two types of amorphous silica that can be found naturally. Other forms, like vitreous silica or fused silica, are produced from some forms of crystalline silica. They first need to be heated up until 1723ºC and then rapidly cooled to be successfully produced. Other type, as precipitated silica or silica gel, are produced synthetically [1].

The principal type of amorphous silica refractories that is commercially available for the users is fused silica. In the low temperature region, this material is known to show smaller thermal expansion when compared to the crystalline silica refractories, which is related to its better thermal shock resistance. Although the interest in its application has grown, knowledge on the fracture behaviour of fused silica refractories has considerable development to be made. During the service life of this amorphous silica, the crystallization of cristobalite will gradually takes place. Further phase transformation can take place, causing critical effects on the thermo-mechanical performance of fused silica refractories [8].

It has been shown that the Young's modulus of fused silica at room temperature decreases after different heating/cooling cycles. This is due to the devitrification of amorphous fused silica to cristobalite, attributed to microcracking of the cristobalite caused by the phase transformation between the high-temperature cubic cristobalite and low-temperature tetragonal cristobalite. During cooling, in the temperature range of 200-250ºC, a volume contraction of about 2.8%–5% is observed. So, in a general manner, the strength of fused silica is dependent on cristobalite content [8]. Acoustic emission technology and fatigue test have been used to prove that the presence of initial microcracks in silica refractories reduces the brittleness and limits the severe damage of this material [9].

2.2 Production of Silica Bricks

Dense shaped silica products like silica bricks must have higher than 93% SiO_2, but generally varying between 95 and 98% [10, 6, 11]. Refractory silica is available in three grades: superduty, regular duty, and coke-oven quality. Silica bricks are the most used refractory material for coke ovens, superstructures of glass-melting tanks and hotblast furnaces. Unshaped silica mixes are used for monolithic structures and repairs [2, 12]. Their popularity is mostly due to their good thermo-mechanical properties, and high chemical resistance. They are able to withstand very high temperature for a prolonged period of time without heavy degradation of their properties.

In the past decades, coke ovens have become larger and the refractory layers thickness reduced. Due to these changes and the increased productivity that resulted from them, silica bricks production has also evolved during that time. Silica bricks properties are strongly related to their crystalline structure, the amount of residual quartz and the manufacturing process. Nowadays, the German standard DIN1089-1 is the international document that states the quality standard for silica coke oven bricks [6].

According to DIN 1089, two types of quartzites to produce silica bricks can be used: chemically solidified fine-crystalline cement quartzite and predominantly tectonically solidified and coarser crystalline rock quartzite. The criteria used to decide the mix of these two quartzites is the chemical composition, specially the contents of Al_2O_3, alkali's and their behaviour in the firing process.

Approximately 2.5 to 4% of $Ca(OH)_2$, some water and sulfite solution are added upon mixing of the crushed and washed quartzites that were previously sieved into defined grain size ranges. The CaO present acts as a bonding and mineralizer agent for the quartz transformation. This first step can greatly impact the strenght of the fired silica brick without noticeably reducing its refractoriness [6].

The process used for manufacturing silica bricks is summarized in figure 2.3. The prepared mix is shaped in a hydraulic press, resulting in "green" bricks with a high degree of homogeneity and size accuracy. For example, in a coke oven, where silica bricks are the chosen material for the application, there could be over 900 different silica bricks shapes and weights. This enforces a big flexibility in the manufacturing process of the factory, and for economic reasons, some very complicated or small pieces are manually moulded in compressed-air ramming technique. These special batches require skilled workers in order to achieve the same properties as the ones that are shaped mechanically. After shaping, the bricks must be handled with extreme care, as the non-dried green brick is mechanically weak and sensitive to stress [6].

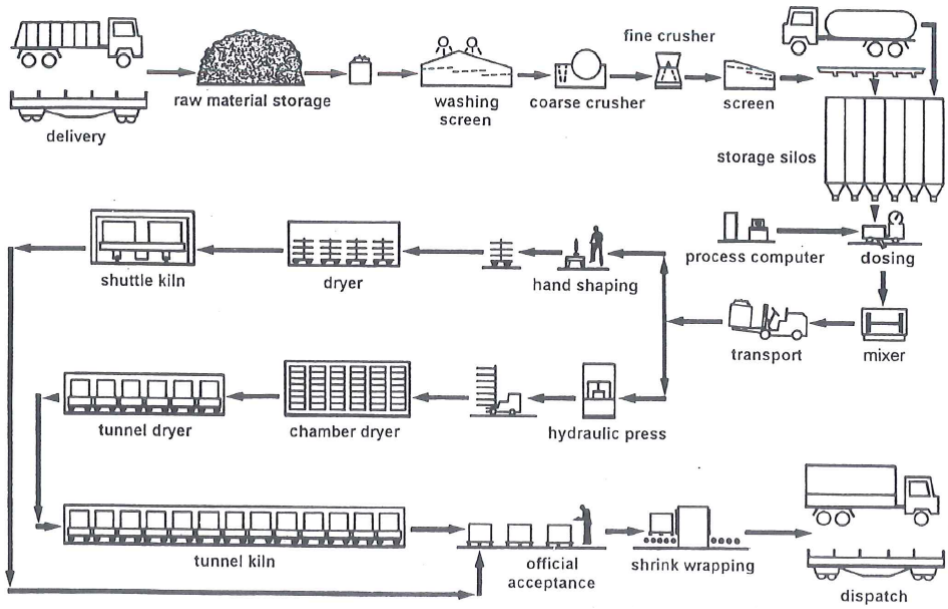

Figure 2.3: Process for manufacture of silica bricks [6]

2.2.1 Brick Firing

Due to the polymorphism and the phase changes related with SiO_2, brick firing is the most complicated process in silica bricks manufacture. Because of the high content of SiO_2, silica bricks undergo extreme volume changes (4 to 5%) during firing. If this process is not done very slowly and with due diligence, cracks can form in the bricks.

The silica transformations have already been discussed and are summarized in Table 2.1. When looking at a specific transformation, the type of quartzite, its amount and distribution will influence the rate of quartz transformation. Generally, fine-crystalline quartzites transform faster than the coarser uncemented quartzite. For the most usual firing parameters, tridymite acts as the stable phase, with a firing that is shape-dependent and takes 1 to 3 weeks at the temperature of 1420 to 1480^{o}C [6]. The process is very long because it involves various changes of crystal form that can disrupt the brick. Heating over 573°C must be slow to account for quartz transformation and cooling between 300°C and 100°C must also be very slow to avoid crack formation when the high temperature forms of tridymite and cristobalite transform to their room temperature modifications [10]. The transformation of cristobalite is much faster than that of tridymite, so cristobalite can be seen in freshly fired bricks. Promoting of tridymite formation should be done by increasing the duration of firing and adding mineralizers. As defined in DIN 1089-1, a well fired brick also needs to contain non-transformed β-quartz, or more commonly known as residual quartz.

Obtaining bricks within a narrow dimensional tolerances is hard, as the firing process and grow rate is also strongly related to grain size of the moulding mix. To guarantee an uniform transformation behaviour for different shapes, firing cycles and firing aggregates need to be well coordinated. A good temperature control and management that lead to a homogeneous temperature distribution over all the bricks are key. Checks of the finished and unfinished products are mandatory, silica bricks applications have high parameters and requirements to attend too [6].

2.2.2 Residual quartz and thermal expansion of silica phases

The thermal expansion of a silica brick can strongly vary depending on the percentages of the three SiO_2 modifications (cristobalite, tridymite and residual quartz) that are present. Silica bricks typical thermal expansion curve is represented in Figure 2.4.

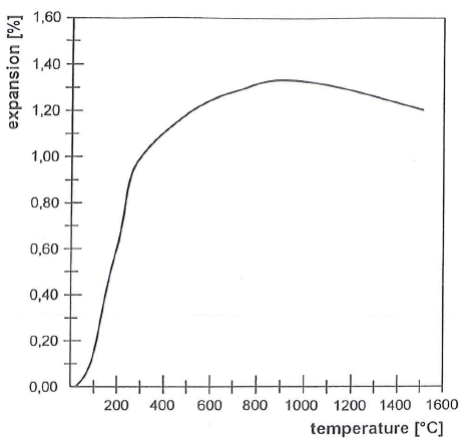

Figure 2.4: Thermal expansion of silica coke oven bricks [6].

During the initial heat up, there is a big expansion of the brick, reaching its peak between 800 and 1000°C, but towards the higher temperature there is a negative expansion behaviour, related to the lattice contraction of tridymite. This negative tridymite expansion can be compensated in practice by a certain amount of residual quartz, as it has a positive thermal expansion at those temperatures. On Figure 2.5 it can be seen the thermal expansion of each phase of silica from room temperature until 1000ºC. The behaviour of tridymite is evident, as well as the mismatch in the thermal expansion ratio of each phase throughout the temperature range.

For use in coke ovens for example, a coarse-crystalline with a mean residual quartz of 2 to 3% can mitigate this problem. However, the presence of residual quartz will cause an after-expansion event at temperatures above 1200°C. If the temperature is increased over 1200°C, this event will happen more intensively, leading to even higher expansion values. The type of quartzite used will also have an influence. If a cemented quarzite is to be used

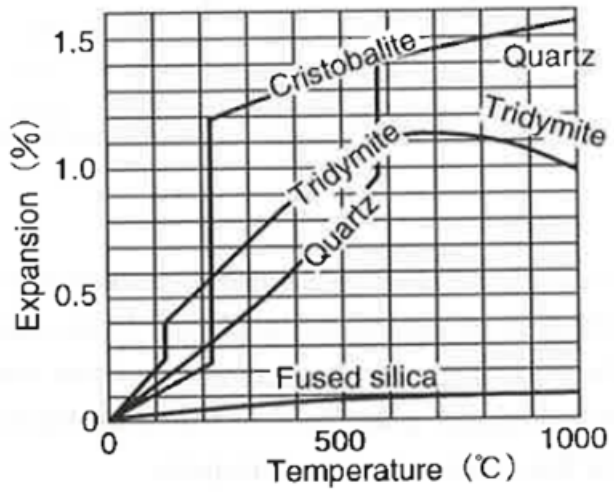

Figure 2.5: Thermal expansion of different silica phases [13].

instead of a uncemented one, for the same amount of residual quartz, the after expansion behaviour is much greater (Figure 2.6).

During the long periods of continuous working time that silica bricks are subjected to when used in coke ovens, there are variations in the structure and composition of the bricks. At the heating side of the coke ovens walls, due to migration of the constituents from this zone to the colder zone, occurs formation of secondary tridymite. This leads to a reduction in the thermal conductivity on bricks with a tridymite/cristobalite ratio of 1-1.2 [6].

2.3 Microstructure and failure of Silica Bricks

Refractory materials microstructure is rather different to the usual ceramic microstructure, mostly due to their manufacturing process. Shaped brick manufacture usually starts from the combination of different powder, commonly combining grains of different mineral types and sizes to form the final product. These powders have a broad particle size distribution which lets smaller particles to pack in the gaps between larger particles. When a coarse particle size distribution of powders is used, it is expected to achieve a complex microstructure of large, discrete aggregate (filler) refractory grain particles joined by a bonding matrix. The end result is a material with a microstructure often containing substantial amount of porosity, grains and a bonding matrix [14].

Refractory silica bricks have the same characteristic microstructure found in refractory material in general. Figure 2.7 represents a typical microstructure for a silica product. Large particle sizes of silica and porosity can be identified (grey and black, respectively).

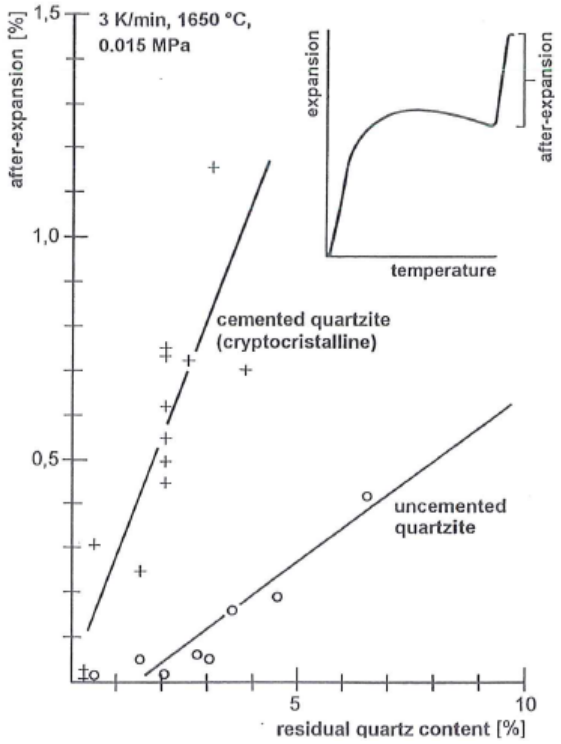

Figure 2.6: After-expansion behaviour of silica bricks for different amounts of residual quartz and different types of quartzite's [6].

At room temperature, there can be found few connections between grains, which explains the lower mechanical properties of the material at that temperature. Several cracks can be spotted in larger grains, which are due to stress induced by the phase transformation during the cooling in the fabrication process. Surrounding the grains there is also calcia present. CaO is mainly present in the matrix and it is not completely diffused in all of the material, due to the firing temperature being lower than the required for proper diffusion of CaO. When subjected to higher temperature for longer periods of time, modifications in the composition and microstructure will be seen [15].

The main source of damage and failure of silica refractories serving in high temperature industrial installations is thermo-mechanical cyclic loads. The degradation of the microstructure during cyclic loading develops as a gradual growth and coalescence of micro cracks [16]. The micro cracks start at pre-existing cavities or flaws in the matrix. These flaws can be introduced either trough the manufacturing process, exposure to aggressive environments or even surface preparation. These act as stress concentration points, that leads to crack propagation and consequent failure if no crack arrest mechanisms are present. [17] Silica refractories are known to have a quasi-brittle behaviour, which is explained by the crack arrest mechanisms that develop under crack propagation [16]. Their fracture exhibits notable deviations from pure linear elastic. This can be at-

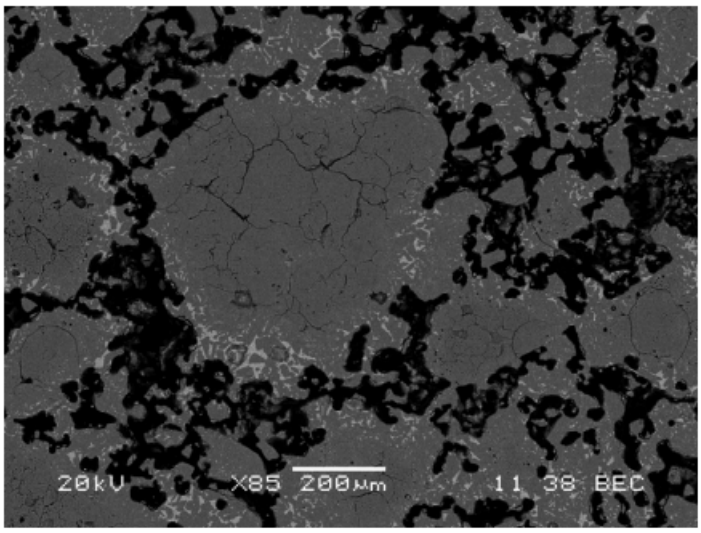

Figure 2.7: Microstructure of a silica refractory material, the matrix is seen in black and silica grains are in grey [15]

tributed to energy-consuming processes ahead (process zone) and behind (process wake) of the crack tip [18].

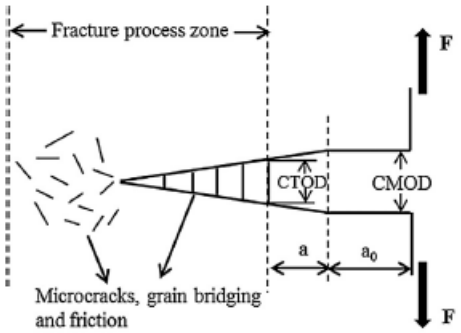

Figure 2.8: Schematic representation of the fracture process zone for refractories, CMOD - crack mouth opening displacement, CTOD - crack tip opening displacement [19]

Figure 2.8 represents the fracture process zone, where microcracking and multiple crack branching are usually observed. Grain bridging and friction of the crack faces are also present, being responsible for consuming energy in the process wake zone. As a result, the parameters that evaluate toughness of refractories are no longer material constants but they are also influenced by the crack extension [20].

The presence of porosity will act as stress intensity sinks during the development of a fracture, resisting the propagation of the cracks. This will lead to an increased fracture energy compared to that needed for crack initiation, as well as a decrease in toughness ratio. On the other hand, microstructure with lower porosity and well sintered composition

have a higher toughness ratio and a higher crack initiation energy needed [20].

For well sintered refractory with a well bonded matrix and grains, like the case of silica bricks, the crack path will tend to show a more straight path, transversing all the grains. This is due to the strength in the bond compared to the toughness of the bond between matrix and grains. On the other hand, for refractories with aggregates stronger than the matrix, the grains will be surrounded by cracks and the crack path will be extremely sinuous [20].

2.4 Fracture Mechanics

Fracture mechanics seeks to predict the behaviour of materials under critical loads. This leads to a need to develop criteria able to characterize the failure of materials. Criteria able to characterize a material was developed from observations and the study of its mechanisms of failure. It is a complex matter, as there are many variables that can influence the way a material will fail, from microstructure, size, weight, defects, temperature, loading rate and environment that they are exposed to.

Silica bricks are known to present different fracture behaviour depending on their composition. In general, silica bricks in a virgin state have high grain cohesion and lack of micro-cracks (compared to heat treated ones) which rates them as brittle. Although, depending on the structure of the brick (microcracks) and type of loading (cyclic loading), they can develop a less brittle fracture [16]. Acoustic emission technology and fatigue tests were used to prove that the presence of initial microcracks in silica refractories reduces the brittleness and limits the severe damage of this material [9]. Monotonic loading, as is the case with 3PB tests, is known to produce more brittle cracks than cyclic loading [16].

Liner elastic fracture mechanics (LEFM) is an accurate way to predict the crack behaviour of brittle materials. Altough a slightly approximation in some cases, LEFM can be used in conjunction with finite element methods to model the fracture of silica bricks in three point bending tests [21].

2.4.1 Stress intensity factor, *K*

The work developed by *Inglis* on material failure criteria, was continued by *Griffith*, who successfully proved the relation between defects in the materials and their fracture strength [22]. His research revolved around the study of brittle materials (glass), stating that for the crack to grow, the elastic energy present in a loaded body must be converted into surface energy of the crack. The source of the elastic energy is the stress applied to the specimen, being this the principle that led to Griffith's equation for fracture stress (based on *Inglis* elastic energy equation):

$$\sigma = \sqrt{\frac{2E\gamma_S}{\pi a}} \tag{2.1}$$

Where:
σ, is stress
E, is Young's modulus
γ_S, is bond energy
a, is crack length

Irwin took on Griffith's work, developing what is know of today as LEFM and the parameter K, stress-intensity factor. K is a function of the loading stress, the geometry itself and the length of the crack, and its knowledge can improve the understanding of the stress distribution around a crack tip in an elastically loaded body [23][24]. For the case of infinite plate with a central crack with a constant unidirectional tension load, a simplified equation for the stress intensity factor can be given by the following:

$$K = \sigma\sqrt{\pi a} \tag{2.2}$$

Where:
σ, is stress
K, is stress intensity factor
a, is crack length

The K_c value, also know as fracture toughness is the value of K at wich the fracture would take place. It can be related with the fracture energy (G_c) and the Young's modulus (E) by the equation 2.3.

$$K_C = \sqrt{EG_C} \tag{2.3}$$

Where:
K_C, is fracture toughness
E, is Young's modulus
G_C, is fracture energy

In a situation where load is applied to a cracked body, the displacement seen at the

surface can be divided into three modes. Mode I refers to case of tensile opening, where the crack opens in a direction perpendicular to the fracture plane, being loaded by tensile stress only. Mode II is also known as the sliding mode, in which the displacement of the fracture happens by an in-plane shear stress normal to the crack front. Mode III or tearing mode, is related to the lateral displacement of both fracture planes, when the torsional shear stress is parallel to the crack plane and the crack front. The fracture modes can take place in a singular or combined manner, being possible to have the three modes present at the same time, a problem that has high complexity [23].

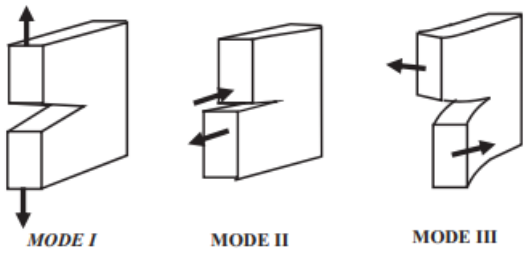

Figure 2.9: Surface fracture modes of a loaded cracked body [23]

For the case of a body subjected to only one loading mode, the stress intensity factor value of a material can be defined according to their type of loading. As mode I is the most common in practical cases (for example 3PB), the stress intensity factor for mode I loading (K_I) is widely used. K_I reflects the level of stress concentration at the crack tip for mode I loading. K_{IC} or fracture toughness for mode I, stands for the stress concentration under mode I loading required to start propagating a pre-existing crack.

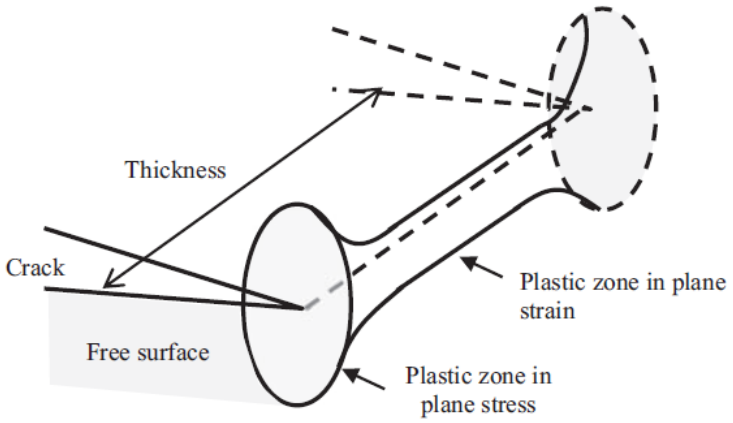

Figure 2.10: Variation of the plane strain, plane stress condition and plastic zone size throughout the thickness of a thick specimen [23]

The thickness of a specimen can influence the K_{IC} value and consequently the load bearing capacity of it in the same direction. For very thin samples and the free surfaces

of thicker ones, the component of stress normal to the free surfaces cannot exist, as it cannot bear loads in that direction. This is the description of what is know as plane stress, the main stresses are parallel to the plane and the force normal to it is constant. On the contrary, a thicker specimens may be constrained on the middle by the surrounding material, developing stress components in the thickness direction. This relates to the condition of a body where the displacements are parallel to the plane, and in the middle, they do not depend on the distance perpendicular to this plane, also known as plane strain. It should be noticed that the condition of plane strain does not apply to the entirety of the body, as it has been subtly mentioned in the previous sentences.

Figure 2.10 represents the plastic zones of both plane stress and plane strain and how the plastic zone varies along the thickness of a thick plate. First, it can be seen that the plastic zone of a plane stress condition is larger than in plane strain, and even for larger specimen, a condition of plane stress is still formed at the lateral surfaces. Altough, in the middle of the specimen, a plane strain condition is formed, and the plastic zone gets progressively smaller as it penetrates into the central part of the specimen and into zone where plane strain is valid.The large plastic zone area seen in plane stress condition helps to distribute the fracture energy over the superior area, leading to higher values of K_{IC}. Looking into Figure 2.11, as you increase the thickness of a specimen, the value of K_{IC} will decrease until the specimen reaches a critical dimension that will cause it to plateau.

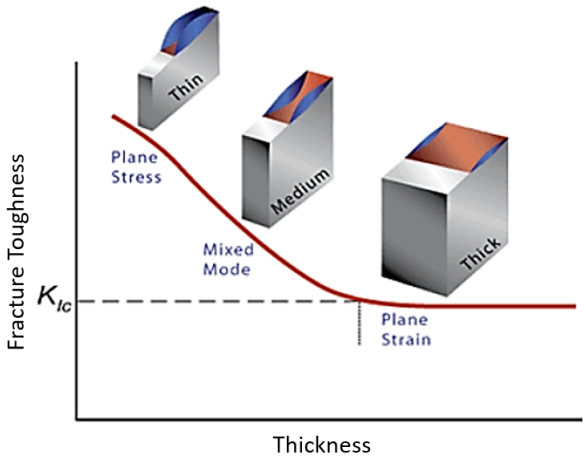

Figure 2.11: Evolution of K_{IC} with the increase in the specimen thickness, leading to more accurate plane-strain assumptions [25]

When K_I reaches a reasonably definitive value, it can be considered a reliable material property named plane-strain fracture toughness K_{IC}. K_{IC} of various materials are available in various sources and books, and the process used to measure it is defined in ASTM Standard E399 [25].

Considering an infinite plate with a stress crack in Mode I, the stress variation in the

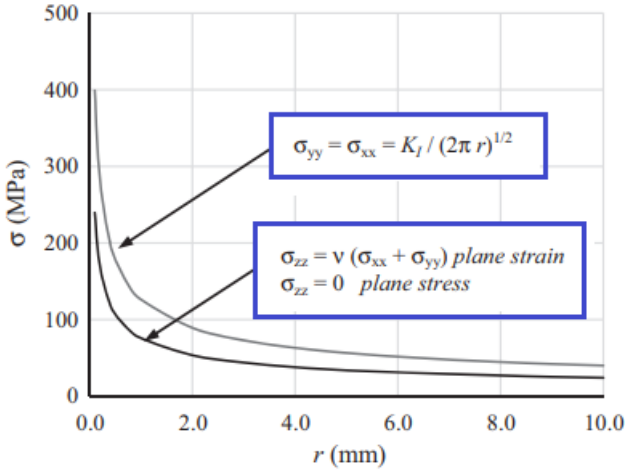

Figure 2.12: Variation of stress in fracture plane in front of crack tip for $\theta = 0$, adapted from [23]

crack plane is represented in figure 2.12. As it has been demonstrated before, around the crack tip there is a development of a plastic zone. By analysing the graph in Figure 2.12, near the crack tip the stress is very high, tending to infinite when a FEM analysis is performed (in practice this does not happen). It is this elevated stress near the crack tip that leads to a formation of a plastic zone around it. The stress levels surpass the yield strength of the material and lead to deformation and plasticity. The formation of a plastic zone does not occur in ceramics, as they have a very brittle failure. According to the graph, away from the crack tip the stress will tend to zero. In reality this is not the case, as the stress away from the crack tip will be equal to the applied stress to the body.

When the plastic zone near the crack tip is small and the load-displacement curve of the material is mostly linear, the stress intensity factor is representative of the stress around the crack-tip region and LEFM can be safely applied. On the other hand, if the material shows significant non-linear behaviour with a bigger plastic region around the crack-tip, K is no longer valid. A correction factor could be added to *Irwin* equation to account for this, but as the plastic zone becomes larger, it reaches a point where it deviates heavily from linear-elastic behaviour, making it not suitable anymore [23].

2.4.2 The energy criterion

The energy criterion is *Irwin's* energy based approach to the point of crack propagation based on a load-displacement behavior of a body under elastic strain behavior. It was based on this energy criterion that the value G, energy release rate, was defined. By definition, it is a measure of the potential energy available for an given increment of crack extension [24].

For a simple case of a wide plate in the plane stress condition and a crack length of 2a, the equation for G is given by

$$G = \frac{\pi\sigma^2 a}{E} \tag{2.4}$$

Where:
σ, is stress
G, is energy release rate
a, is crack length
E, is the Young's modulus

The P versus l curve (applied load vs displacement) of a elastically strained plate with a crack length of a can be used to derive the energy required for crack growth. The line OA represents the load-displacement behavior for a initial crack size a. The line OB stands for the load-displacement behaviour of the plate after a crack extension of δa. Two possible cases for crack extension can be observed in figure 2.13.

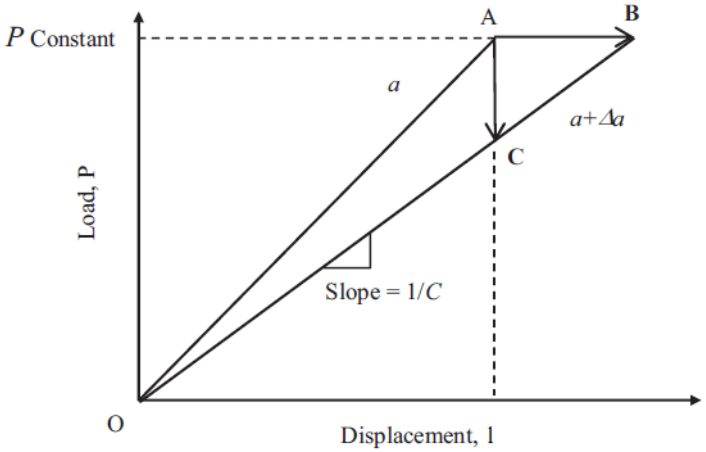

Figure 2.13: P vs l graph of a plate with a single crack loaded in Mode I, representing both the cases for constant load and constant displacement crack growth, adapted from [23]

Looking at the graph, a constant load is aplyed to the plate intil it reaches point A. If for a fixed load, the state of the plate moves from point A to B, there is a crack extension of δa. When unloading the plate and aplying the same load, the P-l curve will follow curve OB, the material is more compliant. If on the other hand, when loading the plate until point A, and the displacement is fixed, the crack will grow δa until point C. And the same would happen if the plate would be unloaded and loaded back again. P-l curve would follow line OC.

The area under the graph, either for the path of constant load or displacement, represents the work done for a crack extension of Δa. From this area, it is possible to determine

the energy release rate G recurring to equation 2.5. G will behave differently for a case of constant displacement or constant loading. In the first case, G will continuously decrease after crack initiation, slowing down the crack until arrest. For the second, G will keep on increasing as the crack extents, meaning more energy is available, and the crack will keep on accelerating its growth.

$$G = \frac{1}{t}\left(P\frac{dl}{da} - \frac{d(1/2)Pl}{da}\right) \tag{2.5}$$

Where:
l, is displacement
G, is energy release rate
a, is crack length
t, is the thickness
P, is the load

In equation 2.5, $1/2Pl$ refers to the area under the load displacement line, representing the stored energy U. The work required to extend a crack can be derived from U, and is designated by R. When the energy release rate reaches a value higher than the work required to propagate a crack ($G > R$), a crack will initiate. The R-curve is known as the graphical representation of the energy release rate. As shown in figure 2.14, a R-curve can be flat or rising depending on the material and its properties.

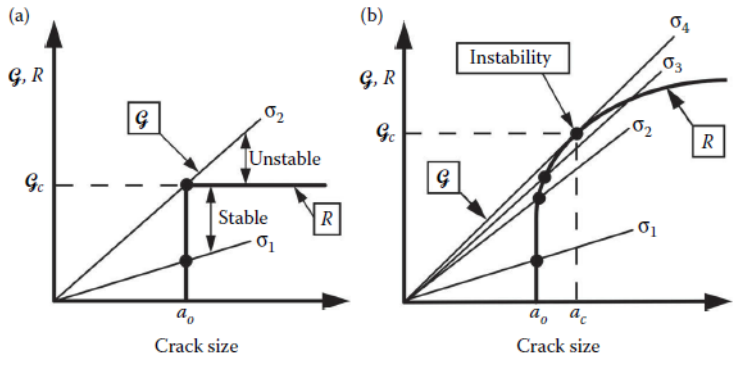

Figure 2.14: a) Flat R curve ; b) Rising R curve, [26]

A flat curve can be defined by one critical value of the energy release rate,G_c, meaning that G_c will be independent of the crack size. This is more typical for britle materials, as is the case with silica bricks. For a flat curve, when $G < R$, for example when an stress of σ_1 is applied, the crack will not propagate, being in a condition of *stability*. For the applied

stress of σ_2, when the crack reaches the length of a_0 and $G = R$, the crack will be self-accelerated due to the increasing available energy. This describes the case of instability.

For a material with a rising R curve, a single value of G is not enough to characterize it. In this case, a material will fail when the stress curve is tangent to the R curve (for the applied stress of σ_4). Materials with nonlinear fracture behaviour are known to have this type of curve.

2.4.3 J-integral

Professor James Robert Rice was the one responsible for the development of the method called the J-integral. It is based on a path-independent integral around a crack tip, that is capable of calculating the fracture energy of a cracked specimen with non-linear load-displacement behaviour [27]. Figure 2.15 represents a crack tip surrounded by an arbitrary path function used for the determination of the J-integral, showing the traction forces and their point of action.

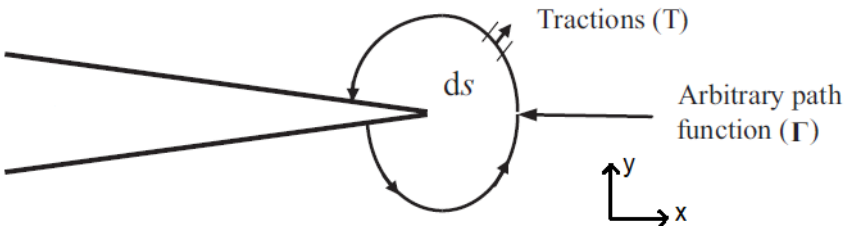

Figure 2.15: Representation of a closed path around a crack for the determination of J-integral, adapted from [23]

The J-integral can simply be defined as a energy balance around an arbitrary and independent closed path around a crack-tip. The work done by traction forces around the crack tip that act on the surface elements of a closed path around the crack is balanced by the deformation energy that is consumed by the crack tip region, inside the crack path. J-integral is said to be independent because it can be calculated close or far away from the crack tip. By calculating it in different positions makes it possible to determine the change of potential energy caused by the crack extension, arriving to more accurate values for the energy release rate. This method can be used for both linear or nonlinear stress-strain behavior materials.

The equation for J-integral for a cracked body is expressed in equation 2.6. T_i defines the traction forces acting in a differential element trough a closed, u_i represents the displacement, and W the deformation energy density.

$$J = \int_{\tau} (W dy - T_i \frac{du_i}{dx} ds) \tag{2.6}$$

$$W = \int_0^{\varepsilon} \sigma_{ij} d\varepsilon_{ij} \tag{2.7}$$

The deformation energy W is directly related to the stress tensor σ_{ij} and the strain tensor ε_{ij} by the equation 2.7. The tractions forces T_i are defined by the stress σ_{ij} normal to the closed path around the crack tip, as shown by equation 2.8.

$$T_i = \sigma_{ij} n_j \tag{2.8}$$

2.5 Three-point bending test

Various three-point bending tests (3PB) tests were performed during the development of this master thesis. The machine available for that purpose at the Ceramics Research Center is denominated of *Zwagnick*. It is composed of a conjunction of a high temperature furnace and a 3PB apparatus, enabling it to perform 3PB tests at high temperatures. The machine was built to perform until temperatures of 1600ºC and forces of 10 kN for multiple samples in sequence. It has a automatic feeding system that removes the sample after testing and replaces it with the next one in line for testing, for a max of 9 samples. As standard, these machines are equipped with a load and displacement sensor for measuring the force and deformation of the sample. The data from this sensors is collected and available at the software that controls the machine. The software shows itself as versatile, many variables can be changed and suited to the required test. Both force or displacement controlled tests can be performed, and the end of test criteria can be either governed by a percentage of maximum force or a maximum displacement. The heat up and cooldown rate, and dwell times are also parameters available to change on the machine.

As is known, 3PB will load the brick under tension, compression and shear. But majority of stress applied and the reason behind failure in the bottom middle of the brick is mode I fracture (tension) [28]. The test will provide the force-displacement graphs for each sample tested, allowing to compare the behaviour of samples that have undergone different thermal cycles. Figure 2.17 show an example of a force-displacement curve for a 3PB test representing both a brittle and ductile material, and what to expect from a test of this sort. Different size samples can be used, but the most common and the ones used in this work is 150x25x25 mm^3.

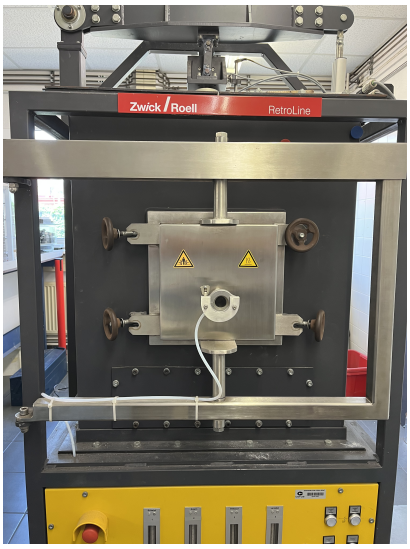

Figure 2.16: Hot Modulus of rupture machine available at the CRC

2.6 IET - Impulse Excitation Technique

Studies have found that there is a correlation between the mechanical resonant frequencies of a material and its elastic properties like E (Young's modulus), G (Shear modulus) and v (Poisson ratio) [30]. This relation is quite straightforward for samples that exhibit simple geometry (rectangular) and are isotropic. Although, this is not the case for objects with complex shapes and anisotropy, which require much more complex analysis to obtain satisfying results. The natural frequency and vibration emitted by the material is also affected by the internal frictions. For example, defects on the structure of a material can lead to a reduction of energy trough internal friction [31].

Inspired by this concept, various apparatus have been developed to measure the resonant frequency of materials. This machines are constructed to perform test under the *impulse excitation technique* (IET). This is a non-destructive technique that uses a small hammer to impact the specimen, which will make it vibrate and emit a frequency that will be picked up by a microphone. The machine used in this work (figure 2.18) was manufactured by the company *IMCE* and follows the same principles described earlier. This machine is capable of high temperatures (1600ºC) and also to perform test under inert atmosphere [31].

The location of impact of the hammer, and the type of support used for the specimen will influence the vibration modes of a specimen. The positioning represented in figure 2.19 is chosen for a few reasons, being one of then the minimization of friction losses in the contact points. This positioning is called flexural mode, and it is the most commonly used in this tests. The brick is supported in two nodes by alumina rods, and the place of impact is on the antinode (as represented in figure 2.19). The precision of the results

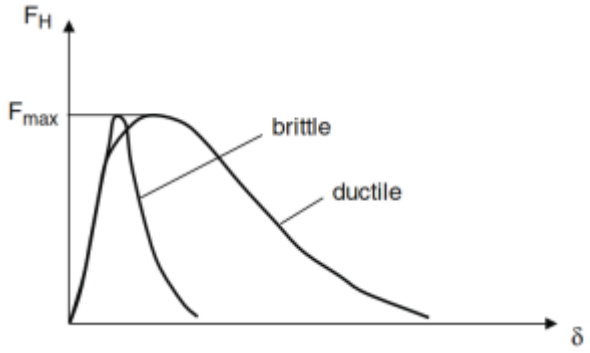

Figure 2.17: Schematic of a force-displacement curves for materials that have undergone 3PB test, adapted from [29]

for the values of natural frequencies (f_r), and consequently the values for the Young's modulus, is not greatly affected by small variations in the positioning of the specimen.

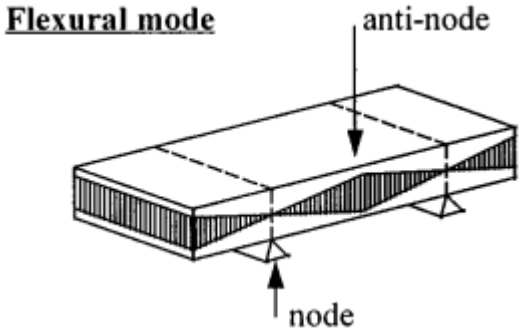

Figure 2.19: Schematic for a rectangular brick under flexural vibration mode, adapted from [31]

The furnace is lined with Al_2O_3 bricks and it is water cooled. Inside, a ceramic tube is positioned close to the specimen top surface in order to guide the acoustic wave out of the furnace to the microphone. Another ceramic tube is place on the bottom, from where the impacting hammer enters the furnace to excite the sample. Another cavity is used to allow an inert gas flow into the furnace in order to produce a non-oxidizing atmosphere when needed.

The excitation is done pneumatically, by firing a small ceramic cylinder with a semi-spherical tip at the bottom of the specimen. Each firing correspond to a measurement, and the signal will be picked-up by a non-contacting transducer (microphone). The signal captured is amplified by the damping analyser, and the program will determine the resonant frequencies (f_r) by a *Fourier* analysis. The frequency can be measured up to a level of accuracy of 0.0001 Hz. Previous studies have found that the repeatability of the f_r value can be determined in the order of 1 Hz. Such small variations will not significantly affect the results. For each test, the algorithm will optimize the parameters by iterations,

Figure 2.18: Impulse excitation technique machine available at the CRC, manufactured by *IMCE NV*

until it gives the final f_r value. Knowing the specimen shape values for the dimension mass and it's shape, the elastic modulus can be calculated from the value of f_r, using the equation 2.9.

$$E = 0.9465\left(\frac{m(f_r)^2}{b}\right)\left(\frac{L^3}{t^3}\right)T_1 \tag{2.9}$$

Lastly, the data recovered from the IET machine can be recovered and analysed. *Microsoft Excel* is the program of choice for the task, permitting the creation of graphs that show (example in figure 2.20) the evolution of the frequency or E in regards to time and temperature.

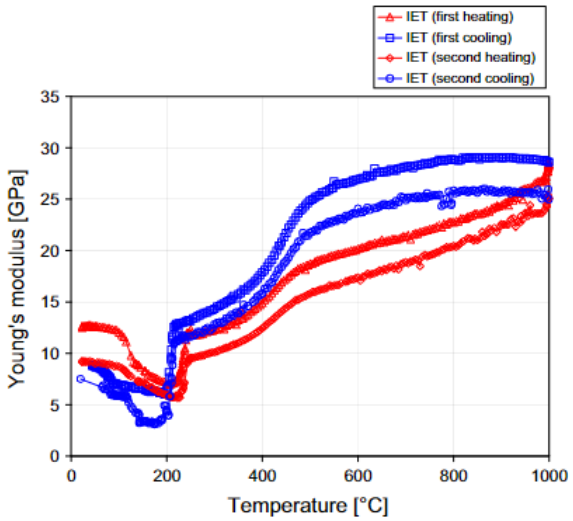

Figure 2.20: Example for a graph obtained from Impulse Excitation Technique testing, showing the variation of the Young Modulus with temperature [32]

2.7 X-Ray Diffraction

X-ray diffraction is a well-known non-destructive method that permits the identification of different crystalline phases of a material. It is best suited for materials with a crystalline or partially crystalline structure. The machine (Figure 2.21), in simple terms, is composed of a X-ray beam production device, a collimation, the sample support and a detection device. The collimation is in charge with producing a relatively thin beam of X-rays with a consistent wavelength and guiding then into the correct direction. The detection device has the job of detecting the scattered X-rays.

A crystal lattice can be defined as three-dimensional distribution of atoms in space. They are arranged in a way that they form a series of parallel planes separated from one another by a distance of d, varying accordingly to the material. For a crystal structure, planes exist in various different orientations, and each with its own specific d-spacing. Diffraction angles of θ will be produced by varying d-spacing in the polycristalline structure, according to Bragg's Law.

$$n\lambda = 2dsin\theta \tag{2.10}$$

Where:
λ, is wavelength
d, is spacing of the crystal layers

Figure 2.21: XRD machine available at the CRC

θ, is incident angle
n, is the integer

If the substance has a structure with a length scale similar to X-ray wavelength (λ = 0.1 to 100 nm), it will interfere with the beam, resulting in a pattern with different values of intensities. By plotting the angular positions and intensities of the resultant diffraction's peaks, the end result will be of a pattern characteristic of the sample. The resulting graph is denominated of diffractogram (Figure 2.22).

The identification of the material components is done trough the analysis of the x-ray diffraction pattern that the diffractogram presents. The pattern is compared to a large database of reference patterns to identify each one. In a diffractogram, the peak positions represent a phase, the height of the peak is equal to the phase concentration, a background bump is related to the amorphous content, and the crystallite size and strain are represented by the peak widths [33].

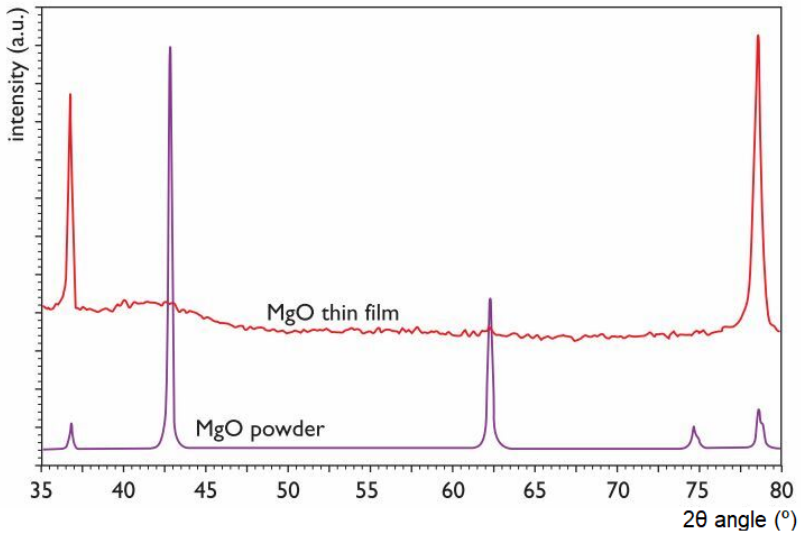

Figure 2.22: Diffractogram for a thin film of MgO and for MgO powder [33]

Chapter 3

Materials and Methods

The materials used for the experimental work were two variants of silica bricks already available at the Ceramics Research Center (*CRC*). The first material is a silica brick composed of crystalline silica (KOK), and the second one, a silica brick mainly composed of amorphous or fused silica (ZEB). From the crystalline brick, is known that it has been fired and pressed in one direction, being evident by the small cracks and pressing defects on the brick. The fused silica one has been slightly sintered after pressing to give rigidity to the brick so it can be handled. Due to that, some crystallization and phase transformation has happened, diminishing the percentage of silica glass in the brick. Table 3.1 has the properties for the crystalline silica sample at both 20ºC and 200ºC. Table 3.2 presents the mineralogical composition of both materials, were can be evidently seen the difference in the amorphous and crystalline content.

Table 3.1: Properties of crystalline silica bricks samples (KOK) [34]

Temperature ºC	Conductivity, W/m/K	Heat Capacity, J/(kg*K)	Density, kg/m3	Linear thermal expansion coefficient, K^1	Dynamic Young Modulus, GPa	Bending Strength MPa
20	1.5	800	1830	3.45E-5	10.0	9.5
200	1.6	1070	1830	3.45E-5	5.0	5.0

Table 3.2: Mineralogical composition of crystalline and fused silica bricks used, provided by CRC

Material	[%] Tridymite	[%] Cristobalite	[%] Quartz	[%] Amorphous	[%] Crystalline matter
Fused (ZEB)	0.6	21.0	0.3	70.9	21.9
Crystalline (KOK)	57.3	26.1	0.4	0.0	100

Different methods were used to achieve the end goal of this work. Finite element modeling was used to simulate three point bending tests. Mechanical tests like 3PB were responsible for the analysis of the force-displacement curves of specimens that have undergone different thermal cycles. Impulse excitation technique (IET) was also used to

study the changes in the Young's modulus of the specimen for different thermal cycles. After this tests, virgin samples also undergo X-Ray diffraction (XRD) to identify the phase proportions. Figure 3.1 show as scheme for the experimental tests and their procedures.

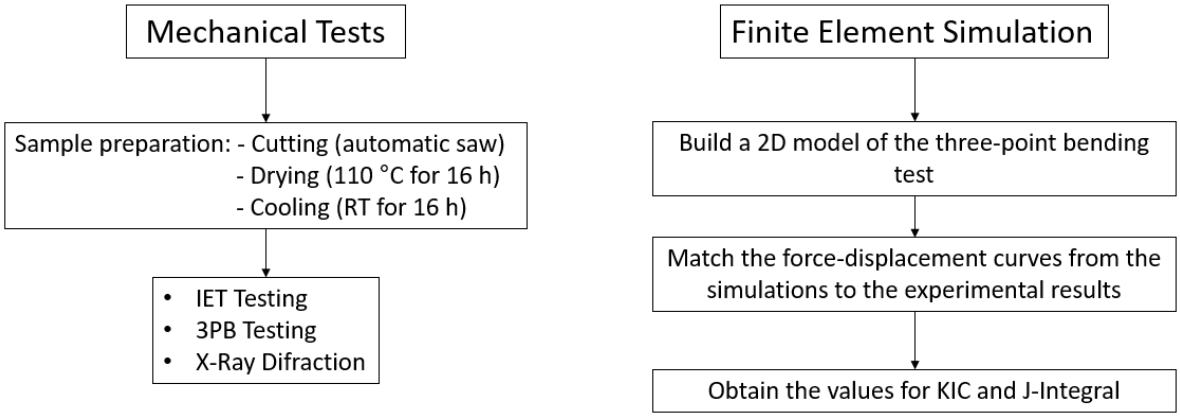

Figure 3.1: Schematic and summary for the experimental and FEM simulation procedure

3.1 Finite Element Modeling

The method used to investigate the viability of characterization of silica bricks using stress intensity factor and J-Integral is the Finite Element Method. The software used will be *Abaqus*, and different crack types will be studied: extended finite element method cracks (XFEM), and contour integral cracks.

The method of analysis started with first doing a preliminary 2D analysis of a 3PB test of a silica brick. The goal of this first analysis was to obtain the force-displacement graphs of the simulation to compare and match them with the experimental results that were supplied for this purpose. To do so, a model of a 3PB test was first developed using *XFEM* crack. Both 4-node bilinear quadrilateral plane stress and plane strain elements (CPS4) were used and the results analysed and compared. The bricks have 145 mm of length, and 25 mm of thickness and height. On this 2D model, a section with 25 mm of thickness was specified. Experimental results for plain bricks, with 4 mm notch and 11 mm notch, were supplied for comparison with simulation. A crack with 0.4 mm size was created and analytical rigid bodies were modeled as the top and bottom tools for the three-point bending test. A displacement of 0.4 mm was assigned to the top tool, having a constant rate of displacement throughout the simulation step time. Damage initiation and propagation criteria had also to be defined in the model (energy release rate = 60 J/m^2 and maximum principal stress = 10 MPa). The 2D model of all this three cases can be seen in figure 3.2.

Figure 3.2: 2D FEM model of three-point bending tests for a brick with no notch, with 4 mm notch, and 11 mm notch

After this first analysis, XFEM was abandoned, and contour integral cracks took its place. The parameters for this contour integral model stayed similar to the previous XFEM one. The only changes made being the mesh, crack length, the crack method and consequently the lack of crack growth.

Using this new model, the first analysis had the goal to arrive to a Young's modulus and crack length value that would be used across the different tests to obtain a consistent value for K_{IC} and *J-integral*. In this model, the same element (CPS4: four node, bilinear, plane stress/plane strain quadrilateral) was used, and a spider web type mesh around the crack tip was assigned, as seen in figure 3.3. Highlighted in green is the crack tip, in red the crack itself, and in yellow the outside of the spider web type mesh.

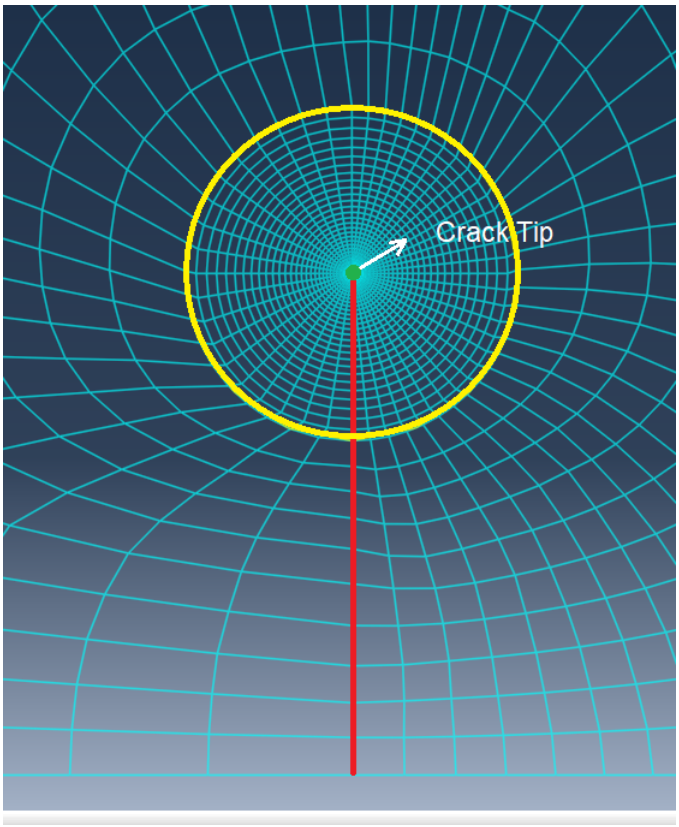

Figure 3.3: 2D FEM model mesh around the crack tip for contour integral crack

First, multiple simulations varying the crack length and Young's modulus was performed, matching the force-displacement curves from experimental results to simulations for every case presented on table 3.3. For each one, a value for E that would better match was obtained, and based on this information, a final value for E and crack length was used in the upcoming simulations.

Table 3.3: Conditions of each simulation ran, varying crack length and notch size

		Notch size		
		No notch	4 mm notch	11 mm notch
Crack length	0.5 mm	E	E	E
	1.5 mm	E	E	E
	4.5mm	E	E	E

Simulations were ran with different crack lengths and notches and, in each case, for both plane stress and plain strain. From each one, the curves for K_I and *J-integral* were obtained. Having the average values for the displacement of failure in each experimental case (no notch, 4mm notch and 11 mm notch), the K_{IC} and *J-integral* at failure could be extrapolated from the curves obtained. Table 3.4 shows all the simulations ran in this step, the conditions and variables retrieved.

Table 3.4: Simulations run in order to analyse the effects of plain stress and plane strain, different crack lenghts and notches

	0.5 mm crack		1.5 mm crack	
	Plane Stress	Plane Strain	Plane Stress	Plane Strain
No Notch	J-int & KI	J-int & KI	J-int & KI	J-int & KI
4 mm Notch	J-int & KI	J-int & KI	J-int & KI	J-int & KI
11 mm Notch	J-int & KI	J-int & KI	J-int & KI	J-int & KI

All these first simulations were performed and compared against values for experimental results that were done previously to this work date, and therefore supplied for this work's purpose.

3.2 Three-point bending

For three-point bending (3PB) testing, the machine used was already introduced in the previous chapter. Rectangular samples with the following dimensions were used in the measurements: 150 mm length, 25 mm height and 25 mm width. The test was performed for both crystalline and fused silica samples. The raw material was supplied in a much larger brick, so samples had to be cut from it. They were cut using a automatic circular saw-brillant 285 from ATM. The machine uses water to lubricate and cool the cutting process, so there is a need to dry the sample after. For that, they are put in a oven at 110ºC for 16 hours, and them are placed at room temperature for 16h in order to cooldown.

Table 3.5: Summary of the 3PB tests performed

		Thermal treatment				
		Virgin	Procedure A	Procedure B	Procedure C	Total
Testing temperature	RT	3	3	3	—-	—-
	1000ºC	3	3	3	3	—-
	1400ºC	3	3	3	3	—-
	Total	—-	—-	—-	—-	33

Table 3.5 displays a summary of the 3PB tests performed. Fristly, virgin samples (no heat treatment performed, just cut and dried) were tested in the machine at room temperature. Each condition of testing was done for three samples for more reliable results (for example in case of having an unorthodox result). Virgin samples were also tested at 1000ºC and 1400ºC, in both cases the samples were put inside the 3PB furnace, heated up at a rate of 6ºC/min. until the desired temperature, where they were left to dwell for 30 minutes so the whole brick arrives at the same temperature. After this, the test is performed until the sample breaks. At the end of test, the transportation mechanism of the

machine will be activated and move the sample forward to replace it with the next one in line for testing. When all the measurements are done, the furnace is turned off and cools down at its natural rate.

The machine possesses an interface that allows for various parameters of the 3PB test to be adjusted. The test was programmed under displacement control (force control also available). The top tool would approach the sample at a velocity of 1 mm/min. until the tool separation would measure 25.3 mm. From there on, the approach would slow down to 0.005 mm/s until a pre-load of 30 N was detected. Consequently, the tool would move until it reached the second level of pre-load, at 60 N, and come back to the 30 N. This is done as a tentative to settle the sample and prevent any deviations in the beginning of the curve.

After this, the actual test would begin, at a displacement of 0.001 mm/s. The failure criteria was also an important parameter to define. In order to identify failure, the program would actively seek for a drop in force greater than a certain percentage value. This parameter together with the displacement velocity were very important in preventing the brick from breaking completely at the end of the test. Too high of a percentage level of drop or displacement would lead to the brick breaking in half, complicating transportation. This problem was mainly a concern with crystalline silica bricks, since it as proven they have a more brittle fracture than fused silica. The percentage of the force drop used for crystalline silica was 30% and for fused silica 60%.

Figure 3.4: Positioning of a brick in testing position inside 3PB machine

On table 3.5, besides the virgin brick tests, there is three other type of testing conditions. These are bricks that have undergone different thermal treatment before testing. Procedure A refers to samples that have been heated up in an external furnace at 6ºC/min.

until 1000ºC, then left to dwell at this temperature for 24 hours, and cooled down at the same rate until room temperature. Procedure B follows the same dwell time and rate of heating and cooling down, but the temperature chosen is 1400ºC. After this, for the samples that undergo both this treatment, they are then tested under the same conditions as the virgin ones. However, procedure C is different, the whole test is done directly in the 3PB machine. The sample is put in the furnace and heated up at the same 6ºC/min. rate and left to dwell at the testing temperature for 24h dwell. After the dwell time, the test is performed at the same temperature. The objective of thermal cycling the samples before testing is to determine and compare the strength of samples that have undergone thermal cycling at 1000ºC, 1400ºC and samples that have not been cooled down, but dwelled for the same period.

3.3 Impulse Excitation Technique

To evaluate the brick's damage caused by the thermal cycles, impulse excitation technique was used to measure and calculate the Young's modulus (E) along different temperatures. Both crystalline silica and fused silica have been tested. The positioning of the brick in the testing position is seen in Figure 3.5. Different thermal cycles were applied to the bricks (Figure 3.6) in order to analyse E and damping through out it . The machine used, and the theory behind it has been introduced in the previous chapter. The machine uses samples with the size of 120x20x25 mm^3.

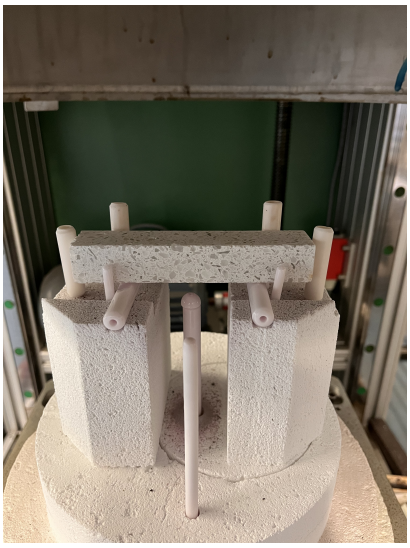

Figure 3.5: Positioning of a brick in testing position inside IET machine

The sample had to be measured and weighted before every test and the data inserted in the program to calculate the Young's modulus. Then, the desired heating cycle had to

be created in the program, the force of impact of the puncture adjusted, and the relevant range of frequency defined.

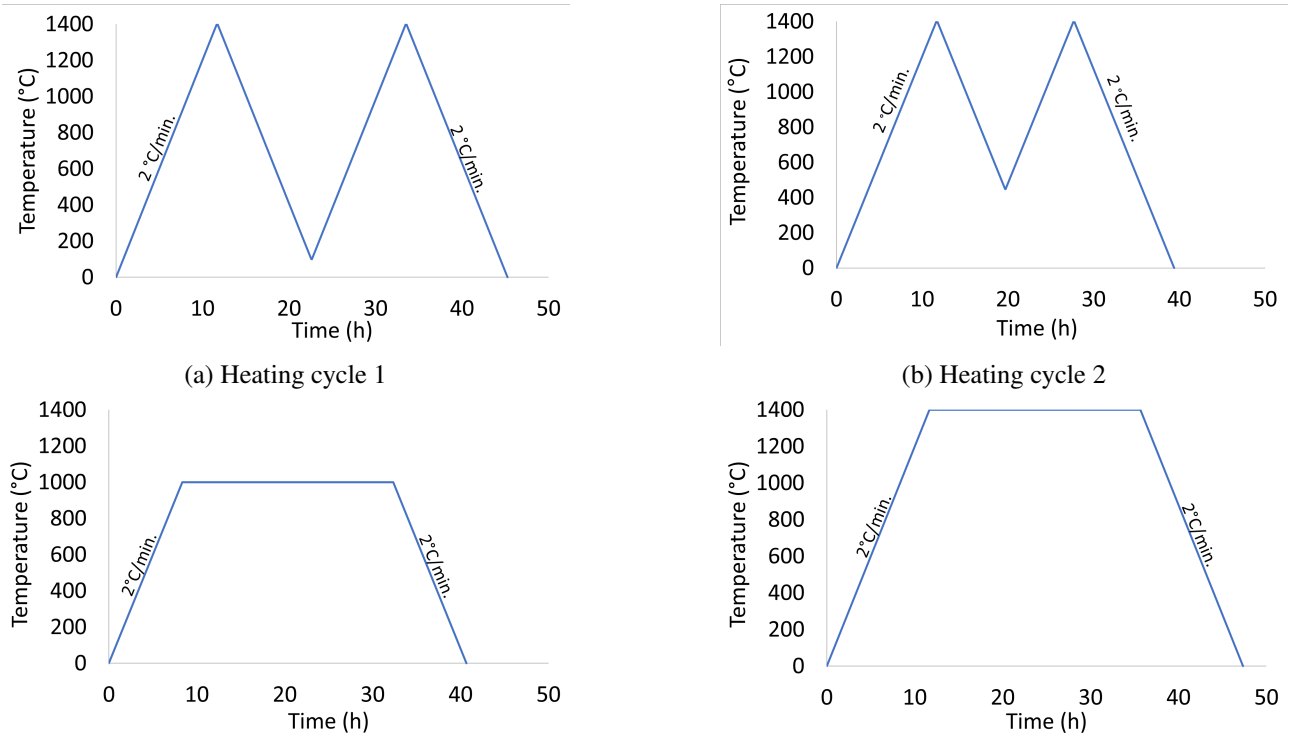

(a) Heating cycle 1

(b) Heating cycle 2

(c) Dwelling at 1000ºC

(d) Dwelling at 1400ºC

Figure 3.6: IET heating cycle's used during testing

3.4 X-ray Diffraction

To identify the temperature of phase transformation and evaluate the mineralogical composition of the brick during the thermal cycle, X-ray Diffraction (XRD) was used. To be analysed in XRD, the samples (originally in brick form) have to be ground in to a powder with a particle size ranging from 2 to 10 μm.

Both virgin samples and already thermal treated ones were tested. The second ones were used as a mean to look into the composition expected after a thermal cycle. Figure 3.8 is a representation of the thermal cycle used during XRD testing. Every 20 minutes a measurement was taken, accounting to 140 data points across the cycle. The data extracted from XRD comes as diffractogram (Figure 2.22). This data has then to be worked and plotted into a graph showing the percentage of each mineralogical component across the temperature range of the test.

The phases expected to see in XRD for these silica bricks are cristobalite, tridymite and quartz in their different crystalline structures. Components with low percentage of inclusion, like impurities, can not be distinguished in this test.

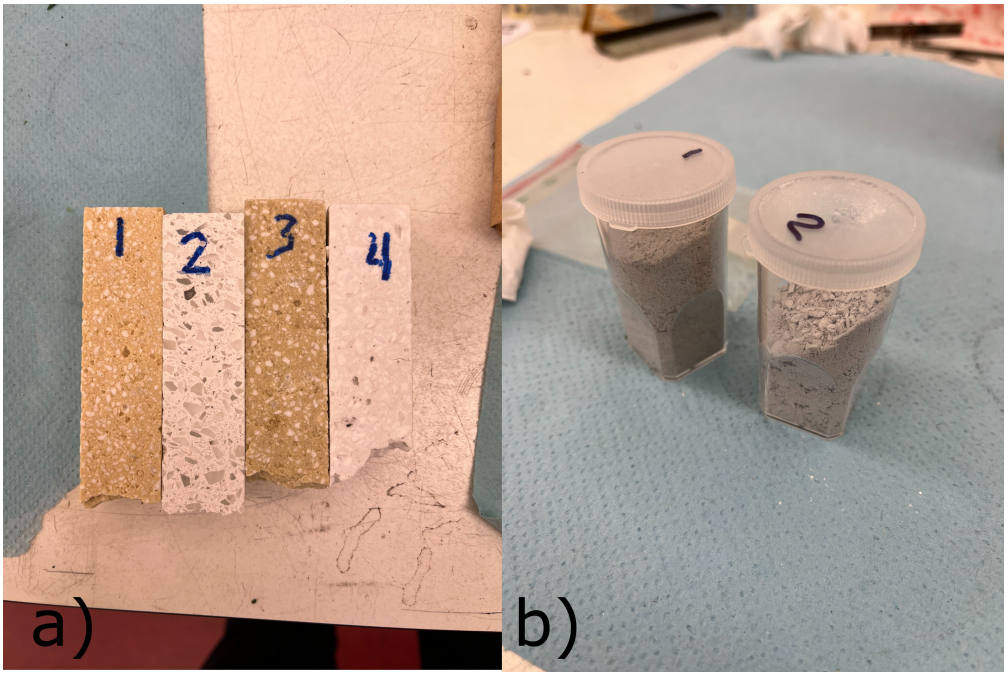

Figure 3.7: a) Brick samples after a piece was broken off then to be ground up, 1- Virgin crystalline silica, 2- Virgin fused silica, 3- Crystalline silica after thermal cycle, 4- Fused silica after thermal cycle; b) Powder from grounding up sample 1 and 2

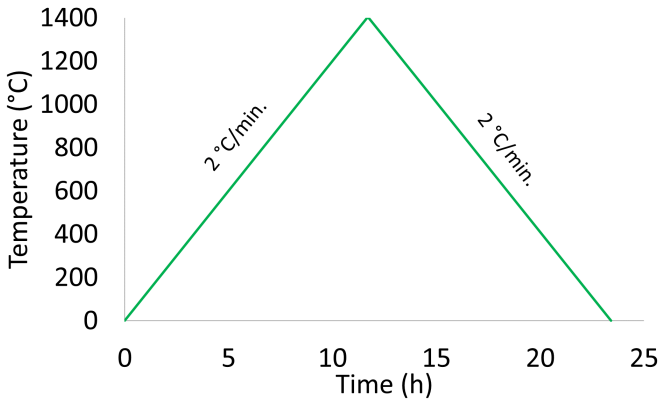

Figure 3.8: Thermal cycle used for testing in XRD machine

Chapter 4

Results and discussion

4.1 Finite Element Modeling Results

4.1.1 2D Modeling XFEM

Figure 4.1 and 4.3 present the force displacement comparison graphs for the 2D XFEM results and the equivalent 2D experimental results. This study started with a sample with 4 mm notch (Figure 4.1).

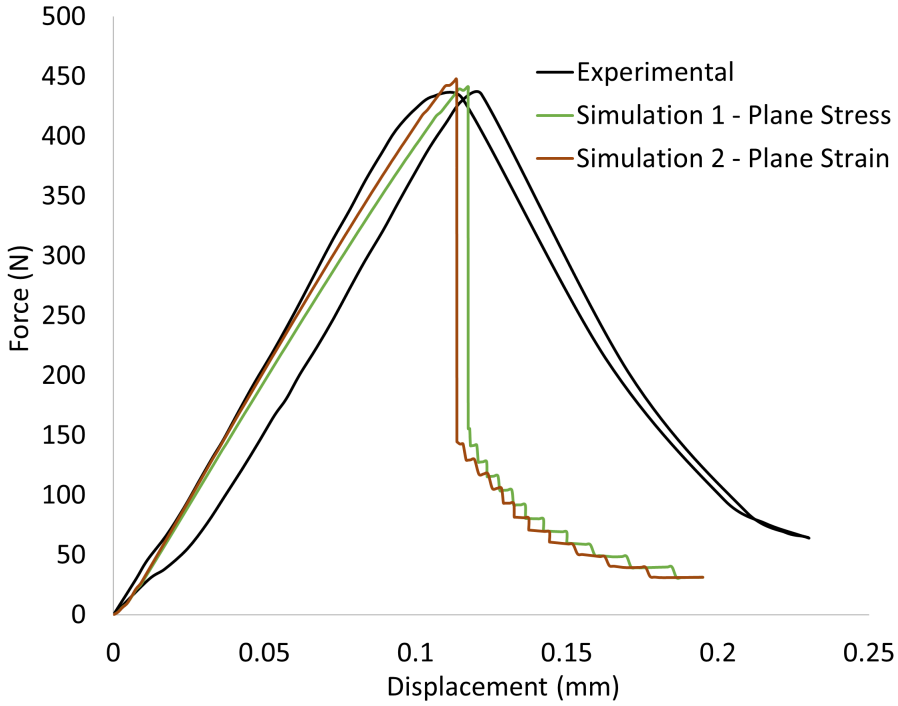

Figure 4.1: Comparison between 2D FEM simulation results and previous experimental results for a sample with a 4 mm notch

Various simulations were performed, adjusting material parameters, improving the mesh, fixing contact problems between the three-point bending supports and the brick, and assuring the correct implementation of the crack method in the model. Not every simulation will be covered in this work, as it is an iterative work and most of them did not withhold pertinent results.

When the modeling and fine tuning process was completed, the time for collecting concrete data and analysing different scenarios had arrived. As *ABAQUS* does not allow for the retrieval of K_{IC} and *J-Integral* values from 2D models with XFEM crack, the endpoint of this 2D simulation was to assess the ability of the model to match the force displacement curves correctly. The experimental results that have been provided for this work were obtained with a brick with 145 mm length, 25 mm width and 25 mm height. To model the thickness effect in the 2D model, it was specified that the FEM elements had a thickness of 25 mm, using plane stress elements first.

The results obtained, as seen in Figure 4.1, were satisfactory, matching the elastic behaviour, force and displacement of failure of the experimental results. Plane strain elements with 25 mm were also used, as seen in Figure 4.1, and comparing plane stress with plane strain, a very small difference was found between these two graphs. So, the choice was made to use plane stress elements for the rest of this XFEM simulation's.

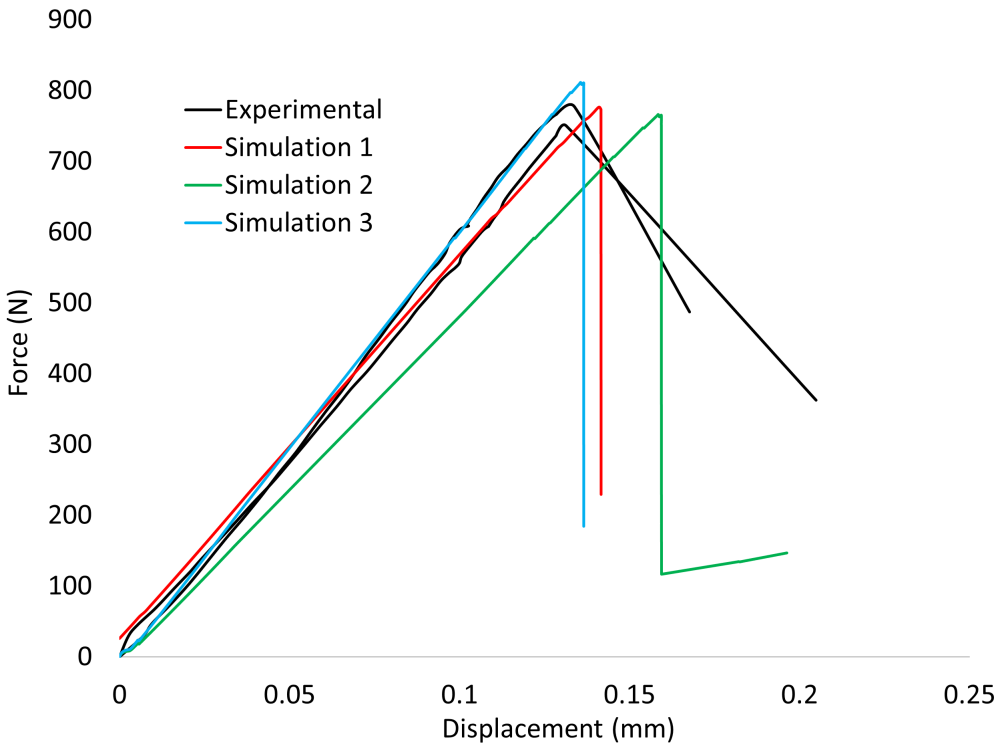

Figure 4.2: Comparison between 2D FEM simulation results and previous experimental results for a sample without a notch

For the sample with no notch, some fine tuning of the model had to be done. Improvements and refinement of the mesh around the contact points and the crack were crucial to reach a good result. The last three simulations done are represented in this graph (Figure 4.2), alongside the two experimental results that were gathered. On the first simulation, contact problems were spotted in the model, leading to an inaccurate result in the first millimeters of displacement of the top puncture. This was fixed by refining the mesh in this areas, which lead to the simulation 2 curve. This curve slope lead to values just under the experimental ones. In order to correct it, Young's modulus was increased from 8 to 10 GPa. Young's modulus being a material property should be consistent across all tests. This difference seen here already points out to some inconsistency in the material properties, something expected, consequence of the manufacturing process.

Lastly, a sample with 11 mm notch was modeled. The model was equal to the previous ones (8 GPa was used), only changing the geometry of the brick. Some contact issues could be observed in the first simulation, evident in the first part of the simulation 1 curve in figure 4.3. As it was the case with the simulation of the sample with no notch, this was due to a contact issue. This was fixed in simulation 2, where the slope matches the elastic part of the curve and peak force quiet accurately.

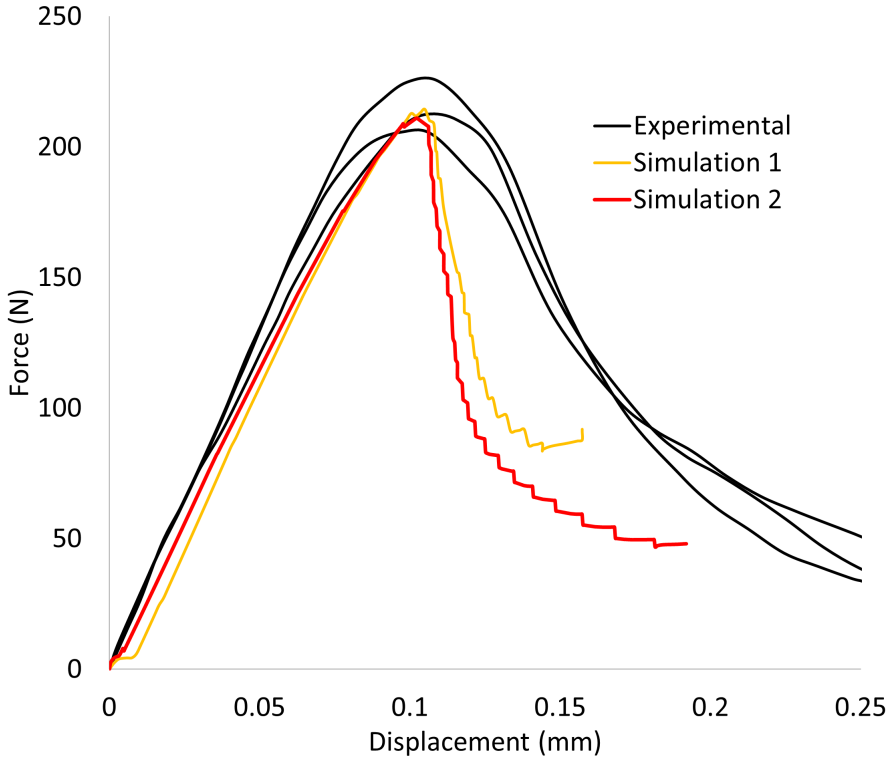

Figure 4.3: Comparison between 2D FEM simulation results and previous experimental results for a sample with a 11 mm notch

In all the cases, a successful modeling of the elastic behaviour and peak force was

achieved. However, the after peak behaviour showed some differences, specially for the 11 mm sample. All the experimental results showed a capability to carry a higher load after failure than the one predicted from FEM simulation. Also, for both samples with notch (more noticeable on the one with 11 mm), a strain softening behaviour can be observed. This is due to the processes that happens behind the crack tip, mainly grain bridging. On samples with crack growth, grains will dislodge from the matrix and wedge themselves in the crack, connecting the two surfaces behind the crack tip by interlocking themselves and allowing force to be transmitted through them. This effect was not object of modeling in this work.

With the force-displacement curves well matched, the next step in this work would be to obtain the values for K_{IC} and *J-integral* from these models. However, *Abaqus* 2D models containing XFEM crack was found to be unable to give these values. This makes it an unviable option for the objective of this work. At this time in the project, a 2D model with contour integral crack was developed to assess the usability of this type of crack for obtaining K_{IC} and *J-integral*.

4.1.2 2D Modeling Contour Integral

A 2D model with a contour integral crack was developed. It makes use of the same parameters as the previous model: the same type of element, similar mesh, same boundary conditions and material properties. The only parameters changed were the definition of the crack and the mesh around the crack tip. Both the previous XFEM model and contour integral model curves are simultaneously compared to the experimental results in Figure 4.4.

It can be seen that the contour integral model matches the experimental results as good as the XFEM crack model. The contour integral has the disadvantage of only being able to model the elastic part of the curve and neither the failure point or the strain softening behaviour that happens at failure for some samples (specially seen in the 11 mm notch samples). XFEM can approximate better to this strain softening behaviour at failure, but not fully. Contour integral models do not have crack growth, so the force displacement curve that the model shows, does not give the point of failure. In Figure 4.4, the curve for contour integral was cut off at the average displacement of failure of the experimental samples to illustrate that, if the right displacement is taken from experimental work, a failure point for the model can be identified, as well as all the parameters in that place in time.

An analysis of the experimental results using contour integral crack on the results for bricks with different notches, as well as varying crack length's (0.5mm, 1.5 mm and 4.5 mm) was performed. The goal is to find the best initial crack length and best value of E that would define the material and the model. Before this, the average displacement of

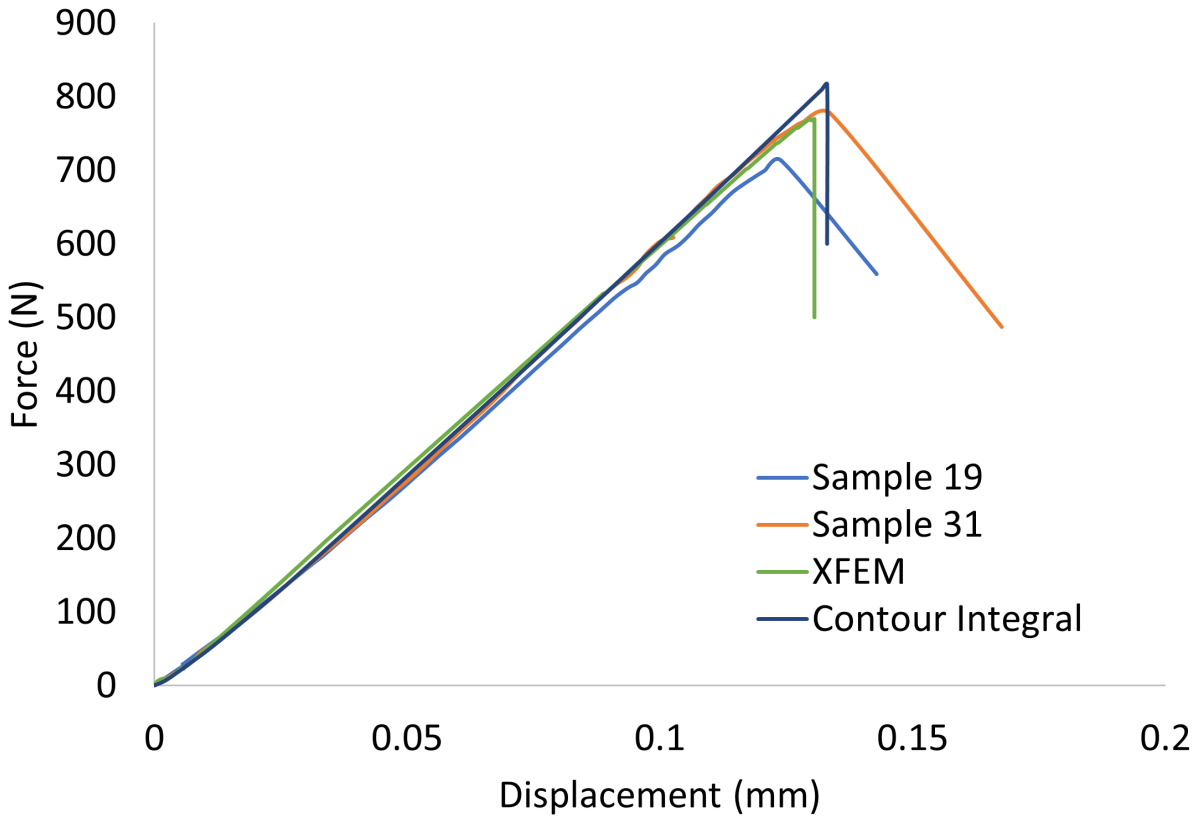

Figure 4.4: Comparison between force-displacement curve of a 2D model for XFEM and Contour Integral for the no notch sample (on the contour integral simulation, the curve was cut at the average displacement of failure of the experimental results)

failure for each case was determined, as well as the average force at the same displacement (Table 4.1).

Table 4.1: Average displacement of failure for each type of brick and equivalent average force at the same displacement

	Average Displacement (mm)	Average Force (N)
No notch	0.133	765.35
4 mm notch	0.114	433.10
11 mm notch	0.107	214.17

Figure 4.5 has the three comparison graphs between experimental and simulation results with different crack lengths for no notch samples. For every case, a different Young's modulus value was achieved.

Figure 4.6 shows the force-displacement curves for experimental and simulation results for every crack length. The experimental curves have a similar slope, although, the one identified in orange, shows a different behaviour in the initial part of the curve (accommodation of the sample in the beginning of the 3PB test moved the curve positively

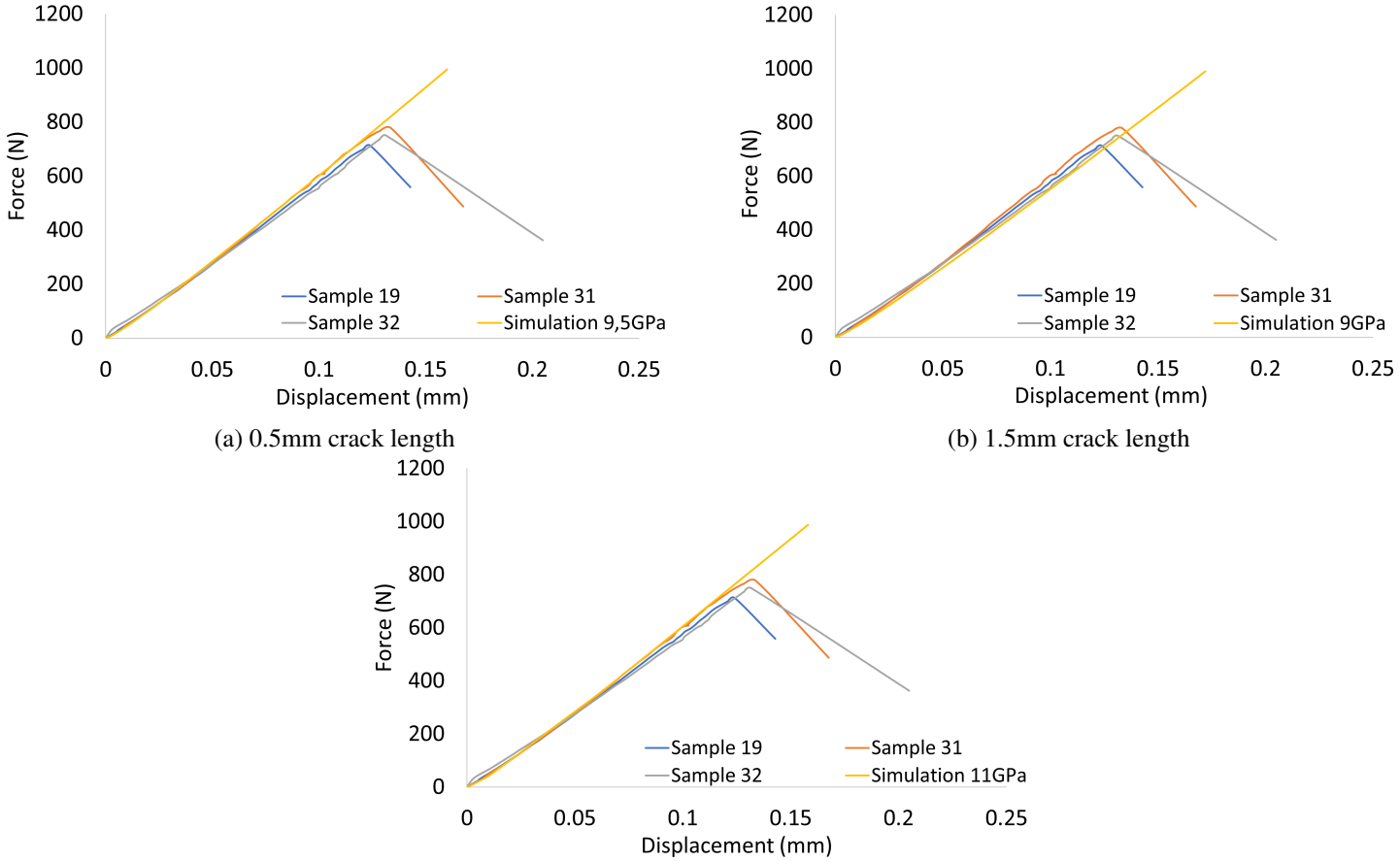

(a) 0.5mm crack length

(b) 1.5mm crack length

(c) 4.5mm crack length

Figure 4.5: Comparative force-displacement graphs of the samples without notch and corresponding simulation results for different crack length

along the x-axis). For this, the curve was closely matched to the experimental result for the curve in blue, as it proves to be a better representation of the behavior of the brick in this conditions.

Figure 4.7 shows the result of the same comparison work done for the 11 mm notch brick. The elastic part of the brick is well matched, but for this case, the silica brick developed a strain softening behaviour at failure that leads to big mismatch between the simulation curve and the experimental one near failure.

In table 4.2 a quick analysis and comparison of the best E that matches the experimental work could be made. For the model's with 4,5 mm crack, was harder to obtain consistent values for E, which makes using a crack of such size not viable. Both 0.5mm crack and 1.5 mm crack show lower deviation between values, being 1.5 mm the lowest. It should also be noted that silica bricks in general have a particle size of approximately 1.18 mm [35]. This material will more likely have defects of similar size, another point in favor using 1.5mm crack to define the model of the brick.

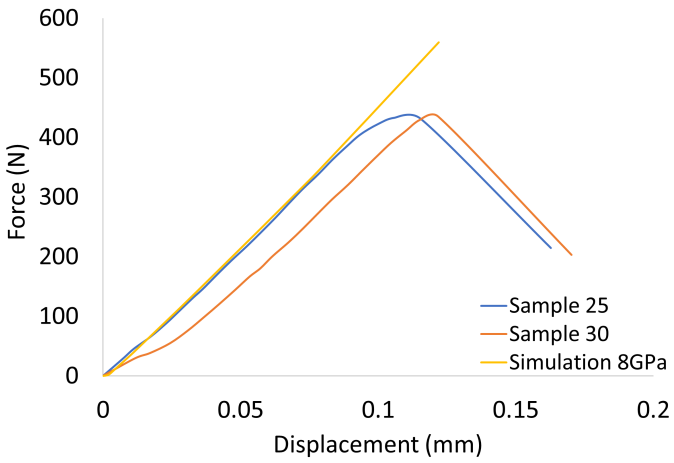

(a) 0.5mm crack length

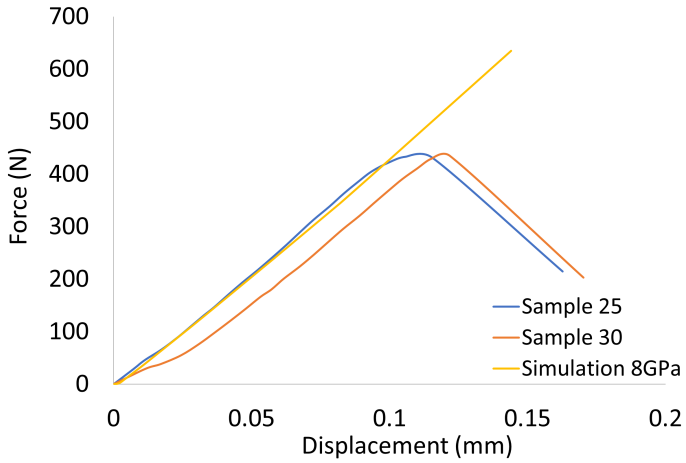

(b) 1.5mm crack length

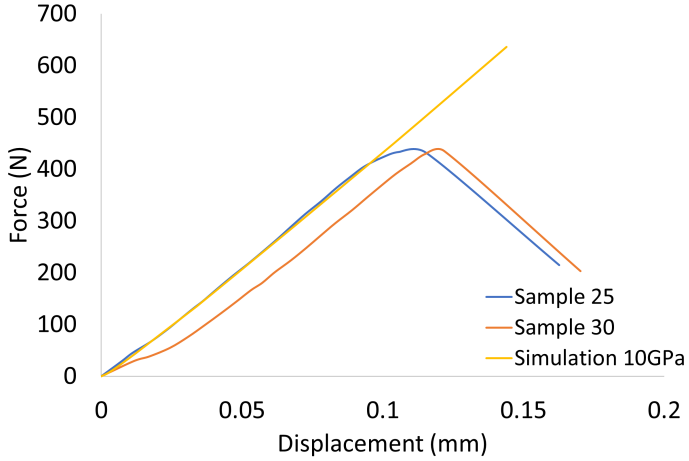

(c) 4.5mm crack length

Figure 4.6: Comparative force-displacement graphs of the samples with 4 mm notch and corresponding simulation results for different crack length

Table 4.2: Comparison table for the values of E from the that better match force-displacement curves

	No notch	4 mm notch	11 mm nocth	Average E	Standard deviation
0.5 mm crack	9.5 GPa	8 GPa	8 GPa	**8.5 GPa**	0.87
1.5 mm crack	9 GPa	8 GPa	9 GPa	**8.7 GPa**	0.58
4.5 mm crack	11 GPa	10 GPa	13.5 GPa	11.5 GPa	1.80

With the information aquired on table 4.2, the decision to persuit and study a model with 1.5 mm and 0.5 mm was made. For this models, the values for K_{IC} (K_I at the average displacement of failure) and energy release rate were retrieved (*J-integral* of a monotonic loading situation leads to the energy release rate value, also retrieved at the avarege displacement of failure).

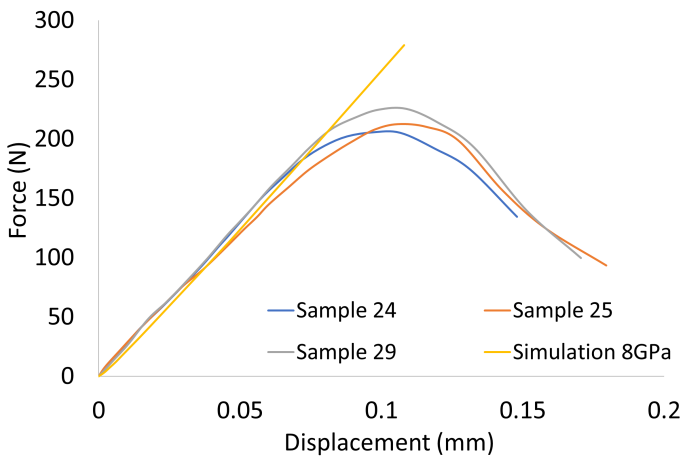

(a) 0.5mm crack length

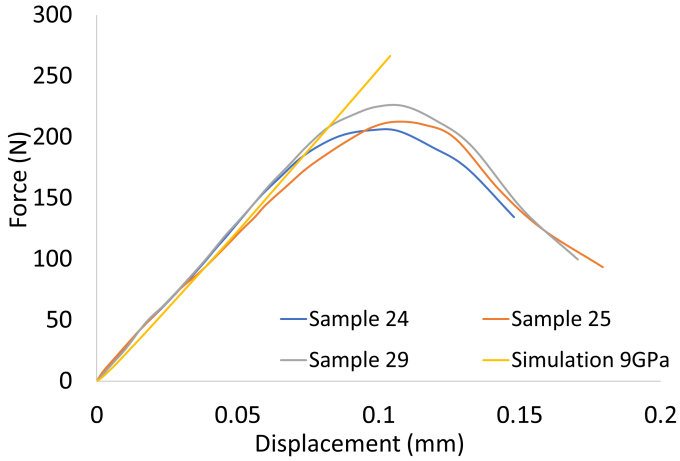

(b) 1.5mm crack length

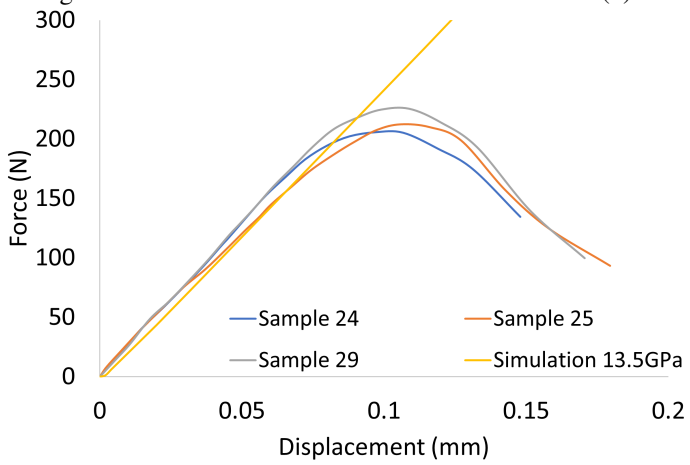

(c) 4.5mm crack length

Figure 4.7: Comparative force-displacement graphs of the samples with 11 mm notch and corresponding simulation results for different crack length

Table 4.3: K_{IC} and *J-integral* values for the model using 0.5 mm crack, in case of plane stress and plane strain

	Plane Stress		Plane Strain	
	K_{IC} $[MPa/\sqrt{m}]$	J-integral [N/m]	K_{IC} $[MPa/\sqrt{m}]$	J-integral [N/m]
No Notch	0.31702	12.94	0.31702	13.64
4 mm Notch	0.65944	54.85	0.69013	54.81
11 mm Notch	0.71802	62.02	0.75390	65.41

Table 4.3 has the values for K_{IC} and *J-integral* for the model with 0.5 mm crack for both plane stress and plain strain. Both of these are material properties, so the expected result was to see similar values across the samples of no notch, 4 mm and 11 mm, since all the samples are made of the same material. A small variation is expected because of the inconsistency of these properties, although the obtained results show values very far apart. For the sample with no notch, both K_{IC} and *J-integral* show the lowest value in all

test, both for plane strain and plane stress. When looking at the values K_{IC} and *J-integral* for 4 mm and 11 mm notch they are rather close to each other. A notch in the sample will lead to a more consistent stress concentration in the area under study, as well as a more predictable stress direction, which in consequence leads to a straighter and more predictable crack path and point of failure.

Table 4.4: K_{IC} and *J-integral* values for the model using 1.5 mm crack, in case of plane stress and plane strain

	Plane Stress		Plane Strain	
	K_{IC} $[MPa/\sqrt{m}]$	J-integral [N/m]	K_{IC} $[MPa/\sqrt{m}]$	J-integral [N/m]
No Notch	0.54887	34.80	0.57650	36.80
4 mm Notch &	0.73693	62.70	0.77093	65.81
(% over no notch)	+34.3%	+80.2%	+33.7%	+78.8%
11 mm Notch &	0.73199	64.46	0.76814	67.90
(% over no notch)	+33.3%	+85.2%	+33.2%	+84.5%

The values for K_{IC} and *J-integral* for the model with 1.5mm crack are displayed in Table 4.4, as well as the percentage difference between each test. Both the 4 mm and 11 mm samples show an almost identical value for K_{IC} and very close value for *J-integral*, either for plane stress or plane strain. Altought, this value is higher (by 34%) when compared to the one for a sample with no notch. This difference can be explained when looking at the difference seen in the force values between the experimental and simulation results at the displacement of failure.

Looking at Table 4.5, the sample without notch matches the peak force at the chosen displacement of failure very accurately. This can also be seen in Figure 4.5, the behavior of the brick is rather brittle, and the curve matches the entirety of the elastic part until failure very accurately. When analysing the difference in force seen between the experimental results and simulation ones for the 11 mm and 4 mm notch samples, a difference was to be expected due to their strain softening behaviour at failure.

By looking at both Figure 4.6 and 4.7, the difference in force at the displacement of failure can be easily spotted. Taking this information into account, and going to the analysis of K_{IC}, the percentage difference in force and K_{IC} between the sample without notch and the 4 mm and 11 mm is rather similar. This was to be expected, as K_{IC}, like the force on a purely elastic situation, will also increase linearly with displacement. In the case of being able to model the strain softening behaviour seen in samples of 4 mm and 11 mm notch near failure, it is predicted that they would have the same K_{IC}, or very similar one, in all three cases.

Table 4.5: Analysis of the force and displacement at failure for the experimental results compared to the simulation ones

	No notch		4 mm notch		11 mm notch	
	Plane Stress	Plane Strain	Plane Stress	Plane Strain	Plane Stress	Plane Strain
Experimental	0.133 mm 765.35 N		0.114 mm 433.10 N		0.107 mm 214.17 N	
0.5 mm crack 8.5 GPa	748.73 N -2.2 %	782.56 N +2.2%	557.83 N +28.8%	582.83 N +34.5	294.61 N +32.2%	307.54 N +43.2%
1.5 mm crack 8.667 GPa	752.66 N -1.7%	771.46 N +0.8%	538.16 N +25%	562.16 N +29.8%	265.73 N +24%	276.76 N +29%

J-integral on the other hand has a much larger percentage difference between the different samples. On the contrary of K_{IC}, *J-integral* increases in a non-linear and exponential way with increasing displacement. This makes it so the mismatch in the force-displacement graph will lead to higher difference for the energy release rate than the K_{IC} value. Besides the increased difference, *J-integral* has very similar values between the samples with 4 mm and 11 mm notch, helping to sustain the explanation and theory here given.

Besides the simulation for no notch with 0.5 mm crack, all others show an increase in force for K_{IC} and *J-integral* when switching from plane stress to plane strain elements. The lack of a significant difference between plane stress and plane strain simulations when using 0.5mm crack, only brings to light the inaccuracy of this crack size simulation. Also, a common trend in all other simulations is that plane strain lead to higher values of force, K_{IC} and *J-integral*.

4.2 Experimental Work Results

4.2.1 IET

Figure 4.8 plots the Young's modulus (E) values as a function of temperature for a sample of fused silica subjected to the thermal cycle 1 (Figure 3.6). Along the two heating and cooling cycles, the sample has many variations of E across the temperature. To better explain the events happening, the curve will be discussed in detail analysing its eighteen main point's of change.

I-II: In the beginning of the heating cycle, E will steadily and slowly increase.

II-III: When the sample reaches a temperature just below 200ºC, there is a abrupt increase of E. The phase transformation of low to high cristobalite happens at this temperature, explaining the sudden increase at this point.

III-IV: It can be said that the phase transformation from low to high cristobalite has finished at just above 200ºC, given away by the change in the curve slope. From point

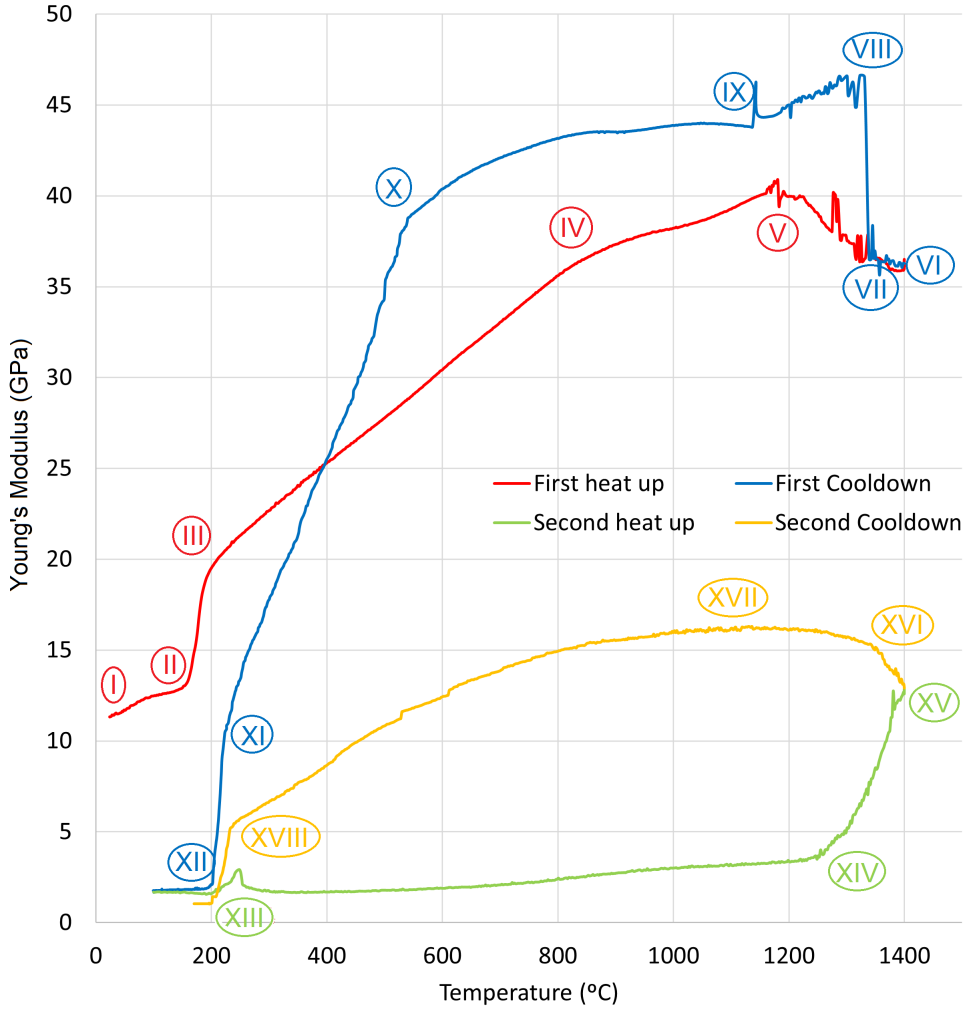

Figure 4.8: Temperature dependence of Young's Modulus in a sample of a fused silica brick subjected to thermal cycling and analysed on IET machine

III to IV, E increases linearly with temperature. This is once again seen because of the behaviour of fused silica, and its high contents of quartz at this phase. It has a very low thermal expansion rate with a consistent value throughout all the temperature range, and this behaviour is reflected on the E [6].

IV-V: At point IV, it can be seen a slight change in the curve's slope. The variation is rather small. This could be both related to the slow transformation of amorphous quartz into tridymite together with the mismatch in thermal expansion ratio of the different phases of the brick that is seen at this temperature. Tridymite thermal expansion rate drops at this temperature, while cristobalite thermal expansion rate keeps on climbing.

V-VI: Above 1200ºC, there is a significant difficulty in picking up consistent values for E. But, a pattern for the behaviour of the brick was successfully obtained. A drop in E is seen from this point on. A hypothesis that could explain this behaviour is that, at this

temperature, the mismatch in thermal expansion between the various components seen in the brick can lead to the formation of voids and internal friction. At the same time, the formation of a low melting phase of silica glass will also soften the sample [36]. These voids together with the presence of the low melting phase, will act as dampening agents, absorbing the impact of the exciting tool of this machine [32, 37, 38]. The dropping of E seen at this temperature is also believed to be related to the appearance of the voids and lower melting phase.

VI-VII: At the beginning of the first cooling down cycle, the curve follows exactly the same path that it took on the heating cycle, having no major changes in this section.

VII-VIII: At this interval, there is a big increase in E. This is a very drastic change, happening at around 1300ºC, and the phase transformations that happen at this stage are reconstructive ones, so this effect cannot be attributed to that. The same hypothesis previously introduced for the section of V to VI can also help explaining this behaviour. It is believed that this lower melting phase that is formed at high temperature is leading to the drop in E, but at the same time, phase transformation of amorphous content into crystalline content (cristobalite) is happening, which will lead to the increase of E. When the brick is cooled down, this lower melting phase will solidify again, leading to the jump in the E seen here.

VIII-IX: After that significant increase, *E's* curve now shows an opposite tendency. From point VIII to IX, a decreasing path for the curve is apparent. These is related to the normal variation of E of the mineral components of silica bricks at this temperature.

IX-X: E shows no major variation with the decrease of temperature, but around the 900ºC, there is a clear negative slope. This could be related to the transformation of quartz into tridymite.

X-XI: Near 550ºC, there is a clear change in the slope. This temperature is closely related to the displacive and reversible transformation of high to low quartz. The abrupt change also suggests that damage, most probably in the shape of microcracks, took place at this time.

XI-XII: Just above 200ºC, the curve's slope has another change. The E decreases at a faster rate than previously shown. This is related to the displacive transformation of high to low cristobalite. This is the highest volume displacive transformation, being linked multiple times to the appearance of damage and microcracks in silica bricks. The value of E, since around 400ºC, has gone under the values previously seen in the heating cycle. This is another evidence that the brick is damaged.

XII: At this point, the brick has reached a value of E far lower than the one seen at the beginning of the test, indicative of severe damage presence in the sample.

XIII: In the second heating cycle, as soon as the 200ºC barrier is reached, there is an increase in E related to the phase transformation of low to high cristobalite. Right after,

at around 250ºC, there is a big drop in the curve. This is unexpected, and could be related to some damage developed after the transformation.

XIII-XIV: In this section, very little change is seen in E. The curve stays flat until around 550-600ºC, and then it gains a very gentle positive slope, increasing the value of E marginally. It could be said that the microcracks previously developed, are working as a sink for the expected changes in the material rigidity, which are related to the phase transformation and the effect that increasing temperature would have on E.

XIV-XV: The value of E sees a big jump, from around 3,5 GPa to 12,5 GPa. This phenomenon is related to crack healing at high temperature. It has been proven that at this high temperature these samples see closure and healing of microcracks, which will lead to the increase in rigidity and consequently higher E. This is consequence of the different thermal expansion ratios of the different phases, leading to both opening of microcracks at lower temperatures and closure at high temperature [39, 40].

XV-XVI: The microcrack closure event seen on heating is also present in the beginning of the cooling cycle. E keeps on increasing at a significant rate until just above 1300ºC.

XVI-XVII: It could be said that at this point there is a change in events. A significant increase in E is no longer present, and the slope tends to a plateau.

XVII-XVIII: This section shows a decreasing E with temperature. The slope tends to increase with the drop of temperature. This is most likely related to some damaging effect of the phase transformation of high to low quartz together with the natural variation of this phase's E with temperature.

XVIII: At this point, the temperature for the high to low cristobalite transformation has been reached and it is clearly shown in the curve. There is a sudden decrease in E, reaching values similar to the one shown in the beginning of the second heating cycle.

This material shows a much higher E after the first heat up, but is heavily damaged when cooled down. Evidence of crack healing was found for this samples, as well as what is believed to be a lower melting phase, both of them reason for the increase in E at high temperature (as well as the crystallization of amorphous content). Cristobalite phase transformation is seen as the main damage source.

A sample of crystalline silica was also subjected to analysis under the same thermal cycle previously mentioned. Figure 4.9 is a plot of the various measurements of E along the thermal cycle. There have been highlighted 10 main points in this graph in order to aid in describing the behaviour of the brick throughout the test.

In the beginning of the first heating cycle, the response of the brick to increasing temperature is a decrease in E. Right after, at around 100ºC, the sample sees a sudden drop in E from point I to II. This temperature range is coincident with the phase transformation of low temperature polymorphs of tridymite, explaining this behaviour.

Point II seems to mark the end of the previous phase transformation, and from there until III, the curve regains the negative slope previously seen. When the sample reaches

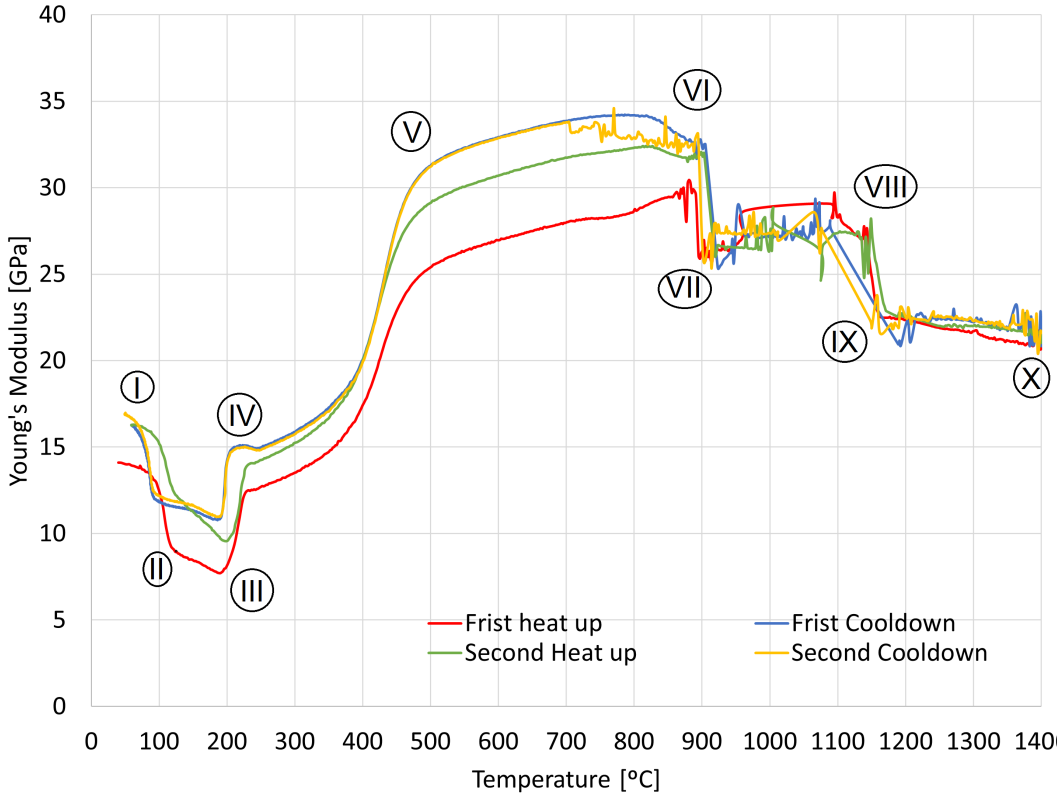

Figure 4.9: Temperature dependence of Young's modulus in a sample of a crystalline silica brick subjected to thermal cycling and analysed on IET machine

around 200ºC, E increases significantly, consequence of the phase transformation of low to high cristobalite.

From point IV to V, the curve exhibits a s-shaped slope. E increases at a fast rate until near 500ºC, where it keeps on increasing but at a slower rate until point VI. Typically, there is not a phase transformation in this temperature range, and this peculiar response could be due to just the thermal expansion and the mismatch of the expansion between the different main constituents of this material (tridymite and cristobalite). A mismatch in the thermal expansion of the different phases of this material will lead to internal stress and closure of voids and microcraks, which will lead to higher E [41]. Altough, further in the study, when analysing the XRD results, we could see that there is another reason behind this behaviour.

Upon reaching around 850ºC, the measurements from there on lack some accuracy. There are big deviations, and makes it harder to take conclusions and identify a pattern. However, after cleaning up the graph and working on identifying the wrong measurements, a tendency could be identified. There are two main steps and two main sections in the temperature range of 850 to 1400ºC, common to every heating cycle. The two drops in E from VI to VII and from VIII to IX, and the sections from VII to VIII and IX to X

show consistent E throughout their range. Both drops are near the temperature ranges of two phase transformations, at 870ºC, the transformation from quartz to tridymite, and at 1250ºC, from quartz to cristobalite.

However, this material is mainly composed of tridymite and cristobalite, so the amount of quartz present is very small, meaning that these phase transformations would hardly impact the material. Besides this fact, these are transformations that require some time to occur. The other explanation related to such behaviour could be the softening of the grain boundaries related to the presence of impurities, alongside the normal variation of E from these mineralogical components. The softening of the grain boundaries and mismatch of thermal expansion of the material is most likely responsible for the inconsistent measurements in this temperature range, as was described for fused silica material.

When comparing all the four curves one to the other, they all share a very similar behaviour and pattern. On the first heating cycle the brick shows the lowest values of E compared to the cycles that come after. The highest values of E are achieved in the cooling cycle of the material. It can be said that the brick did not suffer damage derived from this thermal cycle, and even the opposite could be acknowledge. After 1 cycle, the value of E at room temperature was higher than the one in the beginning of testing. However, some damage is done to the brick on heat up, as the brick does not reach the same values for E that it saw on cooldown. However, it regains it on the following cooling cycle, evidence of crack healing and closure at higher temperature. The source of damage seen in the brick is at lower temperatures, due to both the phase transformation of tridymite and cristobalite, as a significant drop in E is seen.

This behaviour goes against what previous studies have found for such material. A lower E at room temperature and a damaged sample was to be expected after cycling it to these high temperatures [34, 32, 40].

The heat up and cooldown cycle have a slight difference regarding the temperature that the phase transformation of cristobalite takes place, a effect that has been described and documented in other studies [42, 43].

Figure 4.10 represents the results for IET testing of a crystalline silica sample that was tested under similar conditions to cycle 2. In the case of this test, a third extra cooling and heating cycle was made.

The results for this test are very similar to the one seen from crystalline silica cooled down to 100ºC (Figure 4.9). The material shows a very similar behaviour through out the cycle, but with some differences. First it can be seen that on every cycle there is no damage whatsoever in this test. The curve always follows the same path with an exception.

There is a difference in the region between 900ºC and 1100ºC. Both samples show what could be called a three step behaviour: one from 500ºC to 900ºC, another from 900ºC to 1100ºC and from 1100ºC to 1400ºC. The value of E abruptly changes from one to another. As already mentioned, the results above 900ºC should be taken carefully as

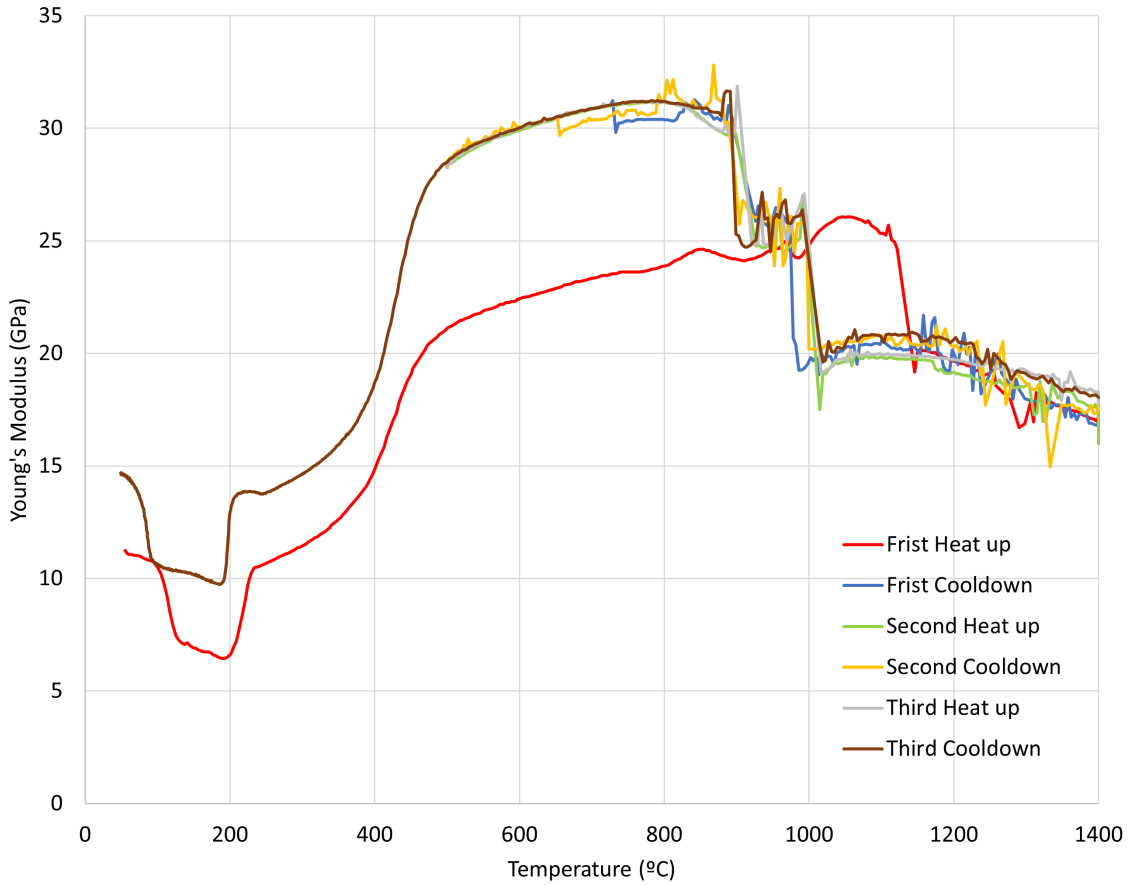

Figure 4.10: Temperature dependence of Young's Modulus in a sample of a crystalline silica brick subjected to thermal cycle 2 and analysed on IET machine

there is a dampening effect and a lower accuracy in the reading of the machine. But, analysing the results given, on the second step (900ºC-1100ºC) there is a clear difference between the two samples and the first heat up and the rest of the cycle. There is no obvious reason to why this happened, and it is believed to be related to the difficulty that IET has to determine the exact dominant frequency (natural frequency) at these high temperatures due to the higher dampening of the sample.

On the other hand, when looking back at the sample of crystalline silica under thermal cycle 1, it showed a slight decrease in E when heated up again, but on cooldown it healed back and E increased. The results from the test seen here once again point out to the same conclusions drawn from the first test with cycle 1. The most probable source of damage is the phase transformation of cristobalite and tridymite at around 200ºC and 100-160ºC, respectively. Since the sample cooled to 500ºC does not pass through it, it does not suffer damage from it.

Both samples showed a higher E at room temperature after the cycle, sample cooled to 100ºC increased E by 21% while sample cooled to 500ºC increased by 30%. This is

both related to the damage seen by cooling the samples across this phase transformation, as well as the higher time that the sample stays at high temperature, leading to more crack healing.

A sample of fused silica was put through heat cycle 2 in order to analyse the effects of not crossing the temperature range of cristobalite transformation (Figure 4.11).

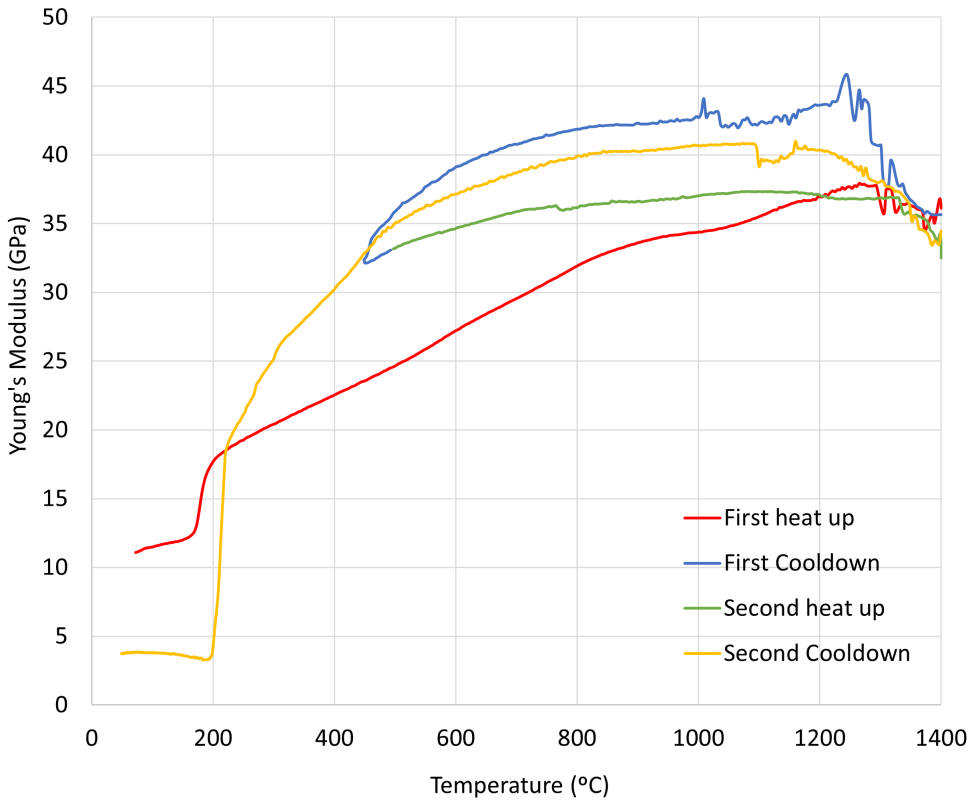

Figure 4.11: Temperature dependence of Young's Modulus in a sample of a fused silica brick subjected to thermal cycle 2 and analysed on IET machine

Comparing cooling the sample to 100ºC (Figure 4.8) to cooling it to 500ºC, there is a clear difference in the second heating cycle. E keeps a much higher value when heating from 500ºC, which is indicative of a sample with a lot less damage and minor degree of microcraks. Still some damage could be seen after cooling to 500ºC, as the second cooldown curve did not match the first cooldown one. This damage is most likely duo the phase transformation from high to low quartz seen at around 550ºC, together with the mismatch seen between the thermal expansion ratio of all the phases. At this point the sample still has a high amount of quartz, making this transformation more impactful at this stage. Also, another evidence of the occurrence of crack healing at high temperature is seen when the second cooldown shows higher E than the ones seen for the second heat up. This increase in E is not solely due to crack healing but also to the process of

crystallization of the amorphous content, since cristobalite and tridymite have a higher E than quartz.

From this test, it can be seen that the drop in E at around 200ºC for the cristobalite transformation, is much higher in the second cooldown than the increase seen in the first heat up. This is due to the higher content of cristobalite that is present in the brick after heating it up, making the transformation a lot more impactful.

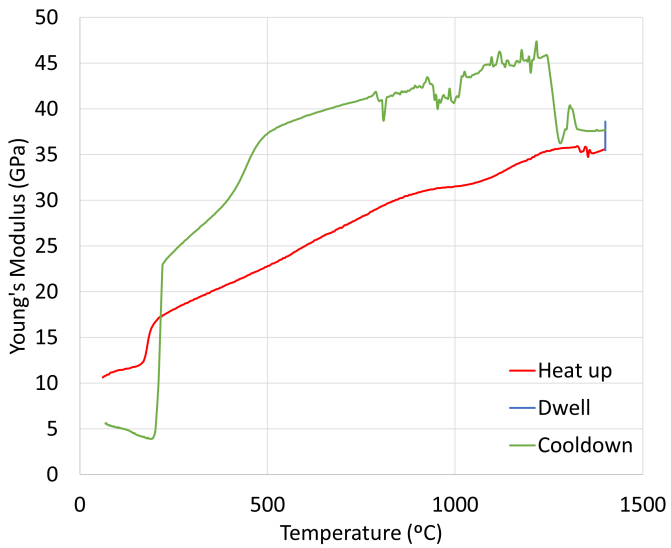

(a) Thermal cycle 3

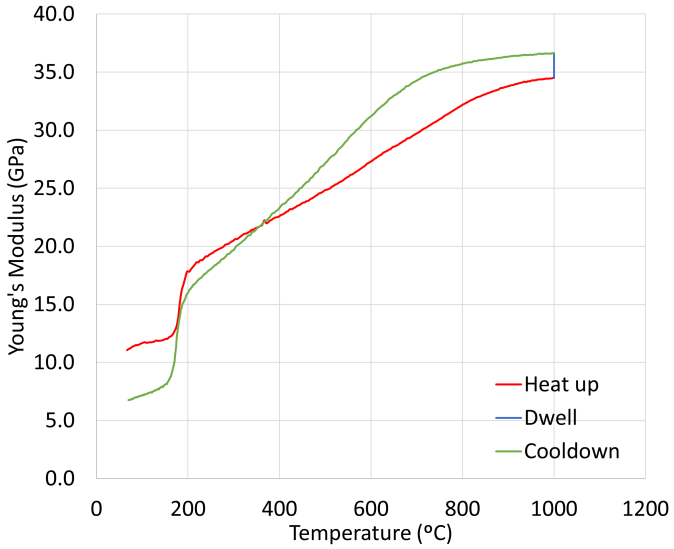

(b) Thermal cycle 4

Figure 4.12: Temperature dependence of Young's Modulus in a sample of a fused silica brick subjected to thermal cycle 3 and 4, analysed on IET machine

In order to analyse the effects of dwelling the sample of fused silica at 1000ºC and 1400ºC, thermal cycle 3 and 4 were performed on IET (Figure 4.12a and 4.12b). The behaviour of both samples on heat up is similar to what previously was seen. Also, both samples showed an increase in E while dwelling at their set temperature. When comparing the sample that dwelled at 1400ºC for 24h and the fused silica one that was just heated momentarily to 1400ºC (Figure 4.8), there is a difference in E at room temperature. The first showed a drop in E of around 47.3%, while the second showed a much higher drop of 84.47%, pointing out to a stronger sample at room temperature when dwelling it for longer periods at high temperature. This higher E is most likely duo to a higher percentage of crystalline content [44].

When looking at sample dwelled at 1000ºC for 24h, it can be concluded that heating a sample to 1000ºC and cooling it down will lead to less damage compared to doing the same for 1400ºC. Looking at E at room temperature after the cycle, a drop in 38.9% was seen, lower than the 47.3% seen for the sample that seen 1400ºC. A common point of both of this samples is the increase in E over the dwelling period. Sample dwelled at 1400ºC got an increase of approximately 1.26 GPa while sample dwelled at 1000ºC

increased by 2.1 GPa. A higher increase in E would be expected for the 1400ºC sample due to the crystallization of the amorphous content, but this effect is counteracted by the lower melting phase that appears at high temperatures. Once again at around 1300ºC, the spike in E seen in the 1400ºC test, at around 1250-1300ºC, is most likely due to the solidification of the lower melting phase.

Also here, it can be seen the difference in the phase transformation of cristobalite for sample heated to 1400ºC and 1000ºC. Heating it to 1400ºC will lead to higher cristobalite content, which in case leads to a more noticeable drop in E when passing trough the cristobalite phase transformation on cooldown.

Figure 4.13 represents the two tests performed in IET under the thermal cycle 3 and 4 for sample of crystalline silica.

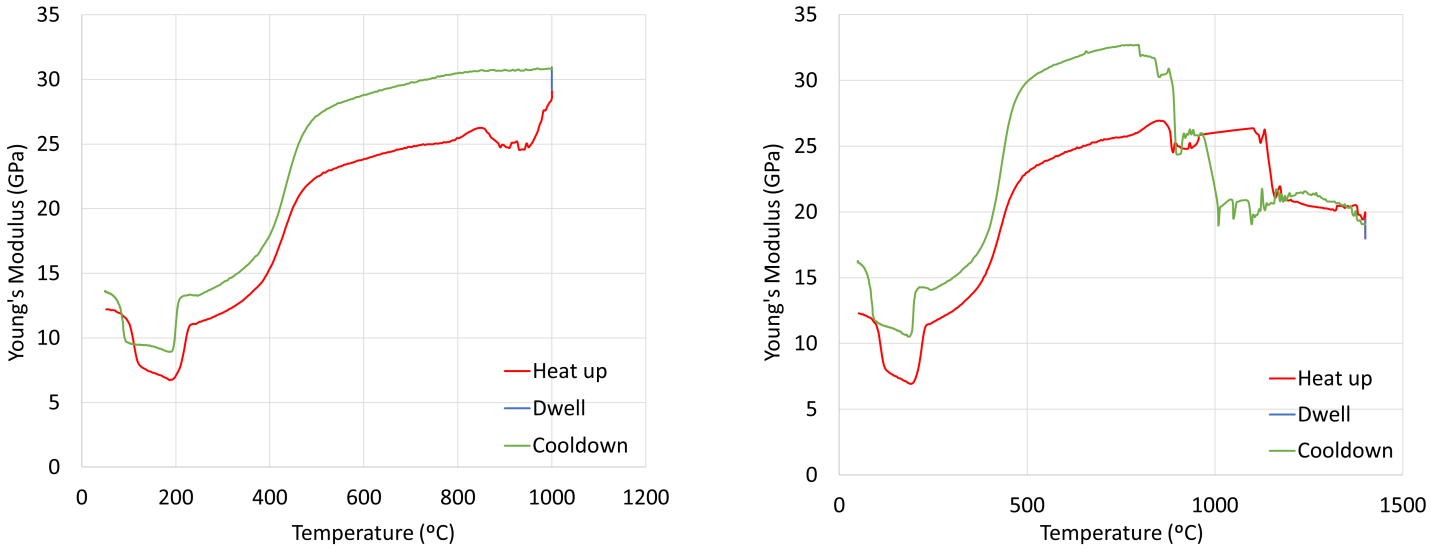

(a) Thermal cycle 3

(b) Thermal cycle 4

Figure 4.13: Temperature dependence of Young's Modulus in a sample of a crystalline silica brick subjected to thermal cycle 3 and 4, analysed on IET machine

First looking at the sample that was heated up to 1000ºC, we see an increase of E after the cycle of 11,8%, with an increase in 1,5 GPa during the dwell time at 1000ºC. When looking at the sample that was heated to 1400ºC, we see a larger increase in E at room temperature (32,6%), and during the dwell time, there was just a slight increase in E of around 0,7 GPa. What this test once again proves, is the occurrence of crack healing at high temperatures, specially above 1000ºC. From literature, it has been seen that crack healing tends do happen at temperatures above 1000ºC, which seems to be in agreement with these findings [32].

4.2.2 Three-point bending

The force displacement results for the samples of crystalline silica tested at room temperature are presented on Figure 4.14. From all the tests done on these samples, a representative of each test scenario was chosen for comparison.

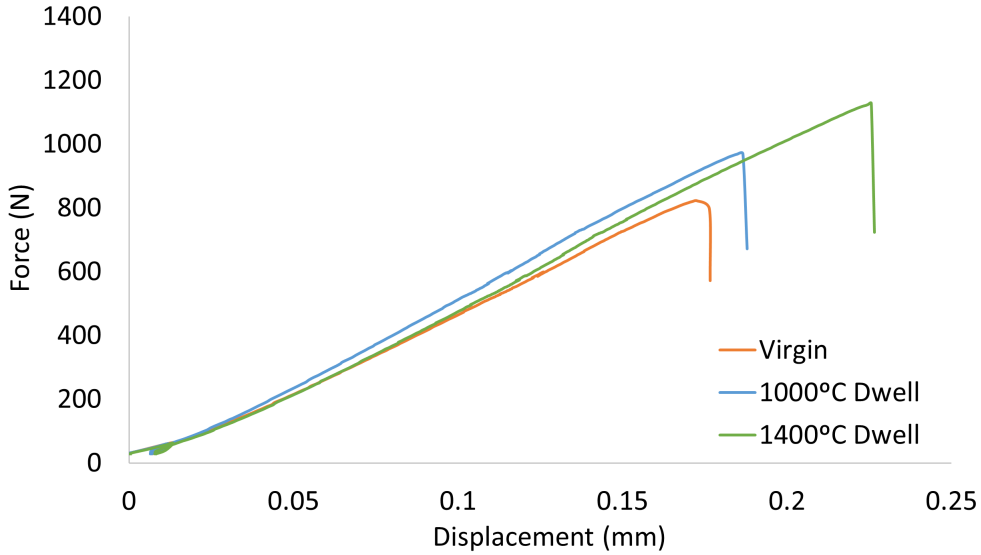

Figure 4.14: 3PB results for the crystalline silica samples tested at room temperature

Analysing the graph on Figure 4.14, the three case scenarios for samples of crystalline silica tested at room temperature are represented: a virgin sample, a sample previous dwelled at 1000ºC for 24h and dwelled at 1400ºC for 24h. All the bricks showed a very brittle behaviour, evident by the force suddenly drooping at failure. All the curves have a very similar slope, which indicates that the samples have a very similar Young's modulus. On the other hand, the displacement and maximum force are not matching. The virgin sample is the less resistant one, failing at a lower displacement, followed by the sample dwelled at 1000ºC and then the sample dwelled at 1400ºC.

When looking back at the results from IET, a rise in E would be expected for both the samples that have been dwelled at 1000ºC and 1400ºC. In these 3PB tests at room temperature, the sample dwelled at 1000ºC did not saw this increase, but the sample dwelled at 1400ºC, besides not having higher E, the higher displacement of this test can be explained with the balance of both the formation of microcracks (leads to higher displacement and decrease of E) together with the effect of the phase transformation of tridymite to cristobalite (increase of E).

The results for the tests performed at 1000ºC for crystalline silica are displayed on Figure 4.15. All three samples that were tested in these three different conditions (virgin, 1000ºC dwell and 1400ºC dwell) show a very similar E and brittle behaviour. Virgin

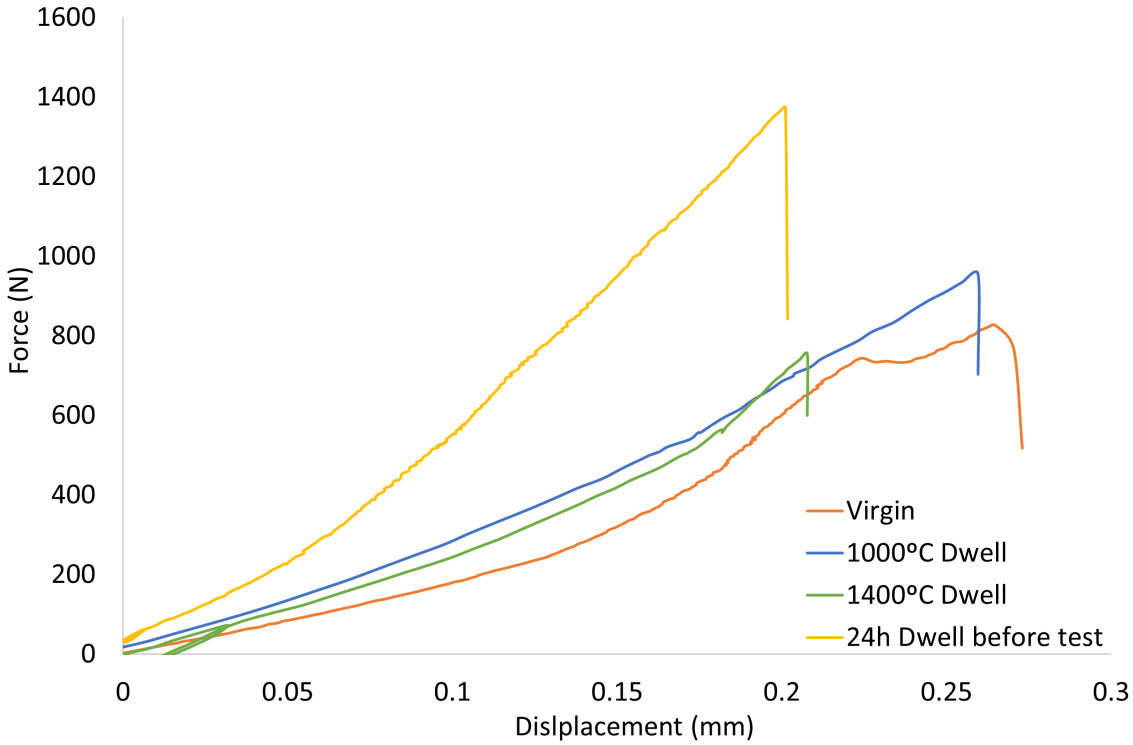

Figure 4.15: 3PB results for the crystalline silica samples tested at 1000ºC

sample shows a behavior near failure that could be explained by a major crack propagating and arresting shortly after leading to these double picks in the curve. Comparing these to IET results, the results expected from 3PB would be for all the samples to have a very similar E, but a E for samples tested at 1000ºC to be higher than the ones tested at room temperature. The first part of these results are confirmed by 3PB, but these samples tested at 1000ºC have a lower E than the the ones tested at room temperature. On the other hand, the sample that was dwelled for 24h before testing inside 3PB, the curve and E are in good accordance with what would be expected to see in IET ($E_{1000C} > E_{RT}$). It can be concluded that for more accurate results, there is a need to dwell the sample for longer period time before testing. This will guarantee that the entire brick will be at an even temperature and that phase transformation's can take place for the brick to show its true behaviour.

Figure 4.16 displays the results for the samples of crystalline silica tested at 1400ºC. The three first tests (virgin, 1000ºC dwell and 1400ºC dwell) show a very similar behaviour. At failure, they show some strain softening, relatable to samples with a certain degree of microcraks. Virgin sample and 1000ºC dwell show an equal behaviour, but a lower E compared to the one from the 1400ºC dwell sample. From IET results, E for all these three samples should be slightly higher than the samples tested at 1000ºC. The sample with 1400ºC dwell shows in fact a higher E, as expected, while the other two samples

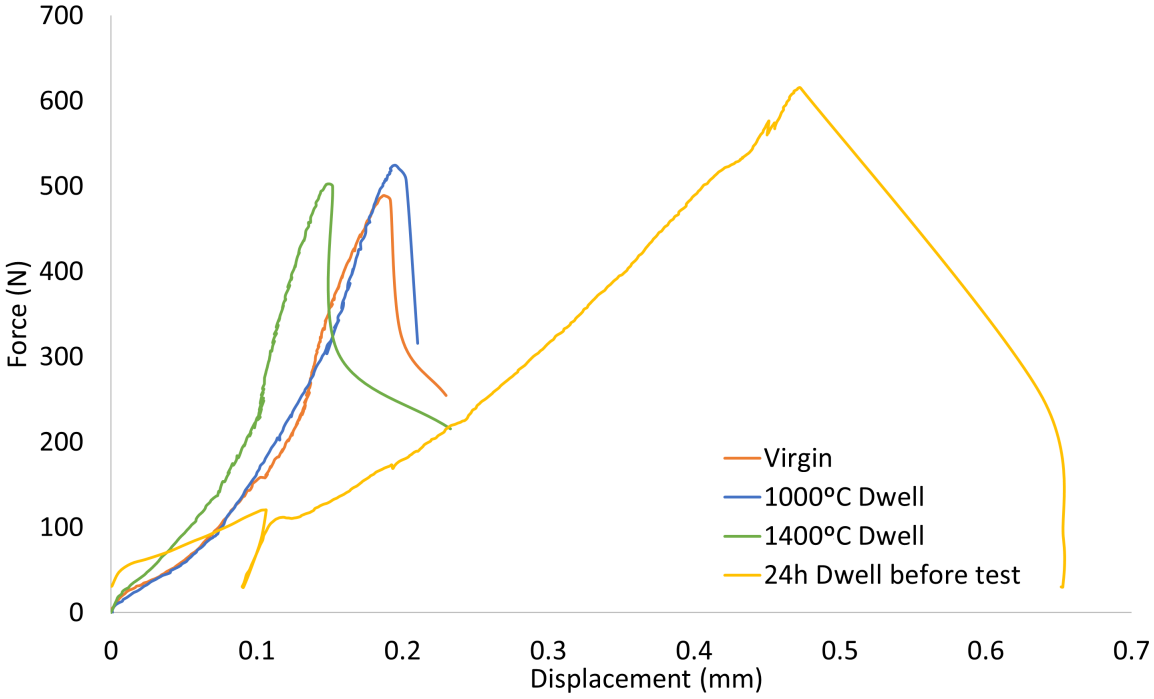

Figure 4.16: 3PB results for the crystalline silica samples tested at 1400ºC

have a similar behavior and curve slope, but a lower E.

IET testing performed on this material under similar conditions, has proven that this material suffers very low damage and even increases its rigidity. After a thermal cycle of heating to 1400ºC and cooling to room temperature, E increased by 30 % at room temperature (according to IET). In general, all these samples should have a higher E than what is seen here (Figure 4.16), but this results also came to prove once again that dwelling a sample at 1400ºC showed a higher E than a virgin or 1000ºC dwell.

When looking at the sample with 24h dwell before testing, the resulting curve from 3PB testing is completely different. This behaviour does not fit in with the results from IET and cannot be justified. It should have a higher E than all the other three tests, and the opposite is seen here. However, the cyclic part of the test is present in the curve (evident in the low displacement part of the curve, it displays a drop around 0.1 mm), and it demonstrates an interesting behaviour. The cyclic part of the curve should have an equal slope to the rest of the curve, representing the purely elastic behaviour of the material. In this case, the slope is completely different, but very similar to the the slope of the other three curves of Figure 4.16. Once again, it demonstrates the importance of using higher dwell times before testing to obtain the correct behavior of the material, but also, that studying the unloading phase of the curve of these material under cyclic loading, could be a more effective method. This behaviour difference between the sample tested after 24h dwell and the others could be related to the time required for phase transformation

(tridymite into cristobalite) and crack healing to happen, leaving it at higher temperature for longer period will lead to these two phenomenon happening in greater scale and the sample being in a more stable form.

In all the 3PB testes performed for this material, the results were very controversial. First at room temperature testing, the samples all showed a similar E, unexpectedly. At 1000ºC the three samples tested with a lower dwell time before testing, showed the same low E, while the 24h dwell before test, had a much higher E, pointing to the need of more testing under these longer dwell times. For the 1400ºC test, the sample dwelled at 1400ºC had a higher E as expected from IET, as well as the very different behaviour of the 24h dwell sample. Overall, this lead to question the methods used for 3PB testing. High temperature testing (1000ºC and 1400ºC) shone light on the importance of using higher dwell times before testing, and the relevance of performing cyclic testing at these temperatures.

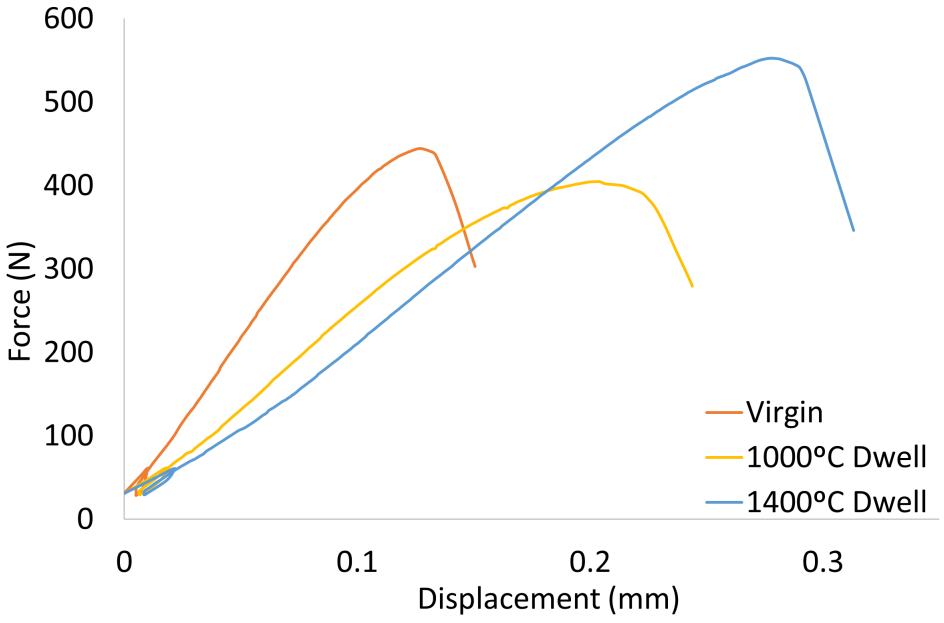

Figure 4.17: 3PB results for the fused silica samples tested at room temperature

The fused silica samples tested at room temperature have their force-displacement graphs displayed in Figure 4.17. All three samples show, to some degree, a strain softening behaviour near the failure point. This behaviour is typical for sample with a higher percentage of amorphous content in their structure. Virgin sample is the most brittle one (and a higher E), followed by the sample of 1000ºC dwell and then the sample with 1400ºC dwell. These results are in good agreement with the ones seen in IET. The formation of microcracks in the samples that have seen heat cycling lead to the drop in E, a less brittle samples and a higher displacement at failure.

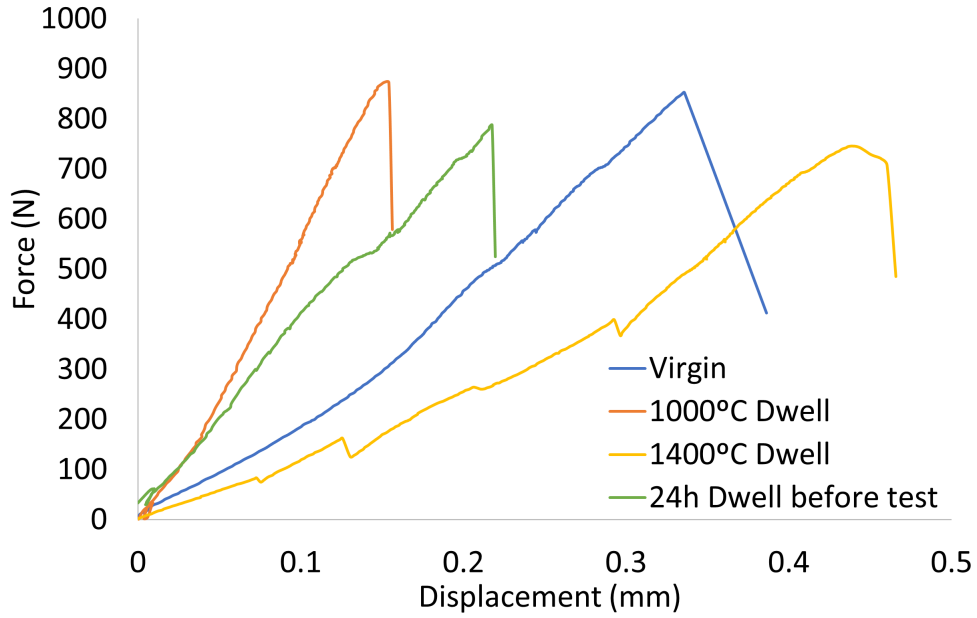

Figure 4.18: 3PB results for the fused silica samples tested at 1000ºC

3PB tests performed with fused silica samples at 1000ºC are summarized in Figure 4.18. From IET testing, it has been proven that heating the sample to 1000ºC or 1400ºC and cooling it down to room temperature has lead to major damage to the sample. The sample of 1400ºC dwell has shown this behaviour in 3PB testing, having a lower E and higher displacement. Although, the sample of 1000ºC dwell and 24h dwell before testing, has a higher E than the virgin sample. These are unexpected results, which could be explained by the these samples in specific not suffering as much damage as expected from micro cracking formation, and the crystallization of the amorphous content leading to the increase in E.

On the other hand, when comparing the sample dwelled at 1000ºC directly to the 24h dwell before test sample, it would be expected that the 1000ºC sample would have lower E, since cooling it down would damage these samples. The opposite is seen, the sample with lower dwell time has higher E, and a reason for this behaviour could not be found.

The 3PB results for the samples of fused silica tested at 1400ºC are available in Figure 4.19. These graph represents the three cases of virgin sample, 1000ºC dwell and 1400ºC dwell. Here, the results for the sample with a 24h dwell before testing are not shown, since the test did not yield valid results [39].

When looking back at the results from IET, the virgin sample is expected to have the highest E, followed by the 1000ºC dwell and finally the 1400ºC dwell. This is the complete opposite from what 3PB force displacement graphs show. The sample with 1400ºC dwell has the higher E and force at failure, followed by the sample of 1000ºC dwell and lastly the virgin one. When looking at the virgin sample, a high degree of

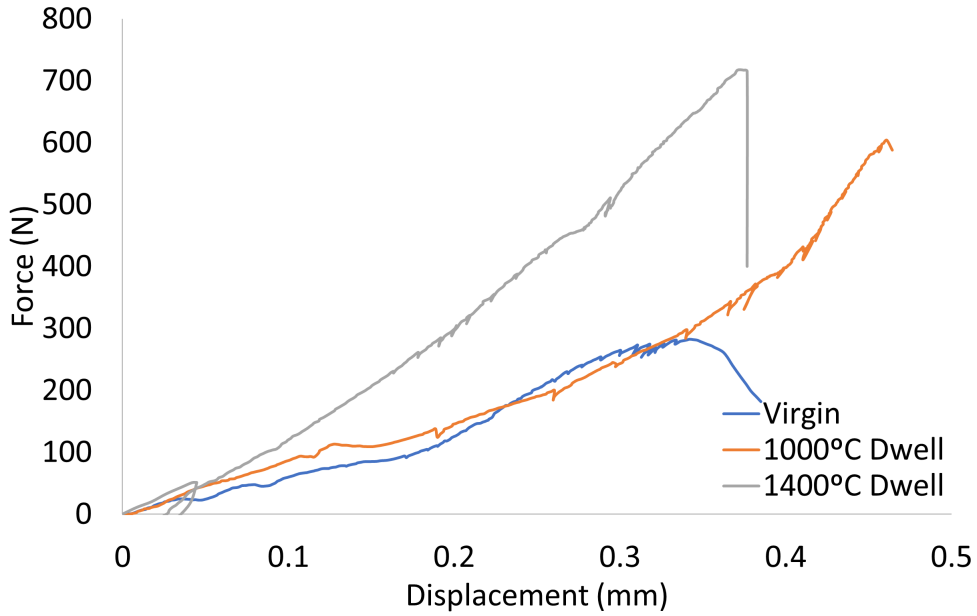

Figure 4.19: 3PB results for the fused silica samples tested at 1400ºC

damage cannot be a reasoning behind the low E of this sample, as the sample as only seen a heating cycle and then tested at 1400ºC. There is not enough data to make solid statements, but a theory can be put together to why this behaviour occurs. It is believed to be related to the formation of a low melting phase of the amorphous phase of silica. In this first heat cycle there is not enough time for formation of high amounts of crystalline content, so the sample is softer at this stage, leading to weaker sample at this temperatures. On the sample with 1000ºC dwell, the sample shows some extra strength, it is able to withstand a higher force and displacement. Following the same hypothesis, this sample will have a higher amount of crystalline content since it already has seen a cycle and dwell at 1000ºC, which will lead to a stronger sample. On this case, the sample with a 1400ºC cycle will have the higher amount of crystalline content, being the strongest. Some crack healing could also be behind the reason why the sample of 1400ºC dwell shows itself with a higher E and peak force.

4.2.3 X-Ray Diffraction results

X-ray diffraction testing was also performed on both samples of crystalline and fused silica, and the results will be presented in this chapter. These results well help better understand and confirm some theories and assumptions previously drawn from IET and 3PB results. After putting a sample of crystalline silica through the heating cycle specified for this testing (heating to and cooling from 1400ºC at 2ºC/minute), the results will be analysed by separating the heating and cooling cycles, as well as the content of cristobalite

and tridymite. Figure 4.20 has in it the graphs with the phase proportions throughout the heating cycle of the test.

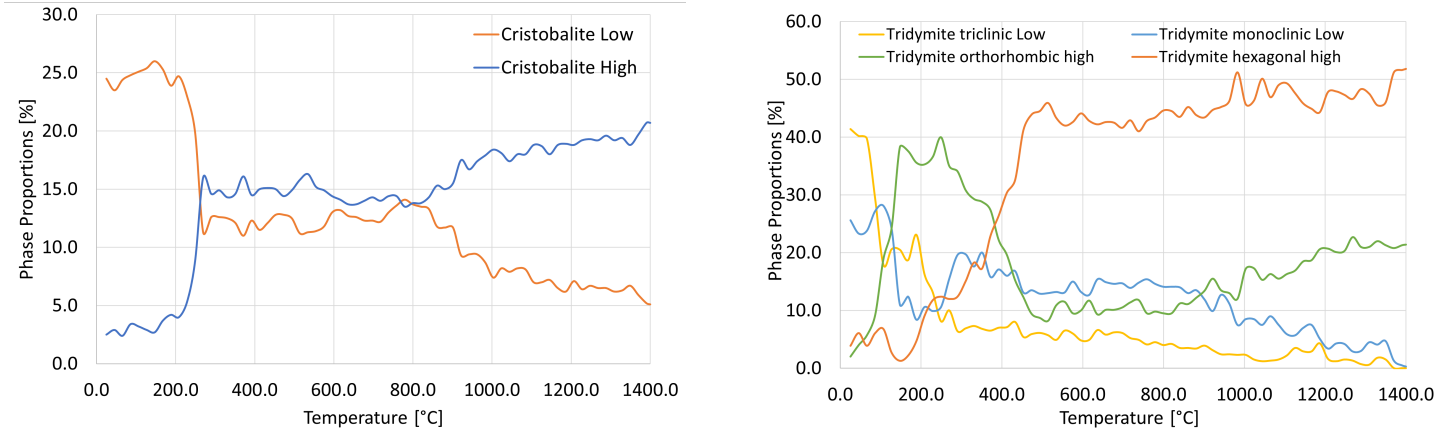

(a) Cristobalite polymorphs content

(b) Tridymite polymorphs content

Figure 4.20: XRD cristobalite content for the heating cycle of a crystalline silica sample

When analysing the graph for the cristobalite content, a very sudden drop in cristobalite low (α) and rise in cristobalite high (β) is seen in the range from 200 to 260ºC. These confirms what has previously seen in IET at this temperature range, the transformation of low to high cristobalite, leading to variations in the E of the sample. From around 800ºC to 1400ºC, there is an increase in cristobalite high which goes along with a similar decrease in cristobalite low. This may lead to believe that there is some phase transformation happening at this stage, but from what is known from this material, such would be very unlikely. Most likely, XRD was just able to pick up on the accurate values for the phase proportions of these materials latter in the test. Cristobalite low and high have a very similar refraction angle, which will lead to some difficulty analysis and differentiation between these two. Also, when looking at the cooling cycle (Figure 4.21), these phenomenon does not repeat.

Looking now at the tridymite phase porpotion graph (Figure 4.20b), XRD is able to pick up on all 4 different polymorphs of tridymite. In the beginning of the heating phase, when the sample reaches 70ºC, there is a decrease in tridymite triclyinc low and tridymite monoclinic low. At the same time, an increase in tridymite orthorhombic high of around the same percentage is evident, until it reaches 170ºC. So a phase transformation of these polymorphs is evidently happening here. From 170ºC until 500ºC, a simultaneous increase in tridymite hexagonal high and decrease in tridymite orthorhombic high appears, with some variations in the the other polymorphs.

When cross analysing this phase transformation of tridymite from 170ºC to 500ºC, and the behaviour of the crystalline silica sample seen in IET testing (Figure 4.9) in the same temperature range, a S-shaped curve is seen in the range from 200ºC to 500ºC. This

sharp change in E seen for this material in IET tests, is most likely related to this phase transformation.

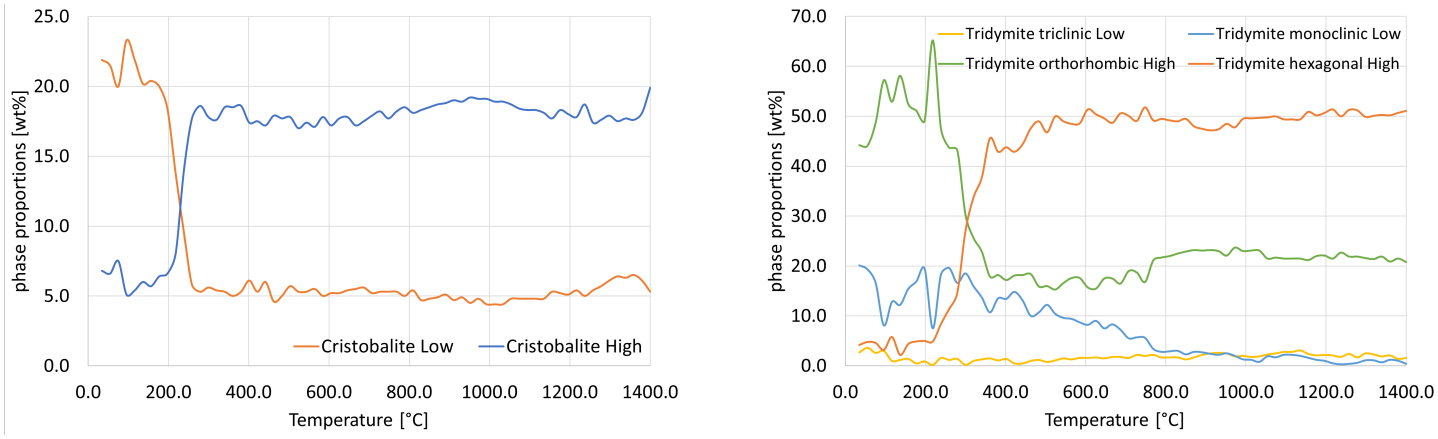

(a) Cristobalite polymorphs content

(b) Tridymite polymorphs content

Figure 4.21: XRD cristobalite content for the cooling cycle of a crystalline silica sample

Figure 4.21 plots the phase proportions of tridymite and cristobalite across the temperature in the cooling cycle of the sample.

From the cristobalite graph, the only variation seen in it, is the increase in cristobalite low and decrease in cristobalite high at around 260-200ºC, evident of the phase transformation of high to low cristobalite.

Looking at the graph for tridymite, when the sample reaches 800ºC on the cooling cycle, there is a shift in the values of tridymite polymorphs. From 800ºC to around 300ºC, an increase in tridymite monoclinic low is evident. This seems to be accompanied with a small decrease in tridymite hexagonal high and orthorombic high. The transformation from trydimite hexagonal high to orthorombic high seems to happen at a much lower temperature than what was seen on the heating cycle. This could be either related to the inaccuracy of this method at times, or there is some variation in the points of transformation for silica's polymorphs.

After the test, some interesting findings were made when analysing the percentage values for the phases at room temperature before and after the testing (Table 4.6). First it should be said that these percentages values are not completely accurate, as XRD does not have enough precision to claim this level of accuracy.

When summing up the content for cristobalite before and after the test, there is 27% of cristobalite in total before and 28.7% after. For tridymite, before there was a total of 72.9% and 71.2% after the test. The same amount of tridymite lost matches the same amount gained for cristobalite after the test. This is evidence of phase transformation of tridymite into cristobalite. This phase transformation is only supposed to happen at temperatures near 1470ºC, but due to the presence of impurities, it is happening at lower

Table 4.6: Phase proportions percentage values for crystalline silica sample before and after XRD testing

	Before cycle (%)	After cycle (%)
Cristobalite Low	24.5	21.9
Cristobalite High	2.5	6.8
Tridymite Triclinic Low	41.4	2.7
Tridymite Monoclinic Low	25.6	20.1
Tridymite Orthorohmbic High	2.0	44.2
Tridymite Hexagonal High	3.9	4.2

temperatures. These phenomenon also help to explain the increase in E at room temperature for samples of crystalline silica after an heating cycle until 1400ºC, since cristobalite has a higher E (65.2 GPa) at room temperature than tridymite (58.1 GPa) [44].

(a) Cristobalite polymorphs content

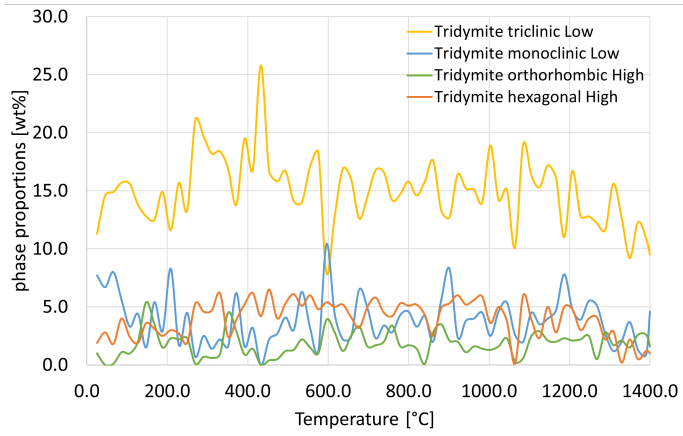

(b) Tridymite polymorphs content

Figure 4.22: XRD cristobalite content for the heating cycle of a fused silica sample

Fused silica sample results for XRD testing on the cooling cycle is represented in Figure 4.22. First, it should be noted that the percentage values for the phase proportions are not correct. This XRD machine cannot effectively pickup quartz, so the percentages here seen are not absolute but relative, only the relation of cristobalite to tridymite can be known. At the beginning of the test, it is known that this sample has an approximate 70% content of fused quartz, so at the beginning of the test, the absolute values can be known. However, when the sample is heated up, the percentage of quartz will change, so no longer can the absolute values for the polymorphs be known.

Analysing the cristobalite graph, once again the point of transformation for cristobalite is the same as seen in IET and 3PB, having a transformation happening from 200ºC to 260ºC. From 260ºC to 1400ºC there is some variation of the values, there is a overall increase of the content of cristobalite.

Tridymite percentage values are rather different for the sample of fused silica. Strangely

enough, the dominant tridymite polymorph along the entire test is tridymite triclinic low. All the polymorphs keep their percentage values very stable throughout the heating cycle, but near the end, above 1300ºC there is a decrease in the overall tridymite content. When connecting the decrease of tridymite with the increase in cristobalite, two things can be said to be happening here. The amount of fused quartz transformed into cristobalite is larger than the transformation into tridymite, leading to a higher proportion of cristobalite to tridymite. Also, as it was seen in the sample of crystalline silica, some phase transformation of tridymite into cristobalite is most likely happening here.

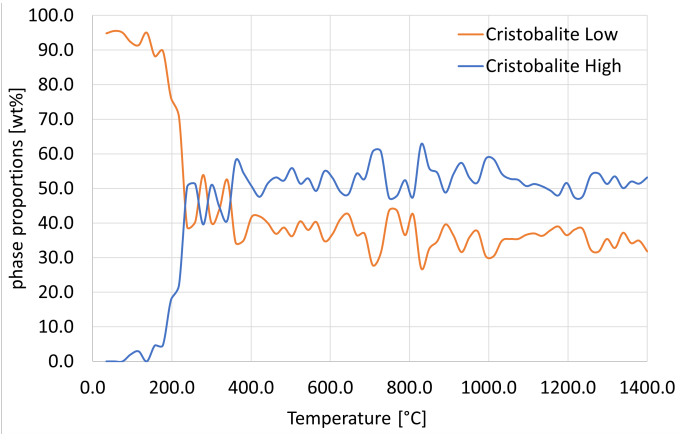

(a) Cristobalite polymorphs content

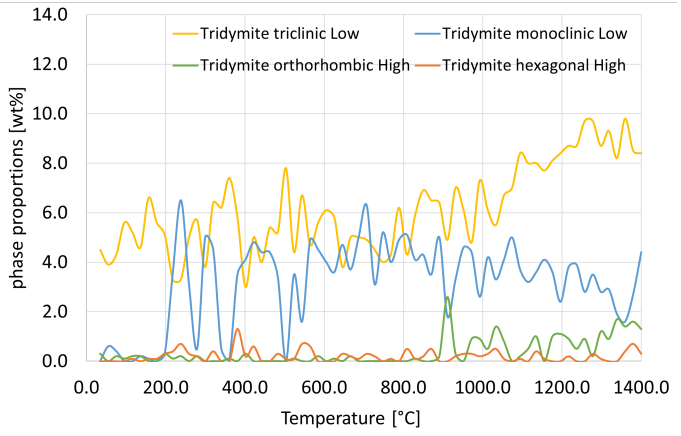

(b) Tridymite polymorphs content

Figure 4.23: XRD cristobalite content for the cooling cycle of a fused silica sample

From the cooling cycle (Figure 4.23), similar conclusions can be drawn from this results. On the cristobalite side, when the sample is cooling down, the values remain very constant until it arrives the phase transformation of low to high cristobalite. Here an increase in cristobalite low is followed by a decrease in cristobalite high.

From tridymite, in the beginning of cooling, tridymite triclinic low values keep on decreasing until around the range of 800ºC to 1000ºC, while tridymite monoclinic low increases slightly. The variation is rather small, and it could be related to a transformation of tridymite into cristobalite together with a low amount of quartz turning into tridymite while most of it is transforming into cristobalite.

When analysing the percentage values of each phase before and after the test, a big difference can be seen (Table 4.7). The cristobalite to tridymite ratio in this sample is much higher than before. This sample is mostly consisted of cristobalite and fused quartz at this point. These results can serve to consolidate the theory that a lower amount of transformation of quartz into tridymite is happening in this sample, and most likely, the lower percentage of tridymite seen here, is also influenced both by the phase transformation of tridymite into cristobalite and a higher rate of quartz transformation into cristobalite.

Table 4.7: Phase proportions percentage values for fused silica sample before and after XRD testing

	Before cycle (%)	After cycle (%)
Cristobalite Low	72.9	94.8
Cristobalite High	5.2	0.0
Tridymite Triclinic Low	6.7	4.5
Tridymite Monoclinic Low	2.6	0.0
Tridymite Orthorohmbic High	3.1	0.3
Tridymite Hexagonal High	6.0	0.0

Chapter 5

Conclusions

This work was divided into two main parts: the FEM simulation, which works towards answering if K_{IC} and *J-integral* were viable properties to characterize silica bricks; and the experimental one, which had the goal to study the fracture behaviour and strength of silica bricks under thermo-mechanical loading.

FEM simulation was performed for a 2D model of a three-point bending test of silica bricks. XFEM crack was first adopted and good approximation to the behaviour of the silica bricks, displacement and force at failure, and E were achieved, while the after failure strain softening behaviour was not able to be fully reproduced.

- XFEM was not able to obtain K_{IC} and *J-Integral* in 2D models, so contour integrals crack was used.
- With the contour integral model the results from 0.5mm crack were not so consistent as the 1.5mm crack one, and this could have been explained by a higher stress concentration in the 1.5mm crack or a unsymmetrical stress direction near the crack tip. On the other hand, both the stress and stress direction were analysed in Abaqus and they did not show enough of a difference to justify the margin seen between these two models.
- The sample with no notch saw the lowest value of K_{IC} in comparison with the other two samples. This can be explained by the fact that the corresponding force-displacement graph at the displacement of failure, did not fully match the experimental one.
- This mismatch happens because of the inability of the model to simulate the strain softening behaviour near failure, which in part will influence the value of K_{IC}, leading to a higher amount than it actually should have.
- With a good matching curve, it would be possible to arrive to a K_{IC} and *J-Integral* that would be equal for every situation.

- K_{IC} and *J-Integral* for this material could be said to be the one achieved for the no notch sample with 1.5mm crack simulation.

Looking at IET, and first at crystalline silica, this material behaved somewhat different from expected:

- After being heated and cooled down from 1400ºC and 1000ºC, it showed an increase in E at room temperature. This material was expected to be damaged at room temperature after a thermal cycle, having a drop in E.
- Flaws and defects are most likely present in them in the form of cracks. When heated up to temperatures above 1300ºC, these cracks will close duo to a crack healing process, and the longer it stays at these higher temperatures, the more crack healing will take place.
- This was also backed up by the healing seen in this material after it was damaged by the phase transformation of cristobalite. As XRD came to prove that some phase transformation of tridymite to cristobalite is happening in these cycles at high temperature, which will also contribute to the increase in E.

From the tests run on IET for fused silica, the results where what was to be expected of this material:

- Fused silica showed a more consistent and predictable behaviour when subjected to thermal cycling.
- The sample had an high degree of damage at room temperature after thermal cycling, enhanced when heated to 1400ºC rather than to 1000ºC.
- This is mostly due to the higher content of cristobalite that is transformed when the sample is heated to 1400ºC, which will increase the damaging effect seen in the phase transformation of cristobalite.
- If the sample is not cooled down below the phase transformation of cristobalite, a significantly lower amount of damage is seen in the sample, part of which is healed back up when heated again.

For both samples, it is believed that the appearance of a lower melting phase is behind the behaviour of the sample at higher temperature, together with the effect of crack healing. The phase transformation of tridymite to cristobalite happens at lower temperature than expected, most likely due to the presence of impurities in the sample.

3PB showed results that were inconsistent when trying to compare and back up the conclusions seen from IET, although, some interesting results came up from these.

- Samples tested with a 24h dwell inside 3PB machine came up with very different results from the other samples.
- Samples tested at higher temperature showed more inconsistent results than the ones tested at room temperature.
- For more accurate testing of sample at high temperature, a higher dwell time before testing is needed in order for all the processes of crack healing and phase transformation to happen and the sample to be in a static state.
- The cyclic part of force displacement curve seen in 3PB should be tested more in depth as it has shown different E than the rest of the curve.

From this study, it could be concluded that the samples of crystalline silica would be ideal for the coke ovens as they are both resistant and can withstand cycling without any damage. On the other hand, this is an unexpected behaviour from this material, therefore more testing needs to be done to confirm the preliminary results of this work.

Fused silica samples main characteristic is the low thermal expansion ratio in the first heat up cycle. This is related to the more consistent increase in E on the first heat up seen in IET. When used in a coke oven, it is ideal for wall repairs, but after heat up, it can never be cooled down to temperatures below 500ºC, or critical damage will occur to this material.

Chapter 6

Future work

Throughout this research, the results obtained opened up some questions that were left unanswered.

Regarding FEM simulation, XFEM testing should be also done for 3D models in order to assess the usability of this crack method on a 3D model and study the variation of K_{IC} and J-Integral across the thickness of the material. It would also be interesting to model the strain softening behaviour seen in some of the sample for contour integral cracks, in order to further validate the results here seen for K_{IC} and J-Integral.

On the experimental side, crystalline silica samples showed some unusual behaviour most likely due to defects, both on IET and 3PB testing. So in future research, it is important to look out for defects in this samples and it would also be important to redo the experiments with a different batch of samples, as it could prove to yield very different results. Microscopic analysis could also be explored in order to identify cracks and defects in the samples, both before and after testing.

On this work, a maximum of 3 thermal cycles were performed in IET. It would be important to study their behaviour when put through IET testing with multiple cycles, hoping to see what damage would occur to these samples (mainly crystalline silica) in the long run. It would be interesting to perform another cycle after performing a 24h dwell on this samples, as then it could be seen if any behaviour change would came from dwelling on the following cycle.

Regarding 3PB, some different parameters should be tested in the future. First, samples should be tested with different dwell times inside the machine, as different behaviour was seen for this cases but needs more information. Also, a study around the unloading curve on force displacement graphs for this samples could also be done. So load cycling the sample and studying the purely elastic behaviour of the unloading phase for samples that have undergone different thermal cycles.

XRD should also be performed with different parameters. The effects of dwelling the samples at high temperature for longer period of time as well as cycling the sample more

then once should also be studied. Both of them can give an insight to how the phase proportions will change with these parameters. Also, further tests need to be performed on these materials in order to better understand the temperatures and conditions at which the various polymorphs of tridymite will transform.

Appendix A

All 3PB results

A.1 Crystalline silica results

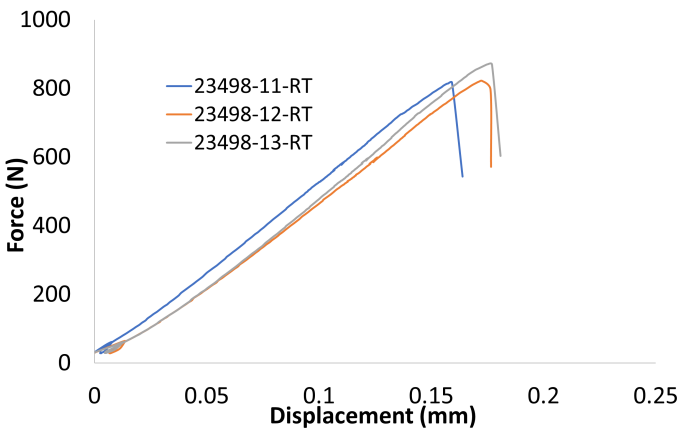

(a) Virgin

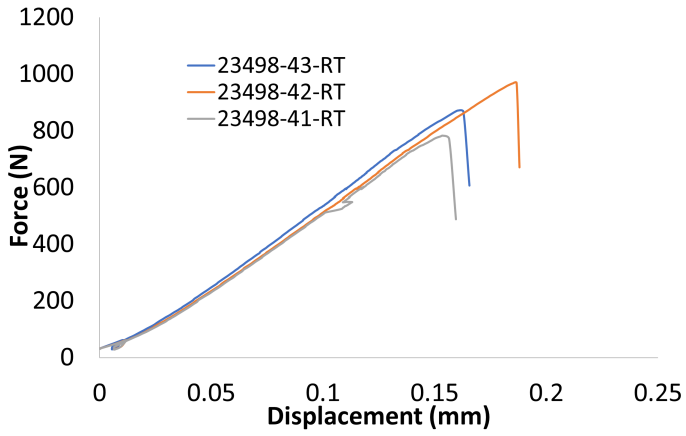

(b) 1000ºC Dwell

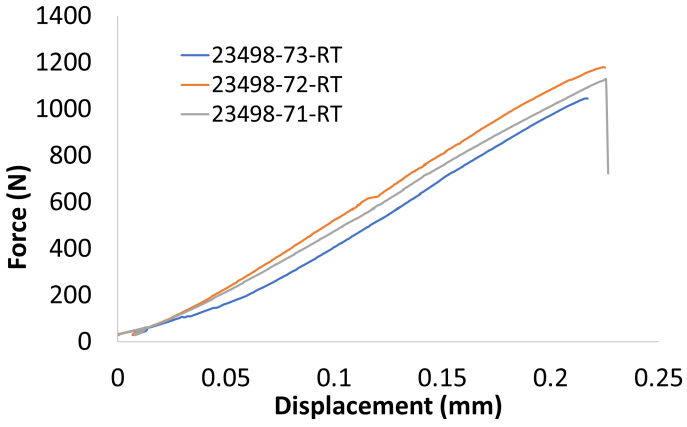

(c) 1400ºC Dwell

Figure A.1: 3PB tests done for crystalline silica at room temperature

All 3PB results

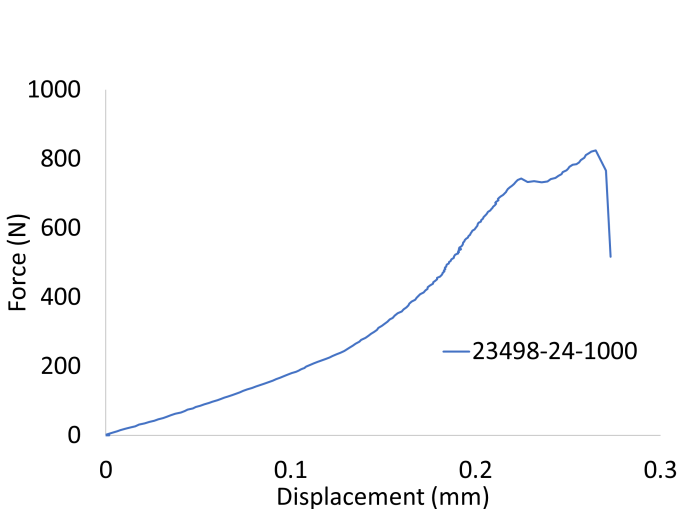

(a) Virgin

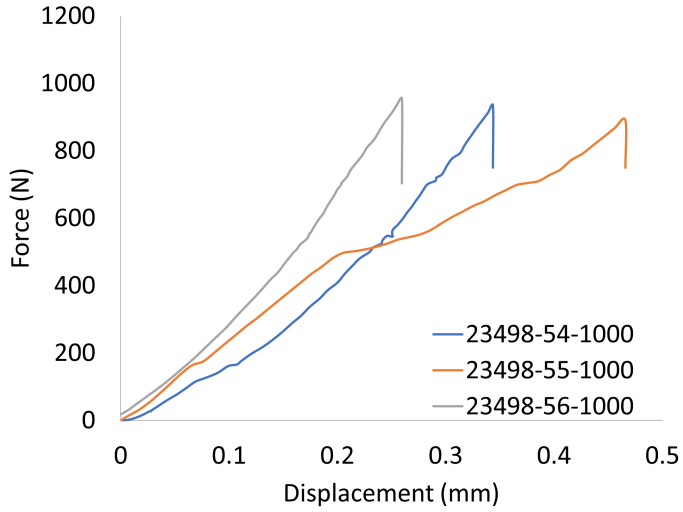

(b) 1000ºC Dwell

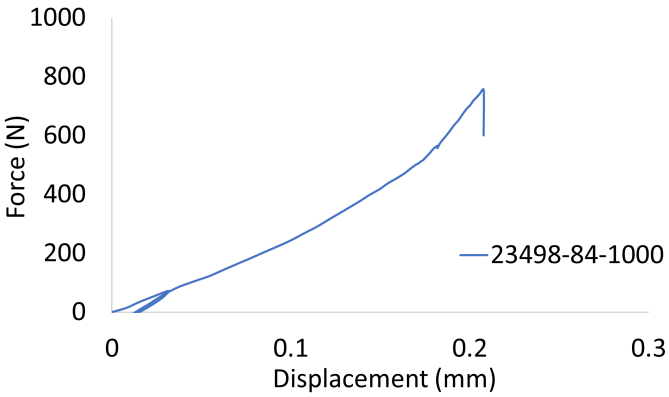

(c) 1400ºC Dwell

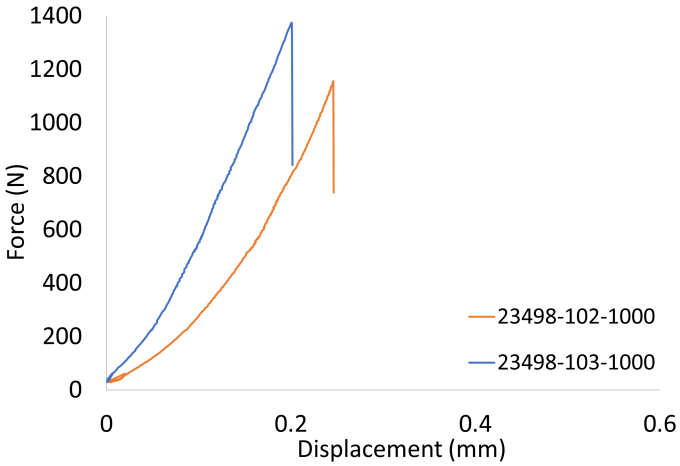

(d) 24h dwell

Figure A.2: 3PB tests done for crystalline silica at 1000ºC

A.1 Crystalline silica results

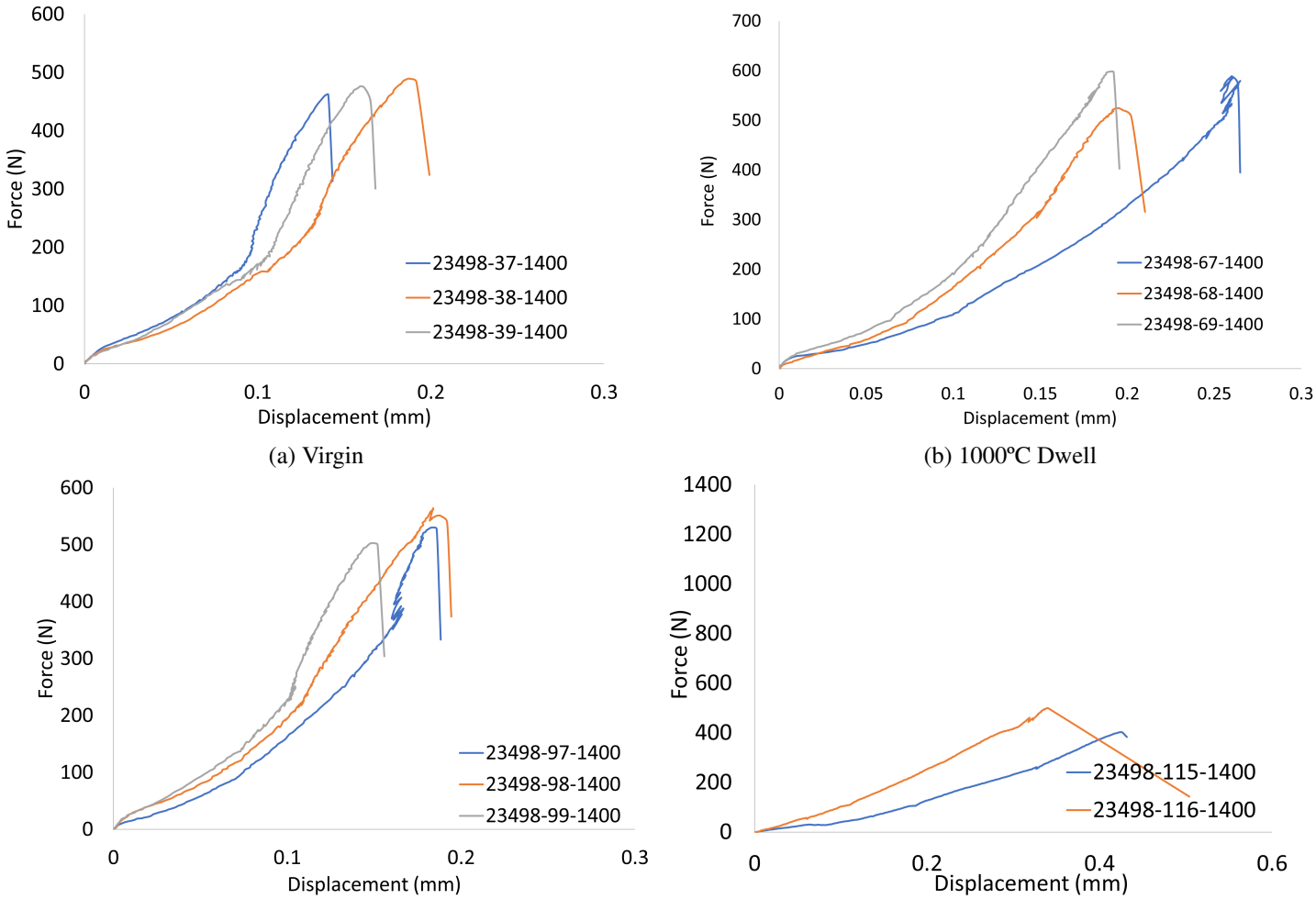

(a) Virgin

(b) 1000ºC Dwell

(c) 1400ºC Dwell

(d) 24h dwell

Figure A.3: 3PB tests done for crystalline silica at 1400ºC

A.2 Fused silica results

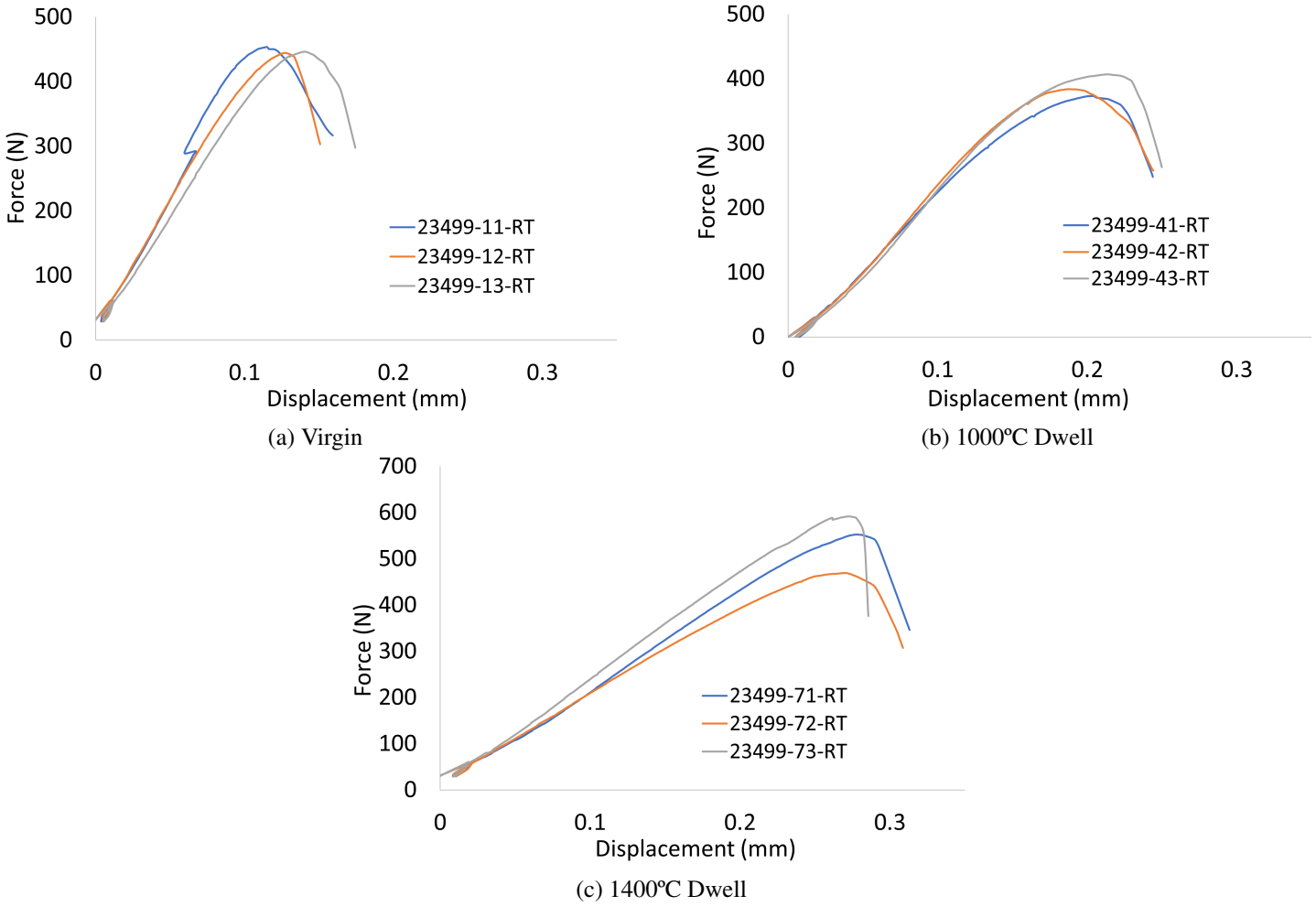

(a) Virgin

(b) 1000ºC Dwell

(c) 1400ºC Dwell

Figure A.4: 3PB tests done for fused silica at room temperature

A.2 Fused silica results

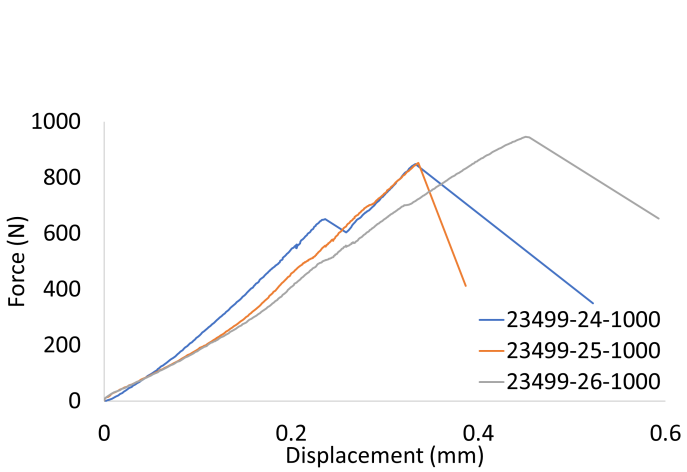

(a) Virgin

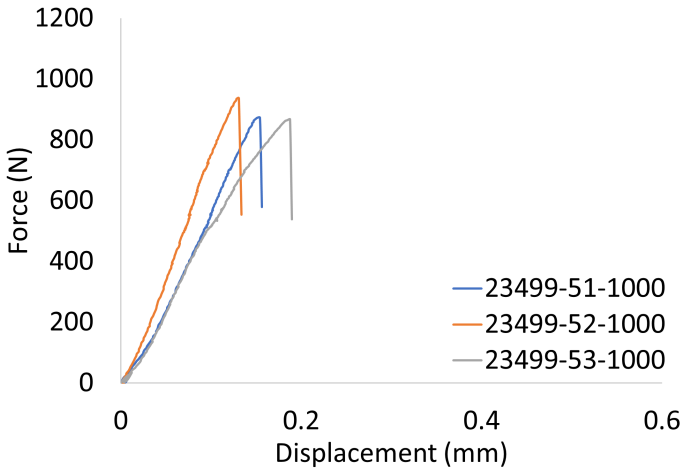

(b) 1000ºC Dwell

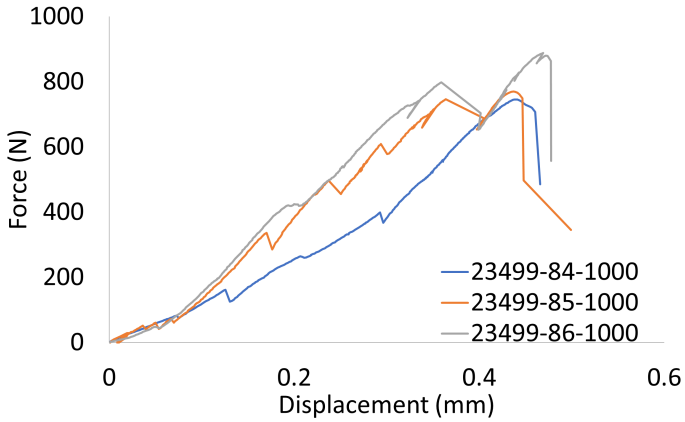

(c) 1400ºC Dwell

Figure A.5: 3PB tests done for fused silica at 1000ºC

All 3PB results

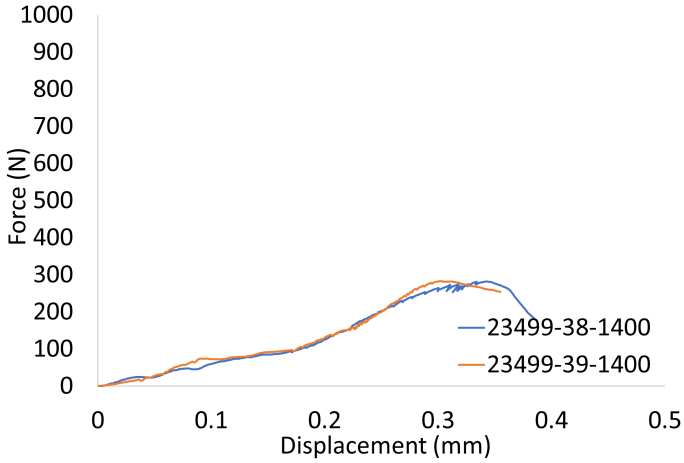

(a) Virgin

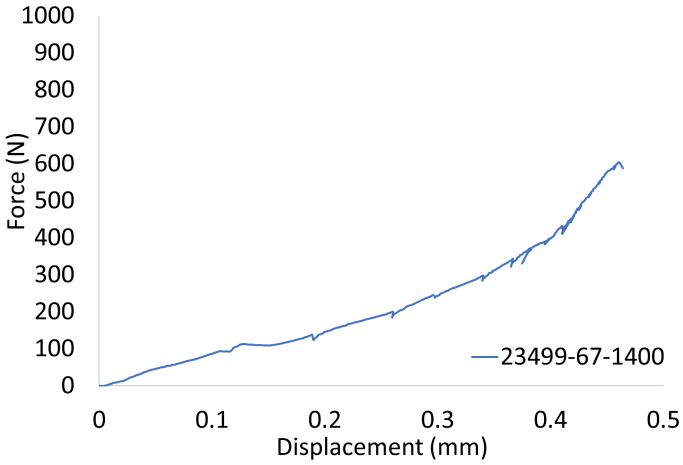

(b) 1000ºC Dwell

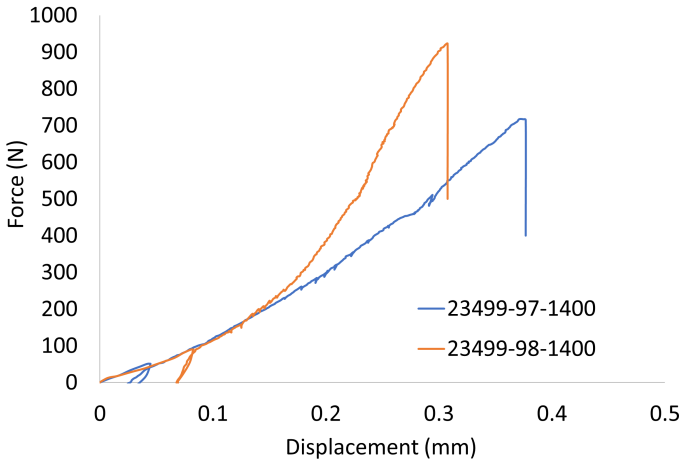

(c) 1400ºC Dwell

Figure A.6: 3PB tests done for fused silica at 1400ºC

In the analysis of this curves, the value for the Young's modulus was the main focus for analysis of these results as well as comparison between the results from IET and 3PB. In order to extrapolate the Young's modulus for these curves, first the curves where all converted to stress-strain graphs by the mean of the following equation:

$$\sigma_f = \frac{3FL}{2bd^2} \tag{A.1}$$

Where:

σ_f, is flexural stress

F, is the load at a given point in the test

L, is the support span

d, is the thickness

$$\varepsilon_f = \frac{6Dd}{L^2} \tag{A.2}$$

Where:
ε_f, is flexural strain
D, is the maximum deflection at the center of the beam
L, is the support span
d, is the thickness

Then, the curves were plotted on excel, and a linear regression of the initial part of the curve was performed. The slope value that was achieved from thi equation equates to the young's modulus of each sample.

References

[1] Antonia Carlene R. Furtado; Marcos C. de Souza Luana da S. Gomes. A sílica e suas particularidades. *Revista Virtual de Química*, pages 1018–1038, 2018.

[2] Fritz Ullmann. *Ullmann's encyclopedia of industrial chemistry*. Wiley-VCH, Fourth edition, 2000.

[3] F. C. Kracek. *Encyclopaedia Britannica*. McMurdie General Editors, First edition, 1953.

[4] D. R. Uhlmann W. D. Kingery, H. K. Bowen. *Introduction to Ceramics*. WileY-VCH, Second edition, 1976.

[5] Jürn W. P. Schmelzer. *Glass, Selected Properties and Crystallization*. De Gruyter, Frist edition, 2014.

[6] F. Brunk. Silica bricks for modern coke oven batteries. *Cokemaking International*, pages 37–40, 2000.

[7] F. Brunk. Silica refractories. *CN Refractories 5*, pages 201–205, 2001.

[8] Yajie Daia, Yucheng Yina, Xiaofeng Xua, Shengli Jinc, Yawei Lia, and Harald Harmuth. Effect of the phase transformation on fracture behaviour of fused silica refractories. *Journal of the European Ceramic Society*, pages 5601–5609, 2018.

[9] K. Andreev, N. Shetty, and E. Verstrynge. Acoustic emission based damage limits and their correlation with fatigue resistance of refractory masonry. *Construction and Building Materials*, pages 639–646, 2018.

[10] J. D. Gilchrist. *Fuels,Furnaces and Refractories*. Pergamon Press, Frist edition, 1977.

[11] *EN ISO 10081-1: Classification of dense shaped refractories - Part 1: alumina-silica products*, 2005.

[12] I. Elstner, H. Leistner, and Feuerfeste Werkstoffe. *Keramik*. II Springer, Sixth edition, 1982.

[13] R. E. Gibbs. The polymorphism of silicon dioxide and the structure of tridymite. *The Royal Society Publishing 13*, page 351–368, 1926.

[14] W. E. Lee, S. Zhang, and M. Karakus. Refractories: Controlled microstructure composites for extreme environments. *Journal of Materials Science*, pages 6675–6685, 2004.

[15] P. Pilate, V. Lardot, F. Cambier, and E. Brochen. Contribution to the understanding of the high temperature behavior and of the compressive creep behavior of silica refractory materials. *Journal of the European Ceramic Society 35*, pages 813–822, 2014.

[16] K. Andreeva, V. Tadaiona, J. Koster, and E. Verstrynge. Cyclic fatigue of silica refractories – effect of test method on failure process. *Journal of the European Ceramic Society*, pages 1811–1819, 2016.

[17] J. Lamon. *Brittle Fracture and Damage of Brittle Materials and Composites*. Elsevier., Frist edition, 2016.

[18] H. Harmuth and E.K. Tschegg. A fracture mechanics approach for the development of refractory materials with reduced brittleness. *Fatigue and Fracture of Engineering Materials and Structures*, pages 1585–1603, 1997.

[19] Yajie Dai, Dietmar Gruber, and Harald Harmuth. Observation and quantification of the fracture process zone for two magnesia refractories with different brittleness. *Journal of the European Ceramic Society*, pages 2521–2529, 2017.

[20] Ana García-Prieto, Manuel Dos Ramos-Lotito, Delia Gutiérrez-Campos, Pilar Pena, and Carmen Baudín. Influence of microstructural characteristics on fracture toughness of refractory materials. *Journal of the European Ceramic Society*, pages 1955–1970, 2014.

[21] K. Andreev, V. Tadaion, Q. Zhu, W. Wang, Y. Yin, and T. Tonessen. Thermal and mechanical cyclic tests and fracture mechanics parameters as indicators of thermal shock resistance – case study on silica refractories. *Journal of the European Ceramic Society*, pages 1650–1659, 2019.

[22] A. A. Griffith. The phenomena of rupture and flow in solids. *Philosophical Transactions Series A*, pages 163–168, 1920.

[23] Jorge Luis Gonzalez-Velazquez. *A Pratical Approach to Fracture Mechanics*. Elsevier, Frist edition, 2020.

[24] G. R. Irwin. Linear fracture mechanics, fracture transition, and fracture control. *Engineering Fracture Mechanics*, pages 241–257, 1968.

[25] IOWA State University. Fracture toughness. Available at https://www.nde-ed.org/Physics/Materials/Mechanical/NotchToughness.xhtml, Accessed last time in Apr 2022, 2022.

[26] T.L. Anderson. *Fracture mechanics, Fundamentals and Applications*. CRC Press, Fourth edition, 2017.

[27] J. R. Rice. A path independent integral and the approximate analysis of strain concentration by notches and cracks. *Journal of Applied Mechanics*, pages 379–386, 1968.

[28] A. A. Roche J. Bouchet and E. Jacquelin. The role of the polymer/metal interphase and its residual stresses in the critical strain energy release rate (gc) determined using a threepoint flexure test. *Journal of Adhesion Science and Technology*, pages 345–369, 2012.

[29] Arief Setiawan, Latif Budi Suparma, and Agus Taufik Mulyono. Developing the elastic modulus measurement of asphalt concrete using the compressive strength test. *AIP Publishing*, 2017.

[30] F. Forster. Z. metallkd vol.29. page 109, 1937.

[31] G. Roebben, B. Bollen, A. Brebels, J. Van Humbeeck, and O. Van der Biest. Impulse excitation apparatus to measure resonant frequencies, elastic moduli, and internal friction at room and high temperature. *American Institute of Physics*, pages 4511–4515, 1997.

[32] Eva Gregorová, Martin Černý, Willi Pabst, Laura Esposito, Chiara Zanelli, Jiří Hamáček, and Jaroslav Kutzendörfer. Temperature dependence of young's modulus of silica refractories. *Ceramics International 41*, pages 1129–1138, 2015.

[33] Peter Grat. X-ray diffraction (xrd). October 2004.

[34] Maria João Margarido Rodrigues. Crack formation and growth during thermal-shock and mechanical cycles in refractories. Master's thesis, Faculdade de Engenharia da Porto, 2019.

[35] Hussein H. Karim, Hisham K. Ahmed, and Oday A. Al-Taie. Manufacturing refractory silica bricks from silica sand. *Engineering and Development Journal, Al-Mustansiriya University*, pages 1093–1207, 2012.

[36] Yuta Hino and Yoshisato Kiyota. Fatigue failure behavior of al2o3–sio2 system bricks under compressive stress at room and high temperatures. *ISIJ International 12*, page 1045–1053, 2012.

[37] J. Zhang, M. N. Gungor, and E. J. Lavernia. The effect of porosity on the microstructural dampening response of 6061 aluminium alloy. *Journal of Material Science 28*, pages 1515–1524, 1993.

[38] C.S.Liu, Z.G. Zhu, F.S. Han, and J. Banhart. Internal friction of foamed aluminium in the range of acoustic frequencies. *Journal of Material Science 33*, pages 1769–1775, 1998.

[39] Peter Greil. Generic principles of crack-healing ceramics. *Journal of Advanced Ceramics 1*, pages 249–267, 2012.

[40] Willi Pabst, Eva Gregorová, and J. Kutzendorfer. Elastic anomalies in trydimite and cristobalite-based silica materials. *Ceramics International 40*, pages 4207–4211, 2014.

[41] Tatiana Gambaryan-Roisman and E. Litovsky. Effect of grain thermal expansion mismatch on thermal conductivity of porous ceramics. *Journal of the American Ceramic Society 82*, pages 994–1000, 2004.

[42] Ryan C. Breneman. Phase changes in silica and their impact on mechanical properties in 3-d printed investment casting molds. Master's thesis, University of Michigan, 2014.

[43] Eva Gregorová, Willi Pabst, Petra Diblíková, and Vojtech Necina. Temperature dependence of damping in silica refractories measured via the impulse excitation technique. *Ceramics International 44*, pages 8363–8373, 2018.

[44] Willi Pabst and Eva Gregorová. Elastic properties of silica polymorphs - a review. *Ceramics – Silikáty 57*, pages 167–184, 2013.